Development of high temperature CO_2 sorbents using solid wastes from power generation

Ili Izyan Syazwani Ramli

Submitted for the degree of Doctor of Philosophy

Heriot-Watt University

School of Engineering and Physical Sciences

September 2014

ABSTRACT

One of various ways to curb anthropogenic carbon dioxide (CO_2) emissions is by using Li_4SiO_4 sorbents to capture CO_2, which have shown high CO_2 uptake capacities (up to 367 mg CO_2/g sorbent) at high temperatures (400 to 600 °C). In this study, solid wastes from coal- and biomass-fired boilers that contain high amounts (>47 wt%) of silica were used as precursors in the development of Li_4SiO_4-based high temperature CO_2 sorbents via solid state (SS) and suspended impregnation (SI) methods. Thermogravimetric analyses (TGA) carried out in pure CO_2 environment at sorption temperatures of 500 to 700 °C showed the waste-derived Li_4SiO_4 sorbents have high CO_2 sorption capacities (up to 263 mg CO_2/g sorbent at 700 °C). This study also experimented for the first time the potential of palm oil mill boiler ash (POMBA) as a waste-derived Li_4SiO_4 sorbent precursor. It was found that POMBA-derived sorbents showed high CO_2 sorption capacities (up to 257 mg CO_2/g sorbent at 700 °C in pure CO_2 environment). These waste-derived Li_4SiO_4 sorbents exhibited CO_2 sorption capacities exceeding some of those in published work (27 mg CO_2/g sorbent). Furthermore, this study analysed the effect of excess lithium on waste-derived sorbents. It was found that depending on the materials used, the amount of excess lithium added during the preparation step affected CO_2 sorption performance of the waste-derived sorbents.

Dedication

In the Name of Allah, the Most Merciful, the Most Compassionate. All praise be to Allah, the Lord of the worlds. Prayers and peace be upon Muhammad, His servant and messenger.

There is none worthy of my highest gratitude other than The Creator. The All Knowing, The Wise, The Guide, Infallible Teacher and Knower. All praises due to Him and only Him, The Self-Existing One upon Whom all others depend. For without Him, there would be no knowledge. For without His guidance, all hope was lost.

The most honourable leader ever existed, Muhammad (may peace be upon him), whom has lead and will continue to lead this Ummah by the best of examples until The End of Time.

A deep debt of gratitude to my supervisor and an inspiring role model, Professor Mercedes Maroto-Valer, for her priceless support in research. To everybody in CICCS, I say thank you for fruitful discussions and collaborations, and also all the good laughs. Not to forget the technicians and staff at Heriot-Watt University for the assistance in times of need.

My wholehearted thanks to my mak, Rohayah Saim, and my ayah, Ramli Muda, for their never-ending love and moral strength through thick and thin. Thousands of miles apart was never an excuse to not provide me with words of motivation and affection. Words will never be adequate to express my appreciation and love to the rest of my family, especially Abalong, Kaklong, Abangah, Kakngah, Aki and Nadeen Ummairah.

Lastly but not by any means the least, to friends. You know who you are.

ACADEMIC REGISTRY
Research Thesis Submission

Name*:*	ILI IZYAN SYAZWANI RAMLI		
School/PGI:	Engineering and Physical Sciences		
Version: *(i.e. First, Resubmission, Final)*	Final	Degree Sought (Award **and** Subject area)	PhD Chemical Engineering

Declaration

In accordance with the appropriate regulations I hereby submit my thesis and I declare that:

1) the thesis embodies the results of my own work and has been composed by myself
2) where appropriate, I have made acknowledgement of the work of others and have made reference to work carried out in collaboration with other persons
3) the thesis is the correct version of the thesis for submission and is the same version as any electronic versions submitted*.
4) my thesis for the award referred to, deposited in the Heriot-Watt University Library, should be made available for loan or photocopying and be available via the Institutional Repository, subject to such conditions as the Librarian may require
5) I understand that as a student of the University I am required to abide by the Regulations of the University and to conform to its discipline.

* *Please note that it is the responsibility of the candidate to ensure that the correct version of the thesis is submitted.*

Signature of Candidate*:*		Date:	

Submission

Submitted By *(name in capitals):*	
Signature of Individual Submitting:	
Date Submitted:	

For Completion in the Student Service Centre (SSC)

Received in the SSC by *(name in capitals):*			
Method of Submission *(Handed in to SSC; posted through internal/external mail):*			
*E-thesis Submitted (**mandatory for final theses)***			
Signature:		Date:	

List of tables

List of figures

Table of Contents

LIST OF PUBLICATIONS

1. Sanna A., **Ramli I.**, Maroto-Valer M. M., 2014, Novel Na-silicates CO_2 Sorbents from Fly Ash. Energy Procedia 63, 739-744.
2. **Ramli I.**, Maroto-Valer M. M., 2013. Development of Development of high temperature precombustion CO_2 sorbents using solid waste from coal-fired power plant. Proc. 12th Annual Conference on Carbon Capture, Utilization and Sequestration, Pittsburgh, Pennsylvania, USA
3. **Ramli I.**, Maroto-Valer M. M., Palm oil mill boiler ash as high temperature CO_2 sorbent. (Draft to be submitted)

Chapter 1 Introduction

1.1. Background literature

Carbon dioxide capture and storage (CCS) is a technological option to reduce anthropogenic carbon dioxide (CO_2) emissions and thus, stabilising atmospheric CO_2 concentration (IPCC, 2005). Under the concept of CCS, CO_2 is captured from large point sources like coal-fired power plants and subsequently transported and sequestered in geologic formations such as depleted oil and gas fields, saline formations and unmineable coal seams (Figueroa et al., 2008; Klara et al., 2003).

The capture of CO_2 can be accomplished by three different routes, namely post-combustion, pre-combustion and oxy-combustion (Figueroa et al., 2008). Post-combustion separates CO_2 from flue gases and can occur anywhere along the flue gas processing stream from combustor to effluent exhaust, where the CO_2 concentration is normally between 3 to 15 vol%. The pre-combustion route involves CO_2 capture after the gasification process and prior to the combustion step (IPCC, 2001). In oxy-combustion, pure oxygen substitutes air as combustion gas producing a stream concentrated with CO_2 and H_2O (GCEP, 2005).

Although CCS provides promising technologies to curb anthropogenic CO_2 emissions, it is not without challenges. The CO_2 capture step contributes to a large portion of the total cost of the CCS chain. The large capture costs are due to the capture materials as well as capital and operational costs of the capture process

itself (IEA, 2004). Consequently, high energy efficiency penalty related to CO_2 capture is one of the biggest challenges for implementing CCS. For example, average net energy efficiency penalty related to CO_2 capture for pulverised coal-fired power plants when a post-combustion amine-based system is applied was reported to be approximately 10 percentage points, which translates to 74% increase in costs without capture. The high energy penalty is mostly caused by the solvent regeneration and CO_2 compression process (IEA, 2011).

Solid sorbents have become an increasingly popular area of research, although liquid sorbents are considered as the most mature CO_2 capture technology, going back to the capture of CO_2 for enhanced oil recovery (EOR) operations in the 1970s (Rao and Rubin, 2002). However, liquid solvents like monoethanolamine (MEA), diethanolamine (DEA) and methyldiethanolamine (MDEA) have been found to have problems of scaling and performance stability (Munoz et al., 2009). Furthermore, liquid solvents are prone to degradation and oxidation resulting in products that are corrosive and may require hazardous material handling procedures (Islam et al., 2011). These problems can be resolved using solid sorbents. Additionally, the energy required for regeneration and moving liquid solvents could be reduced with solid sorbents, if high (more than 132 mg CO_2/g sorbent) CO_2 uptake capacity of the sorbent is achieved (Gray et al., 2008). Furthermore, solid sorbents produce no liquid wastes and offer much wider temperature range applications between 25 and 700 °C (Choi et al., 2009; Olivares-Marin & Maroto-Valer, 2012).

Among the solid sorbents studied thus far, alkaline earth metal oxides such as Li_4SiO_4 have been known to have high CO_2 sorption capacity (up to 367 mg CO_2/g sorbent). Due to the high CO_2 uptake capacity of these sorbents, solid wastes have been proposed as silica sources for lithium-based sorbents in an effort to lower the production cost of the solid sorbents. Additionally, the use of solid wastes as precursors for CO_2 capture sorbents provides a good strategy to solid waste management, as these types of waste materials are known to have environmental and health concerns as most of them ended up in landfills in huge ash lagoons or dumped into the sea (Wang et al., 2008; Blisette and Rowson, 2012).

1.2. Knowledge gaps for high temperature CO_2 sorbents

Despite the increasing number of on-going research on solid sorbents, there are very limited studies on solid waste materials as precursors for high temperature sorbents. Most of the solid sorbents studied thus far are that of pure sorbents including lithium-based Li_4SiO_4 (Kato et al., 2005; Ida and Lin, 2005; Yamaguchi et al., 2007). The preparation of these pure solid sorbents is costly due to the use of high purity starting materials such as Li_2CO_3. Subsequently, this increases the overall cost of capture materials which then contributes significantly to the bulk of the total cost of the CCS chain. By utilising waste materials as precursors for high temperature sorbents, the capture cost could potentially be reduced and at the same time providing an alternative to landfilling.

Improving the CO_2 uptake capacity of high temperature sorbents is an intensive area of research. Even more so, CO_2 uptake capacity of waste-derived sorbents also needs to be further enhanced as the capacity is usually less than that of pure sorbents. Therefore, there is a strong need to investigate different waste materials that could be developed into high temperature CO_2 sorbents. As a general guide, the CO_2 uptake capacity of waste-derived high temperature solid sorbents needs to at least correspond to the commercially available solvents e.g. MEA (176 mg CO_2/g sorbent).

Despite various studies on pure Li_4SiO_4 sorbents, there are limited studies on the development of high temperature Li_4SiO_4 sorbents derived from low-cost solid wastes. These solid wastes have thus far included coal-derived and biomass-derived waste materials, such as pulverised fuel ash and rice husk ash, respectively (Olivares-Marin et al., 2010; Wang et al., 2011). For example, Olivares-Marin et al. (2010) investigated Colombian and Russian coals derived fly ashes that was obtained from coal-fired power plants, while Wang et al. (2011) used ashes deriving from rice husks that was obtained from a rice mill in Wuhan, China (Olivares-Marin et al., 2010; Wang et al., 2011).

Another potential material to be developed as CO_2 sorbents is palm oil mill boiler ash (POMBA). POMBA is a by-product of combustion process in a self-sustainable mill plants, also posed similar environmental and health concerns as other known solid wastes. This material has not been known to be used for producing CO_2 sorbents. In addition, the potential of POMBA as a precursor for high temperature

sorbents has not been reported. Many published studies on biomass-derived sorbents such as oil palm solid waste, durian shell and olive stones are that of low sorption temperatures ranging from 25 to 100 °C (Nasri et al., 2013; Chandra et al., 2009; Roman et al., 2008).

Consequently, studies on effect of CO_2 concentrations, sorption temperature and regeneration of waste-derived Li_4SiO_4 sorbents on the CO_2 uptake are needed to understand the performance of proposed waste-derived sorbents. Previous works reported that these are some of the crucial parameters in determining the performance of CO_2 sorbents. For example, Essaki et al. (2005) reported significant changes in the CO_2 uptake capacity of pure Li_4SiO_4 sorbents in a 15% (280 mg CO_2/g sorbent) compared to a 5% CO_2 (30 mg CO_2/g sorbent) sorption environment (Essaki et al., 2005).

1.3. Research aim and objectives

The aim of this study is to develop high temperature CO_2 sorbents using solid wastes from power generation plants. The materials of interest are hypothesised to be suitable for CO_2 capture at high (500, 600 and 700 °C) sorption temperatures, depending on their chemical and physical characterisation properties. Different methods of synthesising the sorbents and regenerability of the sorbents are hypothesised to affect the sorption capacity. The following research objectives were established to address the hypotheses of this study:

1. To assess the suitability of the materials of interest into solid sorbents by performing chemical and physical characterisations.
2. To synthesise sorbents with CO_2 uptake capacities of at least 100 mg CO_2/g sorbent for waste-derived Li_4SiO_4 sorbents at high temperatures via chemical impregnation method.
3. To investigate the influence of different sorption temperatures (500, 600, 700 °C) on CO_2 sorption capacity of the sorbents.
4. To study CO_2 sorption by sorbents under diluted CO_2 environment.
5. To examine the regeneration performance of synthesised sorbents.

In order to address Objective 1, a series of characterisation analyses including particle size distribution, x-ray diffraction, nitrogen adsorption/desorption isotherm and surface area, x-ray fluorescent, scanning electron microscope and fourier transform infrared were carried out on a series of waste materials and their corresponding prepared Li_4SiO_4 sorbents. The characteristics of waste materials and synthesised sorbents are described in Chapter 4 of this thesis. To address Objective 2, waste materials were subjected to solid state impregnation method. Upon synthesis, the resulting waste-derived sorbents were subjected to thermogravimetric (TG) analysis to determine their CO_2 uptake capacities.

To address Objectives 3, 4 and 5, synthesised sorbents were subjected to thermogravimetric analysis under controlled sorption conditions and the subsequent experimental data are discussed in Chapter 5. Chapter 2 discusses the background to this study, including reviews of relevant published works that have

influenced this study. Finally, Chapter 6 concludes the discussions in previous chapters and provides recommendations for future work. There is also a list of references cited at the end of this thesis.

Chapter 2 Literature review

In this chapter, global CO_2 emissions and mitigation strategies, especially for carbon dioxide capture and storage (CCS), are introduced in Section 2.1 and 2.2, respectively. Next, published work on CO_2 capture by solid sorbents is reviewed in Section 2.3. Finally, a review on CO_2 capture by industrial waste materials is presented in Section 2.4.

2.1. CO_2 emissions and mitigation strategies

2.1.1. *Global CO_2 emissions*

Records have shown that world energy consumption has been escalating since the beginning of 19th century Industrial Revolution (WEC, 2003). In the years between 1971 and 2011, total world energy consumption increased almost two times. The U.S. Energy Information Administration (EIA) has forecasted an increase in world energy consumption of more than 155% from 2010 to 2040 (EIA, 2013). This has caused increasing fossil fuel burning which consequently increases anthropogenic greenhouse gases (GHG), particularly carbon dioxide (CO_2). As a consequence, in 2011, CO_2 emissions to the atmosphere have increased by 40% of those pre-industrial levels (IPCC, 2013).

CO_2 has been identified as the main contributor of anthropogenic GHG emissions, representing about 76% of the total global GHG emission in 2010 (Ecofys, 2013).

In the UK, 82% of the total GHG emission were CO_2 in 2012 (DECC, 2014). Anthropogenic CO_2 is mainly released into the atmosphere by combustion of fossil fuel such as coal, oil and natural gas, as well as renewable energy sources like biomass; as well as deforestation activities including burning of trees for land clearance; and also industrial and resource extraction processes (IPCC, 2005).

Figure 2.1 shows the increasing CO_2 atmospheric concentrations, particularly after the Industrial Revolution. The concentrations were based on the analysis of ice cores obtained from 1987 to 1993 and logged atmospheric CO_2 concentrations from 1958 until 2014 (Etheridge et al., 1998; Scripps, 2014). Figure 2.1a shows that CO_2 concentrations have never exceeded 280 ppmv for more than 800 years until around 1900, where the concentrations reached 300 ppmv and have been increasing continuously since then at an increasing rate (Figure 2.1b) (Keeling and Whorf, 2005). Constant increase in global energy demanded raised fossil fuel burning to meet this demand and also caused a significant impact on CO_2 atmospheric concentrations. In addition, the U.S. National Oceanic and Atmospheric Administration reported that CO_2 atmospheric concentration reached 400 ppm on May 2013 for the first time since measurements began in 1958 in Mauna Loa (NOAA, 2013).

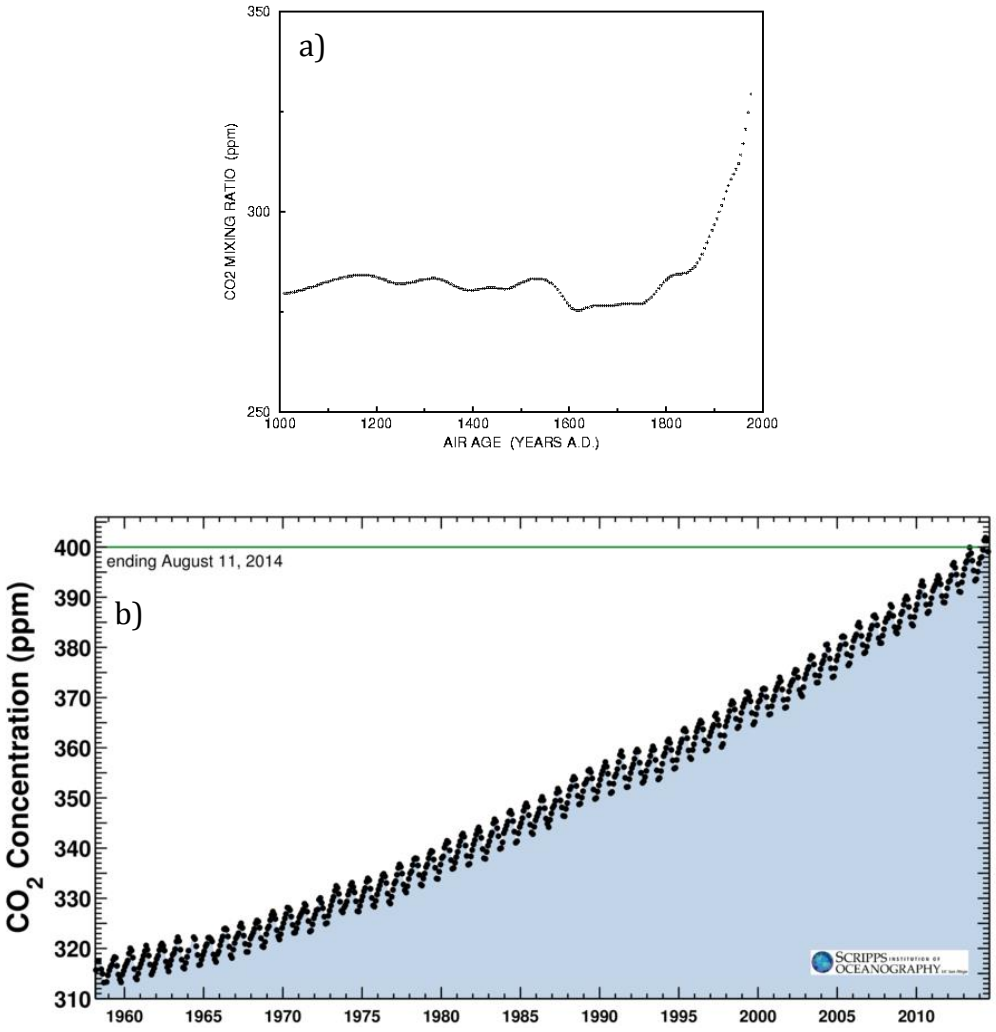

Figure 2.1 a) atmospheric CO_2 concentrations based on the analysis of ice cores for 1000–1997; b) actual atmospheric CO_2 analysis during 1958–2014 (Etheridge et al., 1998; Scripps, 2014)

Increase in GHG emission is being acknowledged as the main contributor to climate change which is estimated to continue throughout this 21st century (IPCC, 2005; IPCC, 2007). Climate change disturbs balanced nature of the Earth, including elevated global average surface temperature, rising global average sea levels and

extraordinary melting of the ice caps (IPCC, 2007). A significant example of climate change impact can be clearly seen by the rapid melting of the Chacaltaya Glacier in Bolivia, where the initial 0.22 km^2 of glacier in 1940 was quickly reduced to 0.01 km^2 in 2005 (IPCC, 2007).

Anthropogenic CO_2 emissions are largely due to the combustion of fossil fuels for power generation, accounting for 41% of the total emissions (NRC, 2010). Combustion of coal emits more CO_2 due to its high carbon content per unit of energy released (about 93 to 99 kg of CO_2 per GJ of energy released, depending on the type of coal being burned), as presented in Table 2.1. Among the different types of fossil fuel i.e. coal, liquid fuels and natural gas, coal emits the highest amount of CO_2 per GJ of energy released with the highest value of 99 kg CO_2/GJ. Liquid fuels emits on average of 69 kg CO_2 per GJ of energy released, while the amount of CO_2 emission of natural gas is approximately half compared to that of coal.

Table 2.1 Carbon content (in kg CO_2 emitted per GJ of energy released) for different types of fuel (EIA, 2012)

Fuel type		kg CO_2/GJ
Coal		
i.	Anthracite	99
ii.	Bituminous	89
iii.	Lignite	93
iv.	Subbituminous	92
Liquid fuels		
i.	Diesel fuel/heating oil	70
ii.	Gasoline	68
Natural gas		52

However, coal has not always been the main CO_2 contributor. In the past, CO_2 emissions from coal were less than that of liquid fuels, but quickly exceeded starting from 2004 (11 billion metric tonnes) and coal is likely to remain as leading source of CO_2 emissions until 2040 (21 billion metric tonnes), as illustrated in Figure 2.2. The natural gas share of CO_2 emissions has been relatively small by comparison at 19% of the total in 1990 and expected to continue the trend at projected 22% of total CO_2 emission in 2040 (EIA, 2013).

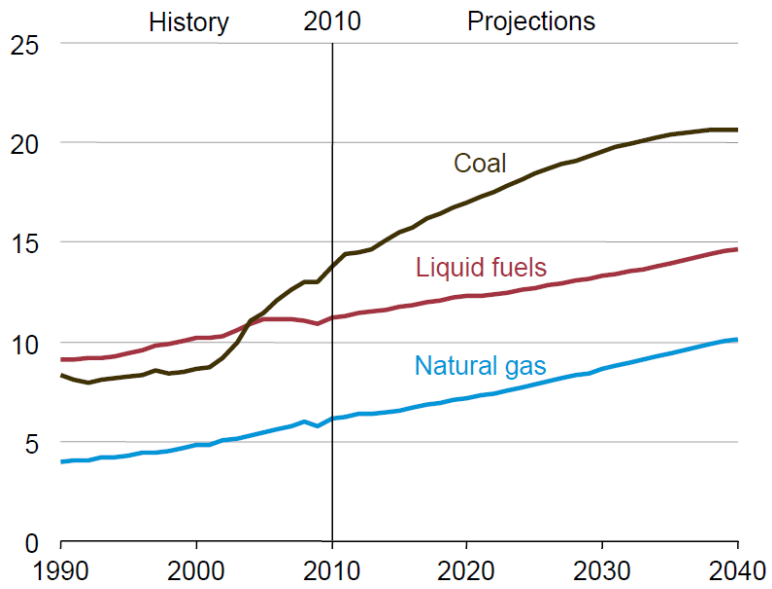

Figure 2.2 Historical and projections of CO_2 emissions by fuel type in billion metric tons (EIA, 2013)

2.1.2. *International regulatory framework*

The United Nations Framework Convention on Climate Change (UNFCCC) was agreed in New York on 9 May 1992 as the direct outcome of the Rio Earth Summit in the same year (UNFCCC, 1992). Its main objective was "to achieve stabilisation of GHG concentrations in the atmosphere at level that would prevent dangerous anthropogenic interference with the climate system". The objective has been the driving force for mitigation initiatives of many GHG, including CO_2, on international levels for years to come since its establishment. The countries of UNFCCC, also known as the Parties, hold annual meetings to discuss feasible methods to achieve this objective.

One of the most important outcomes of the meetings was the Kyoto Protocol. Adopted in Kyoto, Japan on 11 December 1997, it was an international agreement among the Parties to set internationally binding emission reduction targets (UNFCCC, 1998). The Protocol placed heavier burden on developed nations for their current high levels of GHG emissions in the atmosphere as a result of more than 150 years of industrial activities, under the principle of "common but differentiated responsibilities". The Protocol was open for signature from 16 March 1998 to 15 March 1999 and received 84 signatures within the duration. Currently, there are 191 Parties to the Protocol, with the exception of Canada which revoked its ratification status effective 15 December 2012. Although the United States of America is one of the Annex I Parties, which consist of countries committed themselves in aiming to reduce to their 1990 level of greenhouse gases by the year 2000, it has not ratified the Protocol.

The methods applied in the Protocol included the clean development mechanism (CDM). CDM allows emission bargain projects in developing countries to earn certified emission reduction (CER) credits of which each equivalent to 1 tonne of CO_2. CER can be traded, sold and used by industrialised countries to meet a part of their emission reduction targets under the Protocol. Nevertheless, it was not until 2001 at the Convention's seventh meeting at Marrakesh (Morocco) that the detailed rules for implementation of the Protocol were adopted. The Protocol officially entered into force on 16 February 2005. The first commitment started on 2008 and ended in 2012. During this commitment period, 37 industrialised

countries along with European Community committed to reduce GHG to an average of 5% against 1990 levels.

The second commitment of the Kyoto Protocol, also known as the Doha amendment of the Kyoto Protocol, began on 1 January 2013 and expected to end on 31 December 2020 (UNFCCC, 2012). Adopted in Doha on 8 December 2012, the amendment also updated the list of GHG along with several articles of the Kyoto Protocol in agreement with the second commitment. During the new commitment period, it is expected that GHG emission levels are to be reduced by at least 18% below 1990 levels despite altered composition of Parties during the first commitment period.

Other notable negotiations that lead to current commitments include the 2007 Bali Action Plan, the 2010 Cancun agreements, the 2011 Durban as well as the 2013 Warsaw Climate Change Conferences. The Bali Action Plan was established as a direct respond to the IPCC 4th Assessment Report that warned about the change in climate system and that delay in reducing emissions significantly inhibited opportunities to achieve lower stabilisation levels and increased the risk of more severe climate change impacts. Consequently, the Bali Action Plan introduced a comprehensive process to enable full implementation of the Convention through long-term cooperative actions with the establishment of the Ad Hoc Working Group on Long-Term Cooperative Action (AWG-LCA). The focus of the working group included to launch actions on mitigation and adaptation of climate change,

technology development and transfer as well as the provision of financial resources to support these actions (UNFCCC, 2007).

The 2010 Cancun agreements highlighted clear objectives for reducing anthropogenic GHG to keep the global average temperature rise of less than 2 °C. These included realising the Bali Action Plan, while additionally urging global protection of forests as the major repository of carbon, encouraging global participation in minimising climate change and ensuring international transparency of these actions (UNFCCC, 2010). Moreover, the Climate Change Conference in Cancun also emphasised in providing for financial and technology development supports to the developing countries in order for them to realise the outlined actions.

The negotiations at the 2011 Durban Climate Change Conference advanced the implementation of Kyoto Protocol, Bali Action Plan and Cancun agreements. The 2011 Durban outcomes were considered to be a turning point in climate change negotiations, where the Parties were clearly more committed to adopt a universal legal agreement on climate change as soon as possible and no later than 2015. The highlight of the outcomes in Durban conference included the roadmap for implementation, consisting of the second commitment period of Kyoto Protocol, or later known as the Doha amendment to Kyoto Protocol, the launch of new platform of negotiations that critically finding ways to further raise the existing level of national and international actions, more transparent emission reduction and limitation plans in addition to provide supports to the developing countries and

global review of the emerging climate challenge to ensure whether there was a need to revise the maximum two-degree global temperature rise limit (UNFCCC, 2011).

The 2013 Warsaw Climate Change Conference was essentially a preparation of the Parties for a universal climate change agreement planned to be held in 2015. The objectives of the 2015 agreement were essentially to further collectively encourage effective global effort to rapidly reduce the climate change consequences while building adaptation capacity. Among key decisions made during this conference there was the establishment of the Green Climate Fund to support developing countries in realising the action plans, finalisation of monitoring, reporting and verification arrangements for domestic actions, mechanism to address loss and damage caused by long-term climate change impacts. Warsaw 2013 also provided showcase for climate change action by business, cities, regions and civil societies and the Parties were convinced that the solutions to climate change had become available via technological options, wealth as well as knowledge.

2.1.3. *Mitigation strategies*

There is a wide portfolio of technological options to reduce CO_2 emissions, including: i) improving energy efficiency, ii) switching from high carbon intensive fuel such as coal to a less carbon intensive fuels like natural gas, iii) increasing the use of renewable energy sources or nuclear, iv) capturing CO_2 by enhancing the

biological absorption capacity of forests and soils, and vi) capturing and storing CO_2 chemically or physically which is also known as carbon capture and storage or CCS (IPCC, 2005; Plaza et al., 2007).

CCS is a promising choice to reduce the overall mitigation costs and escalating flexibility in reducing GHG emissions. Nonetheless, the extent of application of CCS would depend on technical maturity, costs, overall potential, technology diffusion and transfer to developing nations and their capacity to apply the technology. Social factors such as regulatory aspects, environmental issues and public perception also played important roles to the rate of deployment of the technology (IPCC, 2005).

Positive implications of CCS on CO_2 emission reduction can be explained using the Socolow stabilisation wedges analysis. The analysis derived from CO_2 emission (GtC/year) curves from fossil fuel combustion and cement manufacture which regarded two different scenarios; 1) the business-as-usual (BAU) scenario which assumed zero carbon mitigation initiative and; 2) CO_2 stabilisation at 500 ppm by Wigley, Richels and Edmonds (WRE 500), as shown in Figure 2.3A. The curves are divided into a stabilisation triangle of avoided emissions and continued fossil fuel emissions (Figure 2.3B) which fixed at 7 GtC/year starting 2004 until the WRE500 scenario is ideally applied in 2054. The stabilisation wedges are then referred to as graphical interpretation of activities reducing the rate of carbon build-up in the atmosphere that grows in 50 years at 7 GtC/year (Pacala and Socolow, 2004).

In this analysis, CCS was included as one of the recommended activities in reducing the carbon build-up. The analysis proposed four CCS options; 1) CO_2 capture at baseload power plant; 2) CO_2 capture at hydrogen plant; 3) CO_2 capture at coal-to-synfuels plant and; 4) CO_2 storage in geological formations. CCS would be able to reduce CO_2 emissions by 1 GtC/year within 50 years of employment.

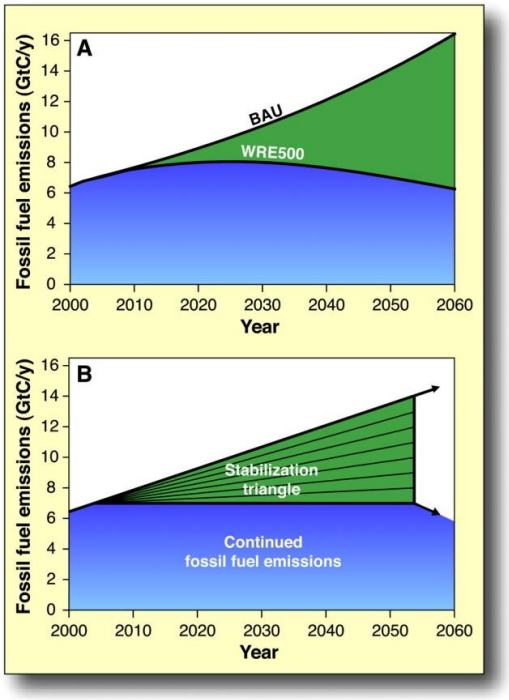

Figure 2.3 CO_2 emission (GtC/year) curves from fossil fuel combustion and cement manufacture with two different scenarios; A) the business-as-usual (BAU) scenario which assumed zero carbon mitigation initiative and; B) CO_2 stabilisation at 500 ppm by Wigley, Richels and Edmonds (WRE 500) (Pacala and Socolow, 2004)

This analysis was reaffirmed in 2011 by the author himself and the core messages of the analysis were found to be still valid as they were in 2004 (Socolow, 2011). However, the wedges needed to fill the stabilisation triangle had increased to nine,

instead of seven in 2004 (Figure 2.4). The additional 2-segment global CO_2 emissions trajectory that started in 2011 instead of 2004 added another 50 ppm to the equilibrium concentration. The delayed trajectory also produced approximately 0.5 ^{0}C rise in the average surface temperature of the earth. This shows the gravity of consequences when the deployment of appropriate activities to reduce CO_2 emissions is delayed. This is backed up by recent IEA report which stated that unless CCS technology is widely deployed, no more than one-third of proven reserves of fossil fuels can be consumed prior to 2050 if the world is to achieve the 2 °C of average global surface temperature rise (IEA, 2012).

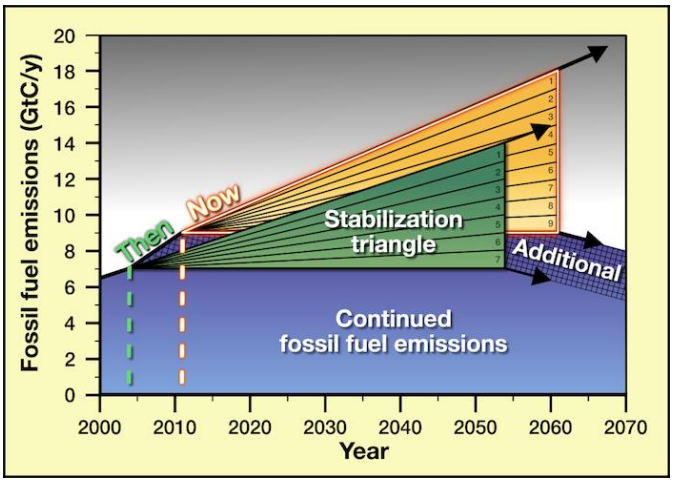

Figure 2.4 Stabilisation triangles in 2004 and 2011 (Socolow, 2011)

The IEA introduced the BLUE Map scenario in the 2008 Energy Technology Perspective, in order to project the ability of the world to reduce 50% CO_2 emission by the year 2050 (IEA, 2008). This scenario served as extension of the Baseline scenario in the World Energy Outlook 2007 (also referred to as WEO

2007 450 ppm case), which was projected up to the year 2030. The BLUE Map scenario took into account the adoption of technologies with marginal costs of up to USD 200 per tonne CO_2. Figure 2.5 shows the source of CO_2 savings in the BLUE Map scenario compared to the World energy Outlook 2007 450 ppm case (IEA, 2008). It is apparent that in order to achieve the optimistic 50% reduction of CO_2 emission by the year 2050, more stringent mitigation strategies have to be deployed. These, among others, include the deployment of CCS technologies in industries as well as power generation.

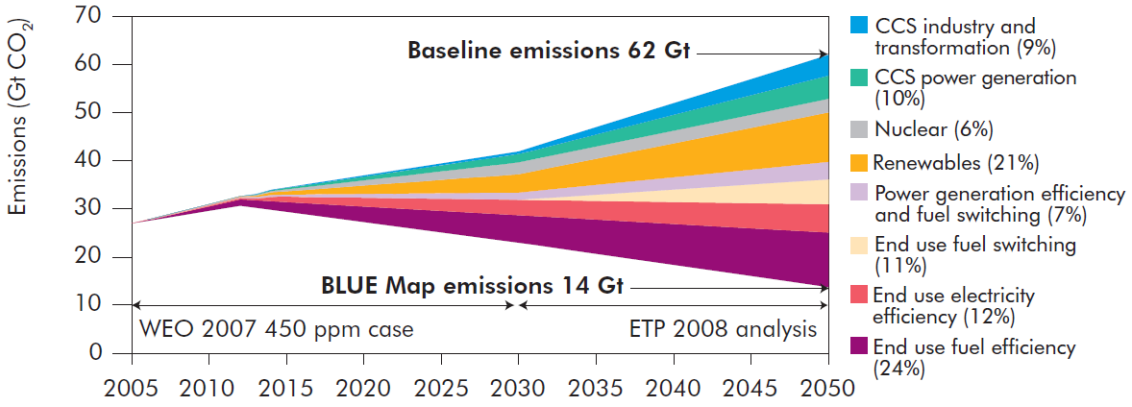

Figure 2.5 The source of CO_2 savings in the BLUE Map scenario compared to the World Energy Outlook 2007 450 ppm case (IEA, 2008).

2.2. Carbon dioxide capture and storage (CCS)

CCS is a technological option to reduce anthropogenic CO_2 emissions. Figure 2.6 provides a general illustration to the CCS chain from the capture plant to geological storage, and including CO_2 transport (GCCSI, 2013a). CO_2 would be captured at large point sources such as coal-fired power plants. Captured CO_2 will be

separated from capture medium, compressed to a high pressure usually at supercritical conditions of approximately more than 200 bar and 250 ^{0}C.

The modes of CO_2 transportation can be divided into two, namely offshore and onshore. Offshore transport includes pipelines and ships. Large amounts of CO_2 can be transported predominantly via pipelines due to the readily available millions of kilometres of pipelines worldwide that transport various types of fluids, including CO_2, and thus would appear to be the most economical and practical (Golomb, 1997; Koorneef et al., 2012). Shipment can be an alternative option for many parts of the world. Europe has been involved in shipment of CO_2 on a small scale, where typically 1000 tonnes food-quality CO_2 is shipped from large point sources to coastal distribution terminals. Shipping larger amounts of CO_2, i.e. 10,000 and 40,000 cubic metres, are likely to be similar to that of liquefied petroleum gas (LPG), which expertise has been developed for decades.

Onshore transport can also include pipelines, as well as road tankers and rails. Transports by road tankers and rails are possible for smaller amount of CO_2 being transported over shorter distances compared to transport by pipelines. Nevertheless, it is unlikely for wheeled modes of transportations to be in significant number based on large amount of CO_2 to be transported to storage sites which are more economical and practical using pipelines (Golomb, 1997; GCCSI, 2013a).

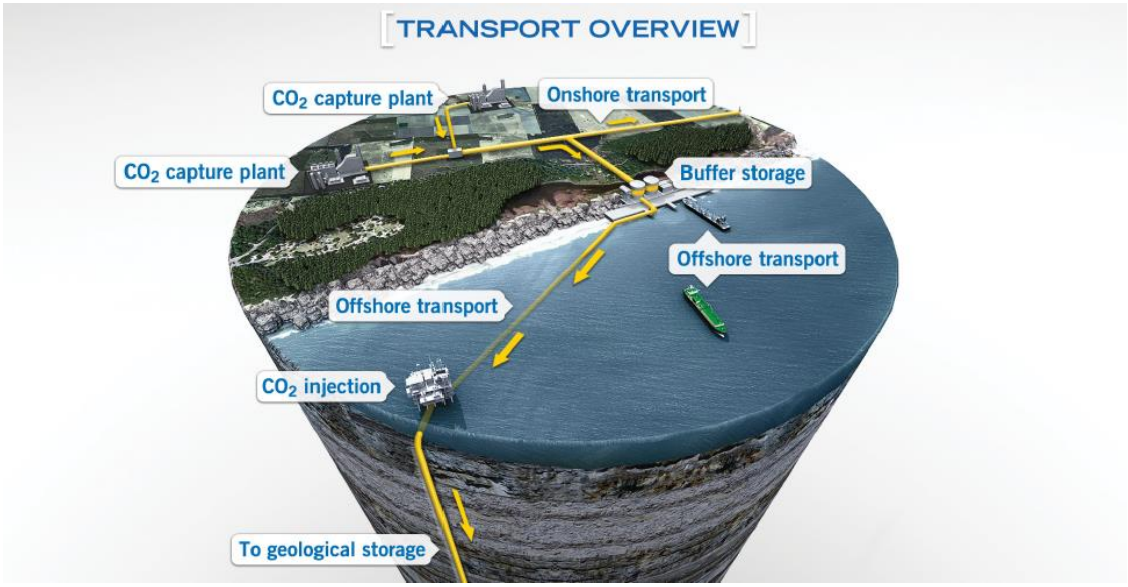

Figure 2.6 The CCS chain with transport overview (GCCSI, 2013a)

Transported CO_2 is then injected and stored in geologic formations (Figueroa et al., 2008; Klara et al., 2003). Figure 2.7 shows different types of CO_2 storage options (IPCC, 2005), where the most common options are saline water-saturated reservoir rocks, oil and gas fields and coal systems. Other options include storage in basalts, oil shales and cavities. CO_2 storage capacity estimates for different geological options are summarised in Table 2.2. These different CO_2 storage options are discussed below.

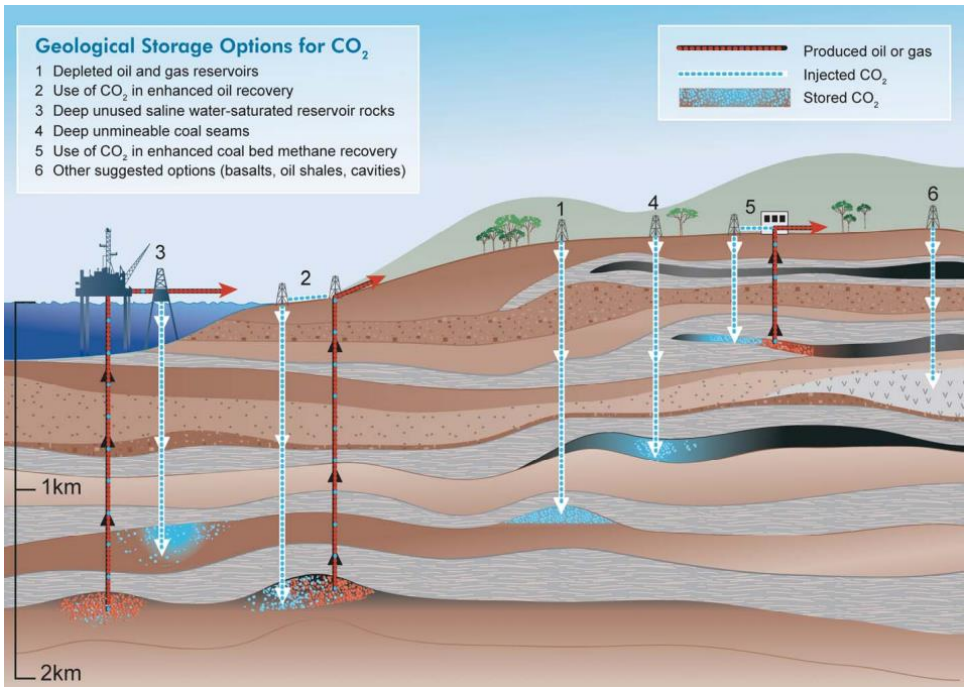

Figure 2.7 CO_2 storage site options (IPCC, 2005)

Saline formations consist of porous sedimentary rocks saturated with formation waters that are considered as unsuitable for human consumption, agricultural or industrial use. Supercritical CO_2 can be stored in deep saline formations due to its ability to retain CO_2 underground at relatively high water formation pressure. Saline formations have been identified as one of the best options for large volume CO_2 storage in geological formation (Bachu, 2000; Bradshaw et al., 2002). Table 2.2 shows the lower estimate of storage capacity in deep saline formations is 1000 Gt CO_2, while the upper estimate is possibly up to 10^4 Gt CO_2 (IPCC, 2005). Nevertheless, these formations are commonly less understood in comparison to shallow freshwater aquifers or hydrocarbon bearing reservoirs and any assessment of their CO_2 storage potential typically includes significant uncertainty because of the scarcity of subsurface data. Additionally, the containment potential

of the seal rock is usually untested and there is uncertainty regarding potential for undiscovered natural resources (CO2CRC, 2008).

CO_2 can be stored in depleted and oil and gas reservoirs. These types of storage are estimated to be between 675 and 900 Gt CO_2 worldwide, as shown in Table 2.2 (IPCC, 2005). CO_2 is also used in still producing oil and gas reservoirs to enhance oil or gas recovery (EOR/EGR) by miscible or immiscible flooding, therefore providing an economic benefit and storing CO_2 at the same time. Storing CO_2 in this way provides an advantage of proven potential containment by retention of hydrocarbon for millions of years. Geological and engineering data for detailed site characterisation are also widely available (Holloway & Savage, 1993; IPCC, 2005). However, possible disadvantages include limited potential storage capacity due to the physical size of the fields, potential leak point caused by the presence of existing oil wells and timing of availability of depleted fields with regards to source of CO_2 (CO2CRC, 2008).

CO_2 storage in coal seams is different from that of other geological formations due to its storage mechanism by adsorption process. Gaseous CO_2 is used in coal seams, instead of pumping liquid CO_2 in other geological formations, and injected into coal micropore surfaces resulting in displacement of the existing methane (CH_4) since coal has higher affinity to CO_2 than CH_4 (Gunter et al., 1997; Bradshaw & Rigg, 2011; IPCC, 2005). Because of the displacement of CH_4 and its higher greenhouse radiative effect than CO_2, CO_2 storage in coal seams is done in conjunction with enhanced coal bed methane recovery (ECBM). Challenges in

storing CO_2 in coal seams include feasibility of injecting CO_2 due to typically low permeability of the coal cleat system, especially with increasing depth. This may compromise the economic viability of ECBM caused by large number of wells that may need to be drilled to overcome injecting issues relating to low permeability. Subsequently, storing CO_2 in unmineable coal seams was deemed to have the smallest storage capacity, as shown in Table 2.2 (IPCC, 2005).

Table 2.2 CO_2 storage capacity estimates for different geological options worldwide (IPCC, 2005).

Reservoir type	Lower estimate of storage capacity (Gt CO_2)	Upper estimate of storage capacity (Gt CO_2)
Oil and gas fields	675*	900*
Unmineable coal seams (ECSM)	3 – 15	200
Deep saline formations	1000	Uncertain, but possibly 10^4

* These numbers would increase by 25% if "undiscovered" oil and gas fields were included in this assessment.

The total CO_2 storage capacity in the European countries was estimated to be approximately 360,000 Mt, with most of that capacity (326,000 Mt) in deep saline aquifers, 32,000 Mt in depleted hydrocarbon fields (EOR/EGR included) and 2000 Mt in unmineable coal (ECBM included) beds (GeoCapacity Consortium, 2009).

About 68% (244,000 Mt) of the total storage capacity is located offshore, while the remaining 32% (116,000 Mt) is onshore (GeoCapacity Consortium, 2009).

Table 2.3 shows the highest CO_2 storage capacity estimates amongst the European countries. Norway shows the highest CO_2 storage capacity in deep saline aquifers and depleted hydrocarbon fields with 29,188 Mt of total capacity. The decreasing order is then followed by Germany (17,080 Mt), United Kingdom (14,400 Mt), Spain (14,179 Mt) and Romania (9,000 Mt) as the top five European countries with the highest CO_2 storage capacity estimates. With the exception of United Kingdom, most of these countries have the largest estimated CO_2 storage capacity in deep saline formations than in depleted hydrocarbon fields.

Table 2.3 Selected CO_2 storage capacity estimates in metric tonnes (Mt) in European countries (GeoCapacity Consortium, 2009). Note that depleted hydrocarbon fields included EOR/EGR and unmineable coal fields included ECBM.

Country	CO_2 storage capacity (Mt)			Total
	Deep saline aquifers	Depleted hydrocarbon fields	Unmineable coal fields	
Norway	26031	3157	-	**29188**
Germany	14900	2180	-	**17080**
United Kingdom	7100	7300	-	**14400**
Spain	14000	34	145	**14179**
Romania	7500	1500	-	**9000**

2.2.1. *Costs of CCS*

The costs of CCS can be divided in to three components, namely capture (including separation and compression of captured CO_2), transport and storage (including measurement, monitoring and verification). The cost of capture dominates the cost of employing full CCS system for electricity generation from fossil-fired power plants. High cost of capture comprises the cost of separating captured CO_2 and compressing it to a high pressure suitable for pipelines, the most common and usually the most economical way to transport CO_2. Compression process of any gas, including CO_2, is a notably energy-consuming process which contributes to high cost of capture (Herzog, 2011).

Table 2.4 shows an estimation of additional electricity cost after CCS employment by CCS components. The cost of capture technology in a pulverised coal-fired (PC) power plant would add approximately 1.8 to 3.4 US$ct/kWh to the cost of electricity without CO_2 capture, 0.9 to 2.2 US$ct/kWh for an integrated gasification combined cycle (IGCC) power plant and 1.2 to 2.4 US$ct/kWh for a natural gas combined cycle (NGCC) power plant. The negative costs shown in the table are coupled with assumed offset revenues from CO_2 storage in EOR or ECSM projects (IPCC, 2005).

Table 2.4 Estimation of additional electricity cost after CCS employment by CCS components (IPCC, 2005)

CCS components	Power plant system	Additional electricity cost after CCS employment (US$ct/kWh)
Capture	PC	1.8 – 3.4
	IGCC	0.9 – 2.2
	NGCC	1.2 – 2.4
Transport and storage	PC	-1 – 1
	IGCC	-0.5 – 0.5
	NGCC	-0.5 – 0.5

Costs of CCS per tonne of CO_2 vary widely according to CO_2 sources, as shown in Table 2.5. CO_2 capture presents the highest costs of the whole CCS chain. CO_2 capture cost for fossil fuel-fired power plants range from 15 to 75 US$/t$CO_2$ captured, while hydrogen and ammonia production as well as gas processing plants range from 5 to 55 US$/t$CO_2$ captured. Other industrial activities capture cost range from 25 to 115 US$/t$CO_2$ captured, which require the highest cost to employ capture technology among other major CO_2 sources. CO_2 transport require the lowest cost of the entire CCS system with cost range between 1 and 8 US$/t$CO_2$ transported. The cost for geological storage of CO_2 is generally small with the exception of mineral carbonation which range between 50 and 100 US$/t$CO_2$ mineralised. These figures were estimated based on assumptions that natural gas prices between 2.8 and 4.4 US$/GJ and coal prices range from 1 to 1.5 US$/GJ (IPCC, 2005).

The cost of capture could be lower by 20 to 30% over the next decade, along with the costs of transport and storage as a result of technology maturity (IPCC, 2005; DECC, 2012). In the meantime, the UK Department of Energy and Climate Change (DECC) outlined drivers for CCS cost reduction (DECC, 2012). The drivers are chosen based on a report by Rubin et al. on "Prospect for improved carbon capture technology" in 2010 which include; 1) technology enhancement in process design and materials; 2) optimisation of construction logistics; 3) economies of scale which justify larger scale units would typically results in reduced costs per unit of capacity; 4) design margins reduction; 5) product standardisation; 6) increased competition; 7) reduction in key input price such as construction labour and services, materials and components; and 8) system integration and optimisation in terms of thermodynamic efficiency and design optimisation (Rubin et al., 2010; DECC, 2012).

Table 2.5 CCS cost range for industrial activities by CCS components (IPCC, 2005).

CCS components	Cost range
Capture	
• Fossil fuel-fired power plants	15 – 75 US$/$tCO_2$ captured
• Hydrogen and ammonia production/gas processing plants	5 – 55 US$/$tCO_2$ captured
• Other industrial sources	25 – 115 US$/$tCO_2$ captured
Transport	1 – 8 US$/$tCO_2$ transported
Geological storage	0.5 – 8 US$/$tCO_2$ stored
• Monitoring and verification	0.1 – 0.3 US$/$tCO_2$ stored
• Ocean storage	5 – 30 US$/$tCO_2$ stored
• Mineral carbonation	50 – 100 US$/$tCO_2$ mineralised

2.2.2. *Current CCS demonstration projects worldwide*

As of 2013, the Global CCS Institute (GCCSI) has identified 65 active large-scale integrated projects (LSIP) worldwide (GCCSI, 2013b). LSIPs are defined as projects that involve all CCS components at a scale of at least 0.8 $MtCO_2$/yr for a coal-based power plant or 0.4 $MtCO_2$/yr for other emission-intensive facilities. There were 20 LSIPs operating or under construction stage with total CO_2 capture capacity of more than 37 $MtCO_2$/yr and 44 LSIPs in planning stages of development with potential capture capacity of approximately 78.5 $MtCO_2$/yr.

In comparison with previous years, the total number of LSIPs that were in planning stage in 2013 of 45 has decreased from 59 in 2010, as shown in Figure 2.8. However, the opposite trend can be observed in the total number of LSIPs in operating or under construction stages of development where 12 were in active stages in 2010 increased to 22 in 2013, with additional 4 operating LSIPs in 2013. The contrary trend is due to some of the planned LSIPs in earlier years have positively passed the financial investment decision (FID), as well as execution phase and commenced the consecutive active stages of development.

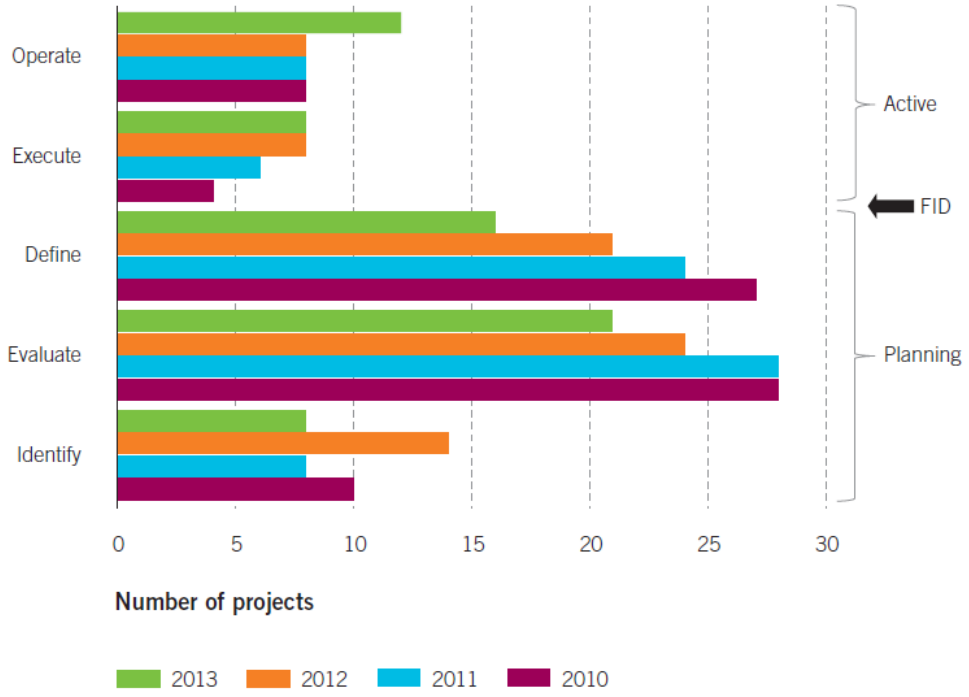

Figure 2.8 Annual comparisons of LSIPs at different stages of development (GCCSI, 2013b)

Despite the increasing number of total LSIPs entering the operating stage in 2013, the total potential mass of CO_2 captured and stored in all stages of development

have decreased over the years beginning in 2010 from 162 $MtCO_2$ to 140 $MtCO_2$, as shown in Figure 2.9 (GCCSI, 2013b). This is due to the change of status of LSIPs to either being cancelled or put on-hold. On the other hand, the volumes of CO_2 captured and stored have increased since 2010 from 12 $MtCO_2$/yr to 17.18 $MtCO_2$/yr in 2013. These values correspond with total volume of CO_2 captured and stored by eleven operating LSIPs around the world, as shown in Table 2.6. The operating LSIPs are dominated by developed nations, particularly in North America and Europe. Technology-wise, most of the operating LSIPs are applying pre-combustion capture and transporting the CO_2 via pipelines with the exception of two direct injection projects, namely, Sleipner CO_2 Injection project in Norway and Petrobras Lula Oil Field CCS Project in Brazil. Two apparent storage types used are deep saline formations and enhanced oil recovery (EOR).

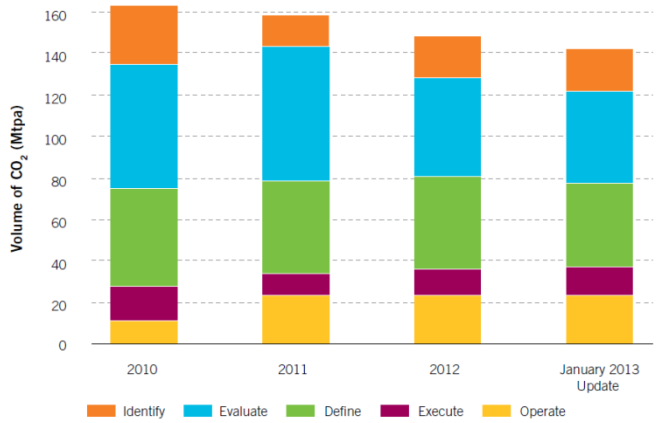

Figure 2.9 Annual comparisons of mass of CO_2 captured and stored from 2010 until 2013 (GSSCI, 2013b)

Table 2.6 Operating LSIPs worldwide (GCCSI, 2014).

Project Name	Volume CO_2 ($MtCO_2$/yr)	Capture Type	Transport Type	Storage Type	Operation Year	Country
Val Verde Natural Gas Plants	1.3	Pre-Combustion	Pipeline	Enhanced Oil Recovery	1972	United States
Enid Fertilizer CO_2-EOR Project	0.68	Pre-Combustion	Pipeline	Enhanced Oil Recovery	1982	United States
Shute Creek Gas Processing Facility	7	Pre-Combustion	Pipeline	Enhanced Oil Recovery	1986	United States
Sleipner CO_2 Injection	1	Pre-Combustion	Direct injection	Offshore Deep Saline Formations	1996	Norway
Great Plains Synfuel Plant and Weyburn-Midale Project	3	Pre-Combustion	Pipeline	Enhanced Oil Recovery	2000	Canada
In Salah CO_2 Storage	1*	Pre-Combustion	Pipeline	Onshore Deep Saline Formations	2004	Algeria
Snøhvit CO_2 Injection	0.7	Pre-Combustion	Pipeline	Offshore Deep Saline Formations	2008	Norway
Century Plant	8.4	Pre-Combustion	Pipeline	Enhanced Oil Recovery	2010	United States
Air Products Steam Methane Reformer EOR Project	1.0	Pre-Combustion	Pipeline	Enhanced oil recovery	2013	United States
Coffeyville Gasification Plant	1.0	Industrial separation	Pipeline	Enhanced oil recovery	2013	United states
Lost Cabin Gas Plant	0.8-1.0	Pre-combustion	Pipeline	Enhanced oil recovery	2013	United States
Petrobras Lula Oil Field CCS Project	0.7	Pre-combustion	Direct injection	Enhanced oil recovery	2013	Brazil

* Injection suspended, future injection strategy under review (GCCSI, 2014).

2.3. CO_2 capture

There are mainly three sources to capture CO_2 from, namely at i) stationary large point sources such as fossil fuel power generation plants, fuel and industrial processing plants; 2) smaller and mobile sources in the transportation, residential and building sectors and; 3) ambient air. However, the concentration of CO_2 in these sources determines the feasibility of capturing CO_2 since higher concentration would provide greater driving force in separating the gases. The highest CO_2 concentration is found in stationary large point sources mentioned earlier and could provide the most feasible profile of technologies. Lower CO_2 concentrations found in small and mobile sources as well as in ambient air would increase the complexity of the separation process and the associated costs required to manufacture such technology (IPCC, 2005).

The capture of CO_2 can be accomplished by three different routes, namely post-combustion, pre-combustion and oxy-combustion, as shown in Figure 2.10 (Figueroa et al., 2008). Post-combustion separates CO_2 from flue gases and can occur anywhere along the product processing stream from combustor to effluent exhaust, where the CO_2 concentration in flue gases is normally between 3 to 15 vol%. The pre-combustion route involves CO_2 capture after the gasification process and prior to the combustion step (IPCC, 2001). The most common configuration involves gasification with air or oxygen. The products undergo a water-gas shift to a high-concentration stream of CO_2 and H_2. The CO_2 is then captured and the H_2 is reacted with air. Finally, in oxy-combustion, pure oxygen substitutes air as

combustion gas producing a stream concentrated with CO_2 and H_2O (GCEP, 2005). However, partial oxygen concentration is also possible to be used in practice due to low resistance of boiler material against high temperature associated with combustion using pure oxygen (Li et al., 2013).

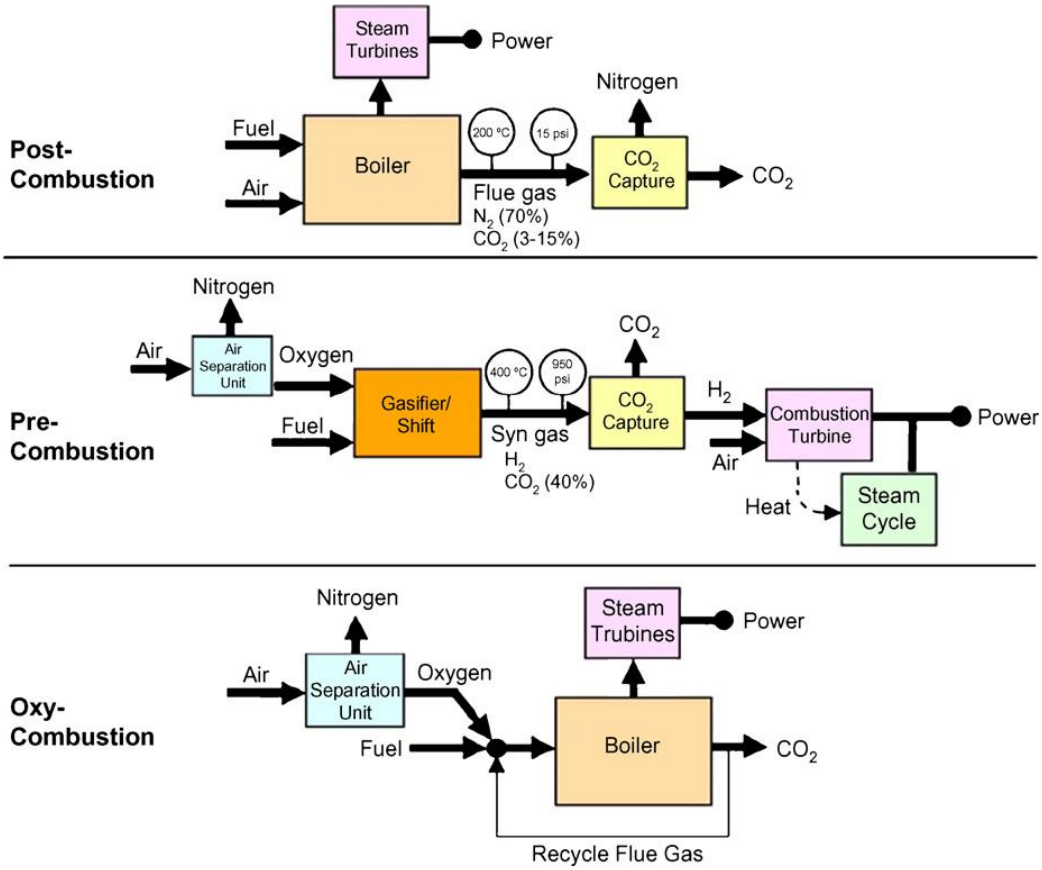

Figure 2.10 Block diagrams illustrating post-combustion, pre-combustion, and oxy-combustion systems (Figueroa et al., 2008)

There are several technology options for CO_2 capture that are being researched including liquid absorption, solid absorption, cryogenics, membranes,

microbial/algal systems and adsorption, as shown in Figure 2.11 (Rao and Rubin, 2002). Under these categories, there are more specific methods like chemical and physical liquid absorption processes, adsorber beds and regeneration solid adsorption methods, as well as gas separation/absorption and ceramic based systems for membranes.

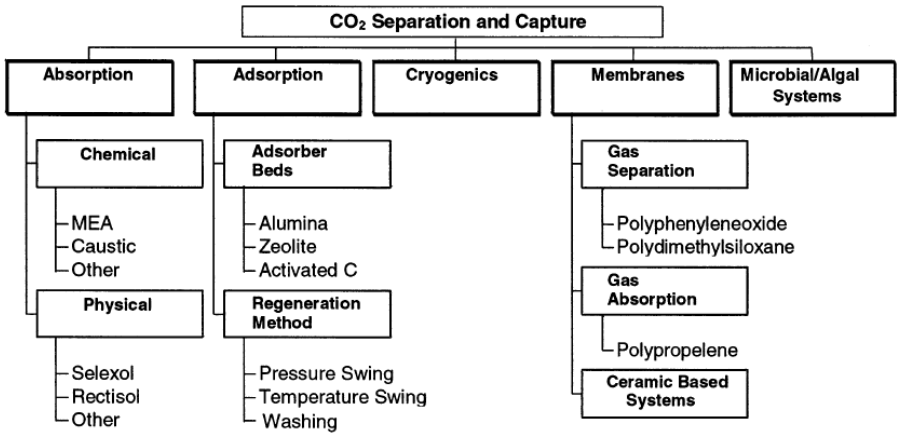

Figure 2.11 Technology options for CO_2 separation and capture (Rao & Rubin, 2002)

Both absorption and adsorption can be divided into two types of processes i.e. physical and chemical. Physical sorption process, also known as physisorption, uses sorbents to trap as much CO_2 molecules as possible by intermolecular forces, without any chemical reaction assisting the process (IUPAC, 1997). This process occurs at low to medium sorption temperatures ranging from 25 °C to 100 °C. Chemical sorption process, or chemisorption, utilises strong chemical bonds between sorbents and CO_2 molecules with the help of high sorption temperatures, usually ranging from 500 °C to 700 °C. Chemical reactions that occur generate strong chemical bonds on the surface of adsorbent that bind the CO_2 molecules.

However, both processes can occur in parallel or alternately at some point in the sorption process.

In cryogenic separation, CO_2 is separated from the flue gas stream by condensation which at atmospheric pressure, CO_2 condenses at −56.6 °C. Taking refrigeration costs into consideration, this kind of separation process is most effective in gas streams with high CO_2 concentrations (Wang et al., 2011). Membranes separate CO_2 from gas mixture stream based on the relative rates at which constituent species permeates. Membranes usually are made of polymeric films of which permeation rates would differ based on the relative sizes of the molecules or diffusion coefficients in the membrane material. The difference in partial pressure of the gases at either side of the membrane is the driving force of the separation process. Microbial/algae are microscopic organisms that usually grow suspended in water and feed on CO_2 to produce O_2, much the same as in photosynthetic process adopted by plants. However, factors like availability of light, pH, O_2 removal, suitable design of the photobioreactor, culture density and proper agitation of the reactor that will affect the process significantly (Kumar et al., 2011).

2.3.1. *CO_2 sorption by solid sorbents*

Solid sorbents have become an increasing popular area of research, although liquid sorbents are considered as the more mature CO_2 capture technology, going back to the capture of CO_2 for enhanced oil recovery (EOR) operations in the 1970s (Rao

and Rubin, 2002). However, liquid solvents like monoethanolamine (MEA), diethanolamine (DEA) and methyldiethanolamine (MDEA) have been found to have problems of scale and performance stability (Munoz et al., 2009). Furthermore, liquid sorbents are prone to degradation and oxidation resulting in products that are corrosive and may require hazardous material handling procedures (Islam et al., 2011).

These problems can be resolved using solid sorbents. Additionally, the energy required for regeneration and moving liquid solvents is reduced by more than 30% with solid sorbents, if high (more than 132 g CO_2/kg sorbent) CO_2 uptake capacity of the sorbent is achieved (Gray et al., 2008). Furthermore, solid sorbents produce no liquid wastes and offer much wider temperature range applications between 25 and 700 °C (Choi et al., 2009; Olivares-Marin & Maroto-Valer, 2012). Because of these reasons, CO_2 adsorption on solid sorbents has become an increasingly interesting option for many industries for various benefits. The following section discusses CO_2 capture at high (over 400 ^{0}C) sorption temperatures, where chemisorption is the dominant sorption process (Wang et al., 2011).

2.3.2. *CO_2 capture by lithium-based sorbents*

In recent years, Li_4SiO_4 has been developed as a potential solid sorbent for CO_2 capture due to its high CO_2 capacity and sorption kinetics, especially at high sorption temperatures. Li_4SiO_4 reacts with CO_2 to produce lithium carbonate (Li_2CO_3) and silicon dioxide (SiO_2), as shown in equation (2.1), with a theoretical

maximum uptake capacity of 735 mg CO_2/g. However, practically, reaction products i.e. Li_2SiO_3, restrict the sorption process. Therefore, the reaction advances according to equation (2.2) instead, which yields the limited CO_2 adsorption of 367 mg CO_2/g sorbent (Yamaguchi et al., 2007).

$$Li_4SiO_4 + 2CO_2 \rightarrow 2Li_2CO_3 + SiO_2 \quad (2.1)$$

$$Li_4SiO_4 + CO_2 \rightarrow Li_2CO_3 + Li_2SiO_3 \quad (2.2)$$

There are a number of studies on pure Li_4SiO_4 sorbents for CO_2 capture at high temperatures (Essaki et al., 2005; Kato et al., 2005; Yamaguchi et al., 2007). Essaki et al. (2005) revealed most CO_2 uptake occurred at 500 ^{0}C (220 mg CO_2/g sorbent) for CO_2 concentration of 5 vol% and 600 ^{0}C for 10 vol% (220 mg CO_2/g sorbent) and 15 vol% (270 mg CO_2/g sorbent) of CO_2. During later parts of their study, an attempt was made to express the variation in sorption with temperature more clearly by evaluating using a wider temperature range from 400 to 700 ^{0}C with a smaller temperature interval for every 50 ^{0}C for only 10 vol% of CO_2. These results agreed with the first study, which showed the fastest and highest uptake at 600 ^{0}C with the same amount of CO_2 uptake. This showed that CO_2 sorption by Li_4SiO_4 is strongly affected by the sorption temperature and the initial rate-determining step changed depending on the CO_2 concentration.

Kato et al. (2005) investigated CO_2 capture using lithium-containing oxides, including Li_4SiO_4 and Li_2ZrO_3. Cylindrical Li_4SiO_4 pellet type sample with added

lithium zirconate (Li_2ZrO_3) was placed in a packed bed reactor before subjected to CO_2 flow. Li_2ZrO_3 was added to suppress degradation of the absorption capacity during regeneration cycle as well as to control grain growth in order to maintain high surface area.

The samples were firstly subjected to pure CO_2 flow at 700 ^{0}C in order to examine the pure reaction between Li_4SiO_4 as well as Li_2ZrO_3 and CO_2. It was found that the reaction between Li_4SiO_4 and CO_2 was 50% larger (350 mg CO_2/g) and reached equilibrium much faster than the reaction between Li_2ZrO_3 and CO_2. They then studied the adsorption process at 500 ^{0}C under 20% CO_2 flow, and found that CO_2 uptake was also about 50% greater (250 mg CO_2/g) than that of Li_2ZrO_3 (150 mg CO_2/g). The same adsorption temperature was then experimented on 2% CO_2 flow, and the result showed that there were still significant amount of CO_2 adsorbed by Li_4SiO_4 (250 mg CO_2/g), whereas Li_2ZrO_3 showed no clear CO_2 uptake.

Cyclic tests were conducted using 20% CO_2 gas flow at a rate of 300 ml/min at 600 ^{0}C for adsorption and followed by 800 ^{0}C for regeneration for 1 hour for each process. The tests were repeated 1, 10, 20 and 50 times. Also, 2 mass% and 5 mass% of Li_2ZrO_3 was added to the samples. The results showed initial sorption rate of 280 mg CO_2/g per hour and decreasing with the increment of time and number of cycles, which is an expected pattern. Different amounts of Li_2ZrO_3 addition also played an important role to the regeneration cycles. It was found that the 5 mass% addition of Li_2ZrO_3 improved the most on the reproducibility of

CO_2 sorption/desorption, by maintaining the sorption rate of more than 90% even after 50 cycles.

Yamaguchi et al. (2007) discussed CO_2 separation using Li_4SiO_4-based powder and membrane sorbents. Firstly, CO_2 uptake on Li_4SiO_4 powder samples was investigated. The samples were heat-treated at 700 and 1000 ^{0}C. Then, sorption tests on powder samples were conducted at 700 ^{0}C under pure CO_2 flow. The results showed that the sample heat-treated at 700 ^{0}C had faster sorption rate and more CO_2 uptake (330 mg CO_2/g within 2 minutes) than the one that was heat-treated at 1000 ^{0}C.

A membrane was then produced using the synthesised Li_4SiO_4 powder. The results proved CO_2/N_2 selectivity between 4 and 6 in the temperature range of 525 – 625 ^{0}C. According to the authors, CO_2 transport mechanism through the membrane was possibly assisted by carrier transport of CO_3^{2-} and O^{2-} by the Li_2CO_3 and Li_2SiO_3 electrolytes. Although this experiment was conducted under pure CO_2 flow which most probably be the reason of high sorption rate compared to previous studies, this clearly showed the great potential for Li_4SiO_4 to be used as solid sorbent for carbon capture compared to other lithium-based, for example Li_2ZrO_3.

Despite various studies on pure Li_4SiO_4 sorbents, there are only two published studies on the development of Li_4SiO_4 sorbents derived from low-cost precursors, as shown in Table 2.7. The highest CO_2 capacity was 324 mg CO_2/g sorbent by sorbent derived from rice husk ash (Wang et al., 2011), while the fly ash derived

Li_4SiO_4 sorbents were able to capture about 20 mg CO_2/g sorbent (Olivares-Marin et al., 2010). In terms of regenerability of both rice husk and fly ash derived sorbents, the CO_2 uptake capacities remained almost unchanged even after 10 cycles.

Table 2.7 Li_4SiO_4-based sorbents using low-cost precursors for CO_2 adsorption at high sorption temperatures (modified from Olivares-Marin & Maroto-Valer, 2012)

Feedstock	Synthesis conditions	Modifications	Maximum CO_2 capacity	Regenerability	References
Fly ash (Coal by-product)	Solid state calcination with Li_2CO_3 at 950 °C for 8h	K_2CO_3 addition.	Up to 107 mg CO_2/g sorbent at 600 °C	Sorbents can maintain their sorption capacities after 10 cycles	Olivares-Marin et al. (2010)
Rice husk ash (Biomass by-product)	Solid state calcination with Li_2CO_3 at 800 °C for 4h	Not evaluated.	Up to 324 mg CO_2/g sorbent at 700 °C	CO_2 uptake in samples remained almost unchanged even after 15 cycles.	Wang et al. (2011)

2.4. Solid wastes from power generating plants

Coal fly ash, or better known as pulverised fuel ash (PFA) in the UK, is a by-product of combustion process at temperature range between 1200 and 1700 °C in coal-fired boilers in power generation plants. The by-product indicates the presence of various refractory mineral matters in the feed coal and some components of the

fuel (Sear, 2001). Fly ash consists of fine particles and usually captured by electrostatic precipitators or other types of particle filtration equipment. Depending on the origin of the coal used in the combustion process, the characteristics of the resulting fly ash vary considerably, although unburned carbon, silica (SiO_2), alumina (Al_2O_3) and calcium oxide (CaO) are commonly found in fly ash.

Blissette and Rowson (2012) estimated that world annual production of fly ash is approximately 750 million tonnes and is expected to increase. Currently, a mere 25% of total fly ash produced is being utilised worldwide with most of the remaining ended up in landfills by storing it in huge fly ash lagoons or dumped into the sea (Wang, 2008). Disposing fly ash in this manner can create major environmental concerns due to the potential leaching of metals and organic compounds and their migration into groundwater or nearby surface water (Blisette and Rowson, 2012). Furthermore, fly ash lagoons have been known to breach and affect human health through direct inhalation of particulates from fly ash. Consequently, it has caused substantial distress to the local community (Wang, 2008).

Amongst 25% of the utilised portion, fly ash is popularly used in the cement industry for their low loss-on-ignition (LOI) value which makes it suitable for cement production under the ASTM C618 specification. However, the modification to low-NOx burners (LNB) have significantly increase the values of LOI in resulting fly ash, making it a less desirable choice in the cement industry (Srivastava et al.,

2005). This reduces the percentage of fly ash being utilised, increases the amount of fly ash being disposed of and consequently leads to a strong need to explore other possibilities of utilising fly ash. One way of doing this is to use fly ash a precursor in the development of CO_2 sorbents.

Another type of solid waste from power generation plants includes oil palm ash, or also known as palm oil mill boiler ash (POMBA). POMBA is a by-product of combustion process in biomass-fired boilers in palm oil mills for self-sustained energy in the mill. The biomass includes the fibres and shells of oil palm, which are the residue of palm oil extraction. Silica (SiO_2), alumina (Al_2O_3), iron oxide (Fe_2O_3) and calcium oxide (CaO) are among compounds commonly found in POMBA. Although, the varieties of proportion of irrigated area, geographical conditions, fertilizers used, climatic variation, soil chemistry, timeliness of production and agronomic practices in the oil palm growth process affect the chemical composition of POMBA greatly (Foo & Hameed, 2009).

The production of POMBA is heavily concentrated in Southeast Asia as many countries in this region are big exporters of palm oil, such as Malaysia. Malaysia is currently the world's largest palm oil producing country and there are 426 operating palm oil mills present in this country in 2011 with POMBA production rate of more than 4 million tonnes per year (MPOB, 2011; Mohamed et al., 2005). This figure is predicted to escalate due to the rapid increase in worldwide demand of palm oil which in turn, increasing the amount of POMBA generated by palm oil mills (Chong et al., 2009). Current ash disposal cost, either in landfills or ash

ponds, at $5 per tonne in developing countries and $50 per tonne in developed countries have further accentuated the urgency of transforming the residue into a more valuable end product (Foo & Hameed, 2009).

2.4.1. *Use of solid wastes for development of CO_2 sorbents*

Development of sorbents for CO_2 capture from waste materials has been widely investigated and a review has been recently published by Olivares-Marin and Maroto-Valer (2012). Solid sorbents of wide range of sorption temperatures were developed according to physical and chemical characteristics of waste materials. For example, carbonaceous waste materials were used as precursors of carbon-based sorbents for CO_2 capture at low temperature range between 25 and 75 °C. Wastes containing high amounts of silica and alumina such as fly ashes were converted into zeolite-based materials, mesoporous silica-based materials and lithium-based sorbents for capture at medium (70 – 100 °C) and high (100 – 750 °C) temperatures, subject to the specific precursor and the route of synthesis and surface modifications.

In this section, only the development of Li_4SiO_4 sorbents deriving from solid waste materials from power generating plant is discussed. Olivares-Marin et al. (2010) studied CO_2 capture using lithium-based sorbents from fly ashes at high temperatures ranging from 450^{O}C to 700^{O}C. The lithium-based (Li_4SiO_4) sorbents were prepared by subjecting three different sources of fly ash samples which contain between 24 to 27 wt% content of silica to calcination process at 950^{O}C in

the presence of lithium carbonate (Li_2CO_3). For reference purposes, pure lithium silicate, indicated by P-Li_4SiO_4 was also synthesised and used in this work. Potassium carbonate (K_2CO_3) was also added to the sorbents as it has been reported to improve sorption capacity, as K_2CO_3 is believed to form eutectic melt during CO_2 sorption on Li_4SiO_4. The molten carbonate shell significantly increased the diffusivity of CO_2 molecules through the Li_2CO_3 shell to the bulk of Li_4SiO_4 particle, and therefore, increasing the CO_2 uptake capacity of the sorbents.

According to their findings, the sorption temperature also strongly affected the CO_2 sorption capacity for the sorbents prepared from fly ashes. When the sorption temperature rises up to 600^0C, the sorption capacity increased. The capture capacity also increased with increased amount of K_2CO_3 added to the fly ash sorbent, but not the P-Li_4SiO_4. At experimental conditions of 600^0C and addition of 40 mol% of K_2CO_3, the maximum CO_2 sorption capacity for the lithium-based sorbent was 107 mg CO_2/g.

In order to study the sorbents performance, multiple CO_2 sorption/desorption cycles were carried out. Results showed that the Li_4SiO_4-based fly ash sorbent can maintain its original capacity during 10 cycle processes and reached equilibrium capture capacity within 15 minutes, while P-Li_4SiO_4 demonstrated a continual upward tendency for the 15 minute of the capture step and attained no equilibrium capacity during the experiment time. This is because the P-Li_4SiO_4 with 20 mol% K_2CO_3 addition has maximum capacity of 244 mg CO_2/g, thus, will

show continual upward tendency for the 15 minute of the capture step until it has captured the maximum capacity of 244 mg CO_2/g.

To the best of the author's knowledge, this is the only study that has been published on the development of Li_4SiO_4-based sorbents using solid waste materials from power generating plants. Thus, this research is aimed to further explore the development of Li_4SiO_4 and sorbent derived from low-cost precursors, including the effects of different waste materials, preparation methods, sorption temperature, CO_2 concentration and regeneration of sorbents.

Chapter 3 Experimental methodology

This chapter describes the parent waste materials and methodology used in the experimental studies. The experimental work is divided into three main tasks, namely, procurement and characterisation of parent waste materials, preparation and characterisation of sorbents and CO_2 capture by developed sorbents. Figure 3.1 shows the flowchart for this study. In the first task, waste materials were selected based on their chemical compositions i.e. high silica (SiO_2) content and subjected to characterisation analyses including particle size distribution and XRD analyses, to name a few.

Then, sorbents were developed via dry or wet chemical impregnation methods. Developed sorbents were also characterised using a variety of analyses such as particle size distribution and x-ray diffraction analyses. Finally, the prepared sorbents were used to capture CO_2 in varying sorption conditions, for example, CO_2 concentrations and sorption temperatures. Regeneration performance of the developed sorbents was also investigated.

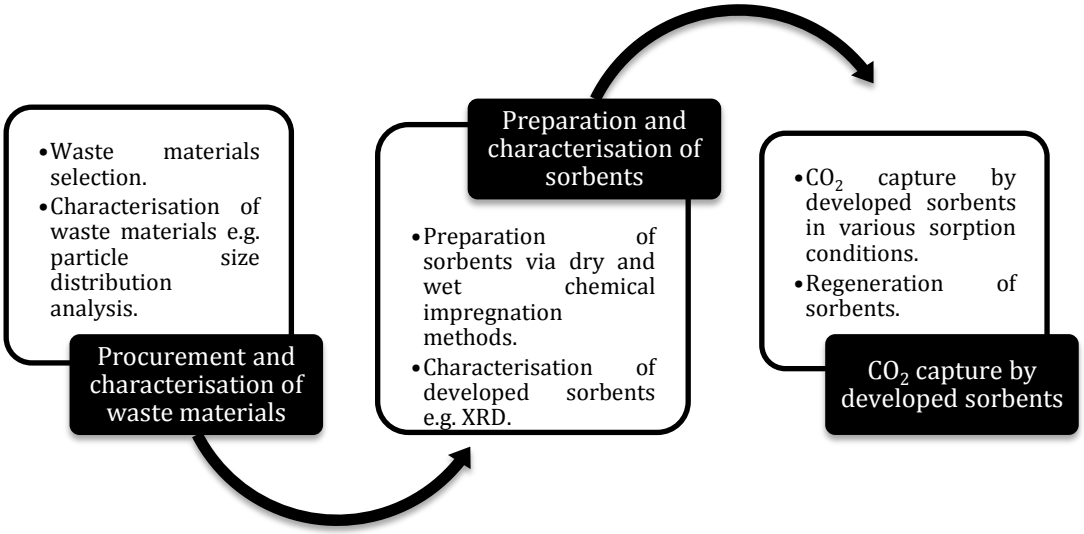

Figure 3.1 Experimental work flowchart

Sorbents were developed from waste materials including fly and bottom ashes collected from a number of coal-fired power plants and a palm oil mill boiler, as detailed in the following Section 3.1. Lithium- and sodium-based high temperature sorbents from high SiO_2 content ashes were developed using dry and wet synthesis methods, namely solid state (SS) and suspended impregnation (SI), which will be detailed in subsequent sections.

3.1. Procurement and characterisation of waste materials

3.1.1. *Waste materials procurement*

A preliminary selection of waste materials which were readily available in sample stock was chosen for chemical composition analysis. This step was conducted to categorise the amount of SiO_2 content in every sample tested. Subsequently,

samples with the highest amount of SiO_2 content were chosen to proceed with further characterisation analyses e.g. particle size distribution analysis and surface area analysis. Table 3.1 shows the waste materials used in this study including two pulverised fuel ash samples (C- and R-PFA) and two bottom ash samples, namely furnace bottom ash (FBA) and palm oil mill boiler ash (POMBA). The feedstock and nomenclatures of every sample are also presented in Table 3.1.

Table 3.1 Waste materials used in this study.

Sample Name	Feedstock	Nomenclature
Pulverised Fuel Ash	Coal	C-PFA R-PFA
Furnace Bottom Ash	Coal	FBA
Palm Oil Mill Boiler Ash	Oil Palm	POMBA

3.1.2. *Characterisation of waste materials*

Following the procurement of waste materials, characterisation analyses were carried out. This included particle size distribution analysis using laser diffraction, x-ray fluorescent analysis for chemical composition determination, nitrogen adsorption/desorption for pore size and surface area analysis, as well as x-ray diffraction analysis for mineralogical study. These characterisation analyses are discussed in subsequent subsections.

It should be noted that the chemical impregnation preparation of all waste-derived Li_4SiO_4 sorbents were carried out entirely by the author. The author appreciates the assistance of experimental officers for their support in operating some of the analytical instruments. These instruments include the 1050 XRD Philips Analytical with a Hilton Brooks 3 kW X-ray generator attachment (operated by Dr. Georgina Rosair at School of Engineering and Physical Sciences in Heriot-Watt University), PANalytical Axios-Advanced XRF spectrometer (operated by Mr. Nick Marsh at the Department of Geology in University of Leicester) and FEI Quanta SEM (operated by Mr. Mark Leonard at School of Engineering and Physical Sciences in Heriot-Watt University).

3.1.2.1. Particle size distribution analysis

3.1.2.1.1. Background of laser diffraction for particle size distribution analysis

Laser diffraction was used to analyse particle size distribution of the waste materials. It measures particle size distributions by calculating the angular variation in intensity of light scattered, collected by an array of detectors positioned perpendicular to the optical axis as a laser beam passes through a dispersed particulate sample (Richardson et al., 2002). Figure 3.2 shows the schematic of the optical system for a reverse Fourier lens arrangement laser diffraction with a liquid flow cell. A light source emits a laser through the beam expander. The expanded laser then passes through the flow cell sensing zone and scatters at an angle and intensity that are dependent on sizes of the particles in the zone. Smaller particles scatter light at relatively low intensity to wide angles, while

larger particles scatter more strongly at narrow angles. Next, high and low angle detectors capture scattered laser patterns accordingly and convert them into particle size distribution using an appropriate model of light behaviour.

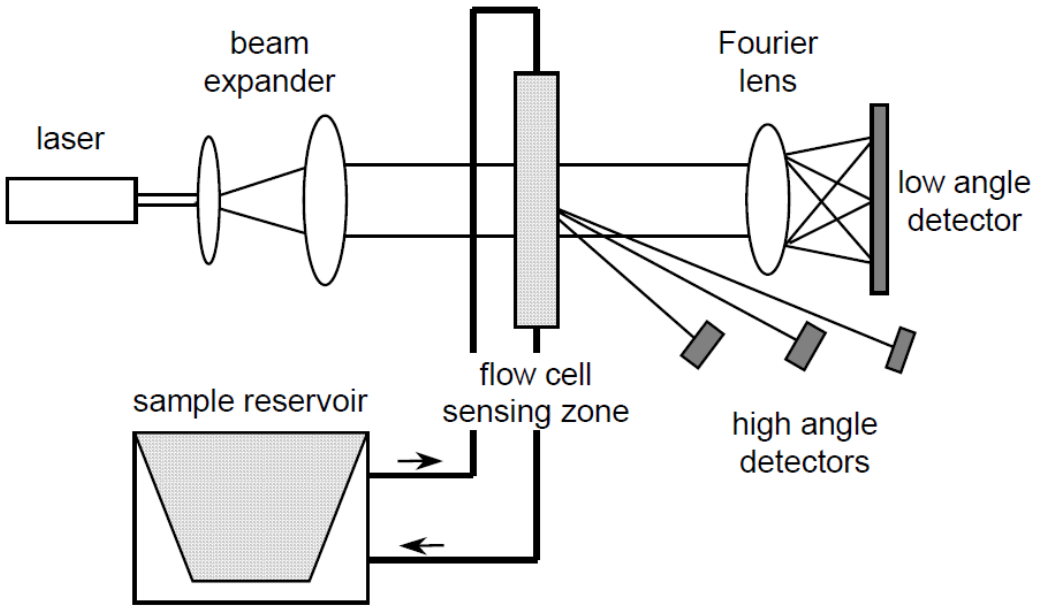

Figure 3.2 Schematic of the optical system for a typical laser diffraction analyser with a liquid flow cell (Hackley et al., 2004).

3.1.2.1.2. Experimental procedures of laser diffraction for particle size distribution analysis

Particle size analyses were conducted by the author using a Malvern Mastersizer 2000E producing a 4 mW He-Ne laser source of 632.8 nm in wavelength and attached to a Hydro 2000SM small volume manual sample dispersion unit. The Mastersizer 2000 software controlled the system for measurement and data

analysis. Particle size range for this instrument was between 0.1 and 1000 μm. Prior to analysis, the flow cell sensing zone was filled with 99.5% propanol as the dispersion medium for the samples via the dispersion unit and the machine was left for 10 to 20 minutes to allow thermal equilibrium to take place.

Propanol was used as the suspension medium due to its ability to suspend and disperse the studied waste materials. This is important to ensure the laser was diffracted by a singular particulate of waste material rather than an agglomeration of particles which would strongly affected the analysis outcome. The instrument then automatically aligned so that the incident path of the laser was in line with the optical arrays. The cleanliness of the system was checked and a background reading recorded. The sample was gradually added into the dispersion unit until ideal concentration was achieved which was approximately 1 g of sample per 1 litre of dispersion medium. The instrument collected and analysed the scattering data to calculate a particle size distribution. The analysis was carried out in triplicates and the error calculated was 1.05%.

3.1.2.2. X-ray Diffraction (XRD) analysis

3.1.2.2.1. Background of XRD analysis

XRD is a non-destructive and versatile technique used to obtained information about the crystallographic structure of materials by comparing the analysed data against a wide set of database. The schematic of an XRD is illustrated in Figure 3.3

(Morris et al., 2012). A solid or powder sample is placed in the diffractometer and bombarded with X-rays generated by copper X-ray tube. The diffracted X-rays are then collected by a detector and send to a computer. The computer then converts them to digital data and produces the diffraction pattern of the sample. The computer also matches the pattern against a database using specialised identification software (Jenkins and Snyder, 1996).

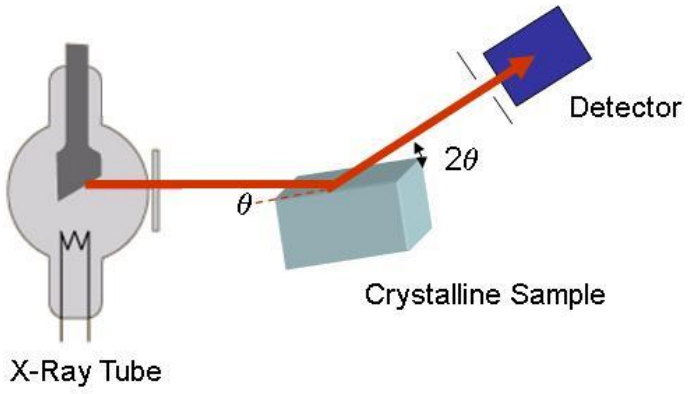

Figure 3.3 Schematic of an XRD (Morris et al., 2012).

3.1.2.2.2. Experimental procedures of XRD analysis

XRD analyses were carried out by the instrument operator in the School of Engineering and Physical Sciences in Heriot-Watt University using a 1050 XRD Philips Analytical attached to a 3 kW X-ray generator Hilton Brooks. The X-ray generator produced copper kα radiation with wavelength of 0.15418 nm. Samples were ground using an agate mortar and pestle to fine powder. About 500 mg of sample was packed into an aluminium holder and subsequently placed in a magazine. The analysis was conducted at angle range of 5 to 65^0 with continuous

scanning rate at 1.2^0/min. Diffraction patterns were analysed using EVA, a software package used for the qualification of crystalline compounds. The error range of XRD measurements was between 2 to 3%.

3.1.2.3. X-ray fluorescent (XRF) analysis

3.1.2.3.1. Background of XRF analysis

XRF is a non-destructive technique to qualitatively and quantitatively analyse elemental composition of a sample. Similar to XRD, X-ray is used in this analysis to irradiate on the sample. As a result of the irradiation step, x-ray fluorescence is generated which possess energy characteristic to each element in the sample. The x-ray fluorescence is then collected by a detector before converted into digital signals. The digital signal is then amplified to be analysed of its elemental composition using spectrometry analysis software. The schematic of an XRF is shown in Figure 3.4.

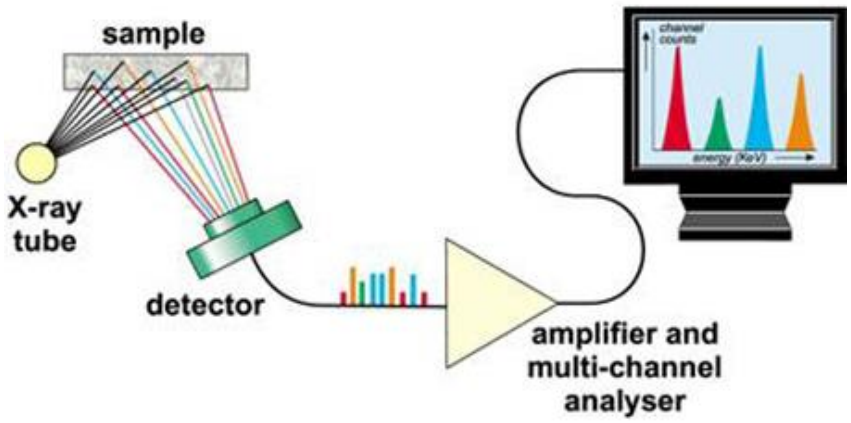

Figure 3.4 Schematic of an XRF (PANalytical, 2014)

3.1.2.3.2. Experimental procedures of XRF analysis

XRF analyses of waste materials were carried out to quantify the elemental composition and were performed by the instrument operator in the Department of Geology at University of Leicester using a PANalytical Axios-Advanced XRF spectrometer. Firstly, approximately 1 g of parent waste material was ground using agate mortar and pestle to fine powder. The fine powder was then ignited at 1100 °C and the subsequent ignited powder was mixed with lithium metaborate and lithium tetraborate flux. The mixture was fused at the same temperature in the furnace which was then used in the XRF spectrometer to determine their quantitative elemental composition in the form of oxides. The standard error for XRF analysis was 1.8% and the analysis was carried out in duplicates.

3.1.2.4. Scanning electron microscope (SEM) analysis

3.1.2.4.1. Background of SEM analysis

Scanning electron microscope (SEM) utilises electron beams to resolve a greatly magnified image of a sample. As shown in Figure 3.5, a SEM comprises basic parts of an electron gun, vacuum chamber containing anode plate, lenses, samples chamber and detectors. To enable control and viewing of the microscopic images generated, a computer is connected to the instrument. In the initial stage of scanning a sample using a SEM, a beam of electrons is first generated. This is done by the electron gun, usually of the thermionic type, is heated up by high voltage. When there is sufficient heat produced, electrons are emitted, resulting a strong

electric force between the electron gun and the anode plate in the vacuum chamber. This produces a beam of electrons which then follows a vertical path down the microscope column, then through the lenses and onto the sample in the sample chamber.

Upon impact with the electron beam, secondary electrons are displaced from the surface of the sample. A secondary electron detector collects the disseminated electrons to record levels of brightness of the sample's image. Backscatter and x-ray detectors gather electrons that reflected off (also known as backscattered electrons) and x-rays emitted from the surface of the sample, respectively, and subsequently producing an image on the computer monitor.

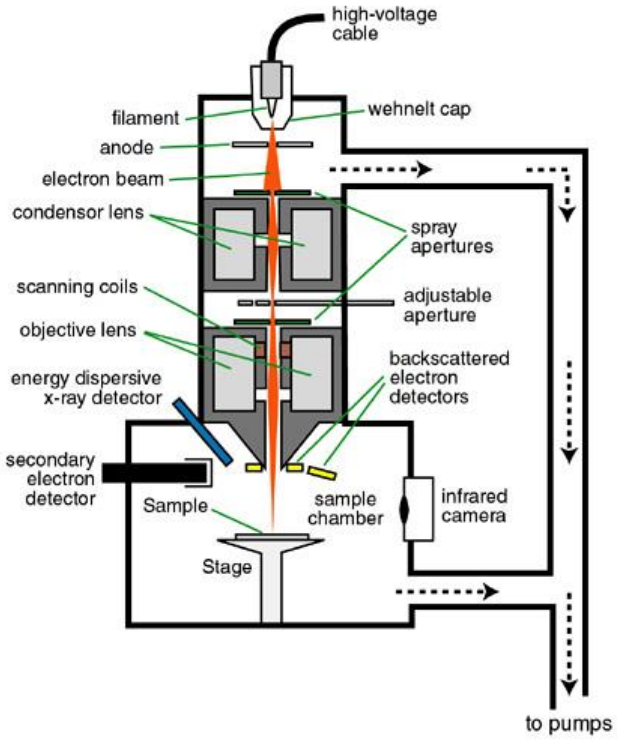

Figure 3.5 Schematic of a scanning electron microscope (Wittke, 2008)

3.1.2.4.2. Experimental procedures of SEM analysis

SEM analyses were performed by the author with the assistance from a technician in the School of Engineering and Physical Sciences using a FEI Quanta SEM. Firstly, an aluminium sample holder stub was prepared by attaching a double sticky carbon tape onto it. Then, the sample (about 3 mg) was evenly adhered to the carbon tape and any excess powder was tapped off to ensure no loose particles will be released inside the SEM chamber. The vacuum was then vented prior to the mounting of the sample onto the sample stage in the SEM chamber. It should be

noted that the controlling of the instrument, including the venting, was done via the instrument software on a computer.

After the sample was mounted onto the sample holder, the chamber door was manually closed and automatically fastened to prevent room air from entering the chamber. Next, air in the SEM chamber was pumped out until it achieved sufficient vacuum for the system to open the column valve and establish an electron beam via the filament. Following the initiation of electron beam, the sample stage was moved to inspection location, which was approximately 10 mm from the end of the column. The positioning of the sample stage was done on the computer and assisted by a video camera located inside the chamber, allowing real-time observation of the stage movement. Inspection of sample was then performed by moving the sample stage and capturing SEM images. Images were captured based on their surface characteristics and image magnification.

3.2. Preparation and characterisation of developed sorbents

3.2.1. Preparation of lithium-based CO_2 sorbents

Lithium-based CO_2 sorbents were developed into i.e. waste-derived Li_4SiO_4 and pure Li_4SiO_4 sorbents. The preparation methods of both types of sorbents are described in the following subsections.

3.2.1.1. Preparation of waste-derived Li_4SiO_4 sorbents

All waste materials were developed into Li_4SiO_4-based CO_2 sorbents via dry preparation method i.e. solid state (SS) impregnation. The sorbents were prepared by mixing Li_2CO_3 powder with the studied waste materials using a Fritsch Pulverisette 2 mortar grinder until the solid mixture achieved homogeneity. Homogeneity of the solid mixture was considered achieved when there was no visible difference in the colour of both solids. The mixing time varied (3 to 5 min) with the type of waste materials used e.g. finer particle size fly ash samples (C- and R-PFA) taking shorter time to achieve homogeneity compared to significantly larger particle size bottom ash samples (FBA and POMBA).

Stoichiometric amount of Li_2CO_3 was used according to equation 3.1, where 2 mol of Li_2CO_3 reacts with 1 mol of SiO_2 to yield 1 mol of Li_4SiO_4 and 2 mol of gaseous CO_2. It is worthy to note that all waste-derived Li_4SiO_4 sorbents were prepared with 0, 5, 10 and 20% excess lithium.

$$2Li_2CO_3(s) + SiO_2(s) \rightarrow Li_4SiO_4(s) + 2CO_2(g) \quad (3.1)$$

Hence, calculating the amount of Li_2CO_3 needed;

$$1\ mol\ of\ Li_2CO_3 = [(6.94 \times 2) + (12.01 \times 1) + (16 \times 3)]\ \frac{g}{mol}\ Li_2CO_3$$

$$1\ mol\ of\ Li_2CO_3 = 73.89\ \frac{g}{mol}\ Li_2CO_3$$

$$1\ mol\ of\ Li_2CO_3 = 73.89\ g\ Li_2CO_3$$

$$2\ mol\ of\ Li_2CO_3 = [73.89\ \times 2]\ g\ Li_2CO_3$$

$$\therefore 2\ mol\ of\ Li_2CO_3 = \underline{\underline{147.78\ g\ Li_2CO_3}}$$

Similarly, calculating the amount of SiO_2 needed;

$$1\ mol\ of\ SiO_2 = [(28.09 \times 1) + (16 \times 2)]\ \frac{g}{mol}\ SiO_2$$

$$1\ mol\ of\ SiO_2 = 60.09\ \frac{g}{mol}\ SiO_2$$

$$\therefore 1\ mol\ of\ SiO_2 = \underline{\underline{60.09\ g\ SiO_2}}$$

Due to the varied amount of SiO_2 content in parent waste materials, the amount of waste samples was calculated according to the amount of SiO_2 needed. For example, there was 49.81 wt% of SiO_2 found in RPFA. Hence, the amount of RPFA needed for a 0% excess Li is as follows;

$$Amount\ of\ RPFA\ needed = \frac{Amount\ of\ SiO_2\ needed}{Weight\ percentage\ of\ SiO_2\ content\ in\ RPFA}$$

$$= \frac{60.09\ g}{49.81} \times 100$$

$$\therefore Amount\ of\ RPFA\ needed = \underline{\underline{120.63\ g}}$$

The amount of excess lithium was calculated by adding 5, 10 and 20 wt% of Li_2CO_3. For example;

$$5\ wt\%\ excess\ of\ Li_2CO_3 = 147.78\ g\ Li_2CO_3 \times \frac{5}{100}$$

$$\therefore 5\ wt\%\ excess\ of\ Li_2CO_3 = \underline{\underline{7.39\ g\ Li_2CO_3}}$$

Thus, the total amount of Li_2CO_3 needed to calcine Li_4SiO_4 sorbent with 5% excess Li:

$$5\ wt\%\ excess\ of\ Li_2CO_3 = 14.78\ g\ + 0.74\ g = 15.52\ \text{g}\ Li_2CO_3$$

Due to the limited availability of waste materials, only 10% of the total calculated amount of parent waste materials, Li_2CO_3, SiO_2 and excess Li were used during preparation method, as summarised in Table 3.2.

Table 3.2 Amount of starting materials required for waste-derived Li_4SiO_4 sorbents preparation. The amounts of parent waste materials needed were calculated according to the amount of SiO_2 contents in each waste material. Fixed amounts of parent waste materials were mixed with varying amounts of Li_2CO_3, depending on excess lithium.

Starting materials	Amount of starting materials needed (g)			
	No excess	5% excess Li	10% excess Li	20% excess Li
Li_2CO_3				
0%	14.8	-	-	-
5%	-	15.5	-	-
10%	-	-	16.3	-
20%	-	-	-	17.7
SiO_2 sources				
Pure SiO_2	6.01	6.01	6.01	6.01
CPFA (55.3% SiO_2)	10.9	10.9	10.9	10.9
RPFA (49.8% SiO_2)	12.1	12.1	12.1	12.1
FBA (47.8% SiO_2)	12.6	12.6	12.6	12.6
POMBA (66.3% SiO_2)	9.06	9.06	9.06	9.06

The mixed powder was weighed (5 g) then calcined in an alumina crucible in a muffle furnace at 800 °C in air for 8 h. During this stage, the SiO_2 component of the waste materials reacted with Li_2CO_3, yielding Li_4SiO_4-based sorbents (Olivares-Marin et al., 2010). After calcination, the resulting products were homogenised using the same grinder. Subsequently, the waste-derived Li_4SiO_4 sorbents were analysed of their CO_2 uptake capacity using procedures as described in Section 3.2.3. Different amounts of excess lithium (5, 10 and 20 wt%) were added to the samples due to the high tendency of lithium to sublimate (Pfeifer and Knowles, 2004; Avalos-Rendon et al., 2010). These amounts of excess lithium were chosen

so that there are sufficiently excess amount of lithium, without significantly exceeding the stoichiometric ratio, as this would produce a completely different substance following the heat treatment.

Following the solid state impregnation method, the effect of different sorbent preparation methods was also investigated. However, only POMBA was used for this purpose due to the highest CO_2 uptake by its corresponding SS-B-Li_4SiO_4 sorbents, as reported in Chapter 5. A wet preparation method (henceforth will be identified as the suspended impregnation (SI) method) was adopted from Chang et al. (2001), where the solid SiO_2 precursor (in this case, POMBA) suspended in a solution of lithium salt before subjecting it to thermal treatment (Chang et al., 2001). A detailed procedure on the calcination of waste-derived Li_4SiO_4 sorbent using SI method is explained below.

A desired amount of lithium nitrate ($LiNO_3$) was dissolved into deionised (DI) water. The amount of $LiNO_3$ used was determined by the stoichiometric ratio of Li:Si of Li_4SiO_4. Once the clear solution of $LiNO_3$ was prepared, the required amount of POMBA was added to the solution. After 20 minutes of stirring and mixing, the mixed solution was subjected to rotary evaporation at a pressure of 600 mbar at 140 ^{0}C for 1 hour, followed by a pressure of 100 mbar at the same temperature for 2 hours. The prepared powders were then subjected to heat treatment at 500 ^{0}C for 2 hours.

3.2.1.2. Preparation of pure sorbents (P-Li_4SiO_4)

Pure Li_4SiO_4 sorbents were prepared for comparison with the waste-derived sorbents, where pure SiO_2 powder was used and reacted with Li_2CO_3 powder to produce pure Li_4SiO_4 sorbents. Similar to the preparation of waste-derived sorbents, pure SiO_2 was mixed with Li_2CO_3 powder using a Fritsch Pulverisette 2 mortar grinder until the solid mixture achieved homogeneity. The mixed powder (approximately 5g) was then calcined in an alumina crucible in a muffle furnace at 800 ^{O}C in atmospheric air for 8h. After calcination, the resulting products were homogenised in the same grinder to ensure there was no agglomeration in the end product.

3.2.2. CO_2 capture by sorbents

3.2.2.1. CO_2 capture by sorbents in pure CO_2 environment

CO_2 capture analyses were conducted using a TA Instruments Q500 Thermogravimetric Analyser (TGA) in a controlled gas flowing environment. Initial weight (about 15 mg) of the sorbents was recorded. Prior to CO_2 sorption testing, the sorbents were preconditioned and dried in flowing N_2 at 5 ml/min. The sorption temperature was elevated and held at the target temperature (500, 600 or 700 °C) for 30 minutes at atmospheric pressure.

Then, the flowing gas was changed to 100% CO_2 gas at 100 ml/min to allow determination of CO_2 sorption capacity. The weight increase due to CO_2 sorption

was measured as a function of time at constant temperature and concentration of CO_2 at atmospheric pressure. The analysis continued for 120 minutes to allow sufficient time for the sorption process to occur. The flowing gas was then changed back to N_2 to allow desorption of CO_2 to take place. It is worthy to note that while this type of CO_2 desorption procedure may not necessarily represent the actual technique applied at an industrial scale, it is considered an established practice in a laboratory-scaled analysis, as reported in published work (Kato et al., 2005; Olivares-Marin et al., 2010). Finally, the sorbents were subjected to N_2 for another 120 minutes to ensure adequate time was provided for CO_2 desorption.

3.2.2.2. CO_2 capture by sorbents in CO_2/N_2 environment

Similar to CO_2 capture by sorbents in pure CO_2 environment, initial weight (about 15 mg) of the sorbents was recorded. Prior to CO_2 sorption testing, the sorbents were preconditioned and dried in flowing N_2 at 5 ml/min. The sorption temperature was elevated and held at the targeted reaction temperature (500, 600 or 700 °C) for 30 minutes at atmospheric pressure.

Then, the flowing gas changed to 14 vol% CO_2 with balance N_2 at 100 ml/min to allow reaction and determination of CO_2 sorption capacity. This particular composition of reaction gas was chosen to simulate the volumetric concentration of CO_2 in a typical flue gas composition which could be somewhere in between 10 and 15 vol% for a coal-fired power plant (GCCSI, 2012). It should be noted that the reaction gas for this part of the analysis was supplied by a gas cylinder of pre-

mixed gases. The weight increase due to CO_2 sorption was measured as a function of time at constant temperature and concentration of CO_2 at atmospheric pressure. The analysis continued for 120 minutes to allow sufficient time for the sorption process to occur. The flowing gas was then changed back to N_2 to allow desorption of CO_2 to take place. The sorbents were subjected to N_2 for another 120 minutes to ensure enough time for CO_2 desorption.

3.2.2.3. Regeneration studies of sorbents

To examine the sorbents durability, CO_2 capture analyses were followed by regeneration steps. The same procedures as for single cycle (Subsection 3.2.1.1) were followed up until the desorption step, where 30 minutes of desorption time was used instead of 120 minutes. Shorter desorption time was employed to allow adequate CO_2 desorption and at the same time the analysis duration did not get excessively prolonged. The sorption/desorption cycles were repeated 9 more times to represent 10 cycles of regeneration steps. Parameters for analysis include number of cycles before the impregnated samples lose their ability to adsorb further CO_2 as well as the percentage of sorption decay rate of the samples.

3.2.2.4. Devolatilisation of parent waste materials

Devolatilisation of parent waste materials was determined in a TA Instruments Q500 Thermogravimetric Analyser. The procedures followed that of CO_2 capture in pure environment (Section 3.2.2.1), with the exception of the flowing gas.

Instead of pure CO_2, this analysis was conducted in pure N_2 environment. Other parameters such as operating temperatures (500, 600 and 700 °C) and analysis duration (120 minutes) remained the same. The analysis came to an end once the 120-minute analysis duration was completed.

Chapter 4 Characterisation of waste materials and Li_4SiO_4 sorbents

This chapter discusses the characterisation studies of the parent waste materials used in this research (Section 4.1) and the developed waste-derived Li_4SiO_4 sorbents (Section 4.2). Finally, Section 4.3 summarises the characterisation studies of all the materials investigated and also the potential performance of proposed CO_2 sorbents on the basis of physico-chemical properties.

4.1. Characterisation of parent waste materials

Four waste materials were selected as precursors for the development of high temperature sorbents, including two fly ash samples (CPFA and RPFA), one furnace bottom ash sample (FBA) and one palm oil mill boiler ash sample (POMBA), as listed in Table 3.1 in Chapter 3. These waste materials were selected from a large suite of samples based on their chemical compositions, in particular, high silica (SiO_2) content, as the sorbents developed from these precursors are Li_4SiO_4-based.

4.1.1. Particle size distribution

The particle size distributions of as-received CPFA, RPFA, FBA and POMBA samples were analysed using laser diffraction method, as described in Section 3.1.2.1. The D(0.1), D(0.5), D(0.8) and D(0.98) values presented in Table 4.1 indicate that 10%,

50%, 80% and 98% of the particles measured were less than or equal to the size stated in the table, respectively. CPFA contained the smallest particle sizes with D(0.1), D(0.5) and D(0.98) values of 2.75, 13.14, 31.67 and 102.32 μm, respectively. The sequence is then followed by RPFA (4.52, 41.89 and 103.32 μm, respectively), FBA (57.68, 181.72 and 697.89 μm, respectively) and POMBA (86.35, 239.41 and 718.76 μm, respectively). As expected, the bottom ash sample FBA contains larger particle sizes compared to fly ash samples CPFA and RPFA, as bottom ash consists of particles that are too large to be carried in the flue gases and impact on the furnace walls or fall through open grates to an ash hopper at the bottom of the furnace.

In industrial applications, POMBA is produced by burning palm oil shells and husks in palm oil mills to produce steam for electricity generation, which is essential in extracting crude palm oil. For best performance and also considering environmental pollution control, 80% palm husk and 20% palm shell are typical proportion used in a steam boiler for electricity generation in a palm oil mill (Borhan et al., 2010). Hence, the particle sizes of the resulting ash determined by the size of the disintegration of the raw materials fed into the boiler. Consequently, there are significant differences between particle sizes of POMBA and its coal-derived ash CPFA, RPFA and FBA samples.

Table 4.1 D(0.1), D(0.5), D(0.8) and D(0.98) values of particle size distribution of waste materials.

Sample	Particle size distribution			
	D(0.1) (μm)	D(0.5) (μm)	D(0.8) (μm)	D(0.98) (μm)
CPFA	2.75	13.14	31.67	102.3
RPFA	4.52	41.89	109.4	240.4
FBA	57.68	181.7	344.5	697.9
POMBA	86.35	239.4	465.3	718.8

Comparing the particle size distribution shown in Table 4.1 and other similar samples found in published studies proved to be in good agreement. Olivares-Marin et al. (2010) reported similar particle size distribution of coal-derived fly ash samples, where 98% of the particles measured were less than or equal to 250 μm (Olivares-Marin et al., 2010). Consoli et al., (2007) reported similar particle size distribution of their coal bottom ash sample having average diameter D(0.5) value of 144 μm (Consoli et al., 2007). However, the particle size distribution values of palm oil boiler ash reported in other studies varied significantly. Chong et al., (2009) reported particle size distribution of oil palm ash within the range of 75 to 2000 μm, with 35% of the particles measured were larger than 1000 μm, 59% of the particles measured were in between 100 and 1000 μm and the remaining of the sample volume having less than 100 μm in size (Chong et al., 2009).

4.1.2. Loss-on-ignition (LOI) and major oxides composition analysis

Table 4.2 shows the LOI values and major elements presented as their oxides form for the parent waste materials. LOI value is a measure of unburnt carbon in the waste materials and can also be used as an indicator for the efficiency of the combustion process (Levandowski and Kalkreuth, 2009). Some differences are immediately evident, although in general LOI values of waste materials were found to be relatively low with the largest value reported for FBA (8.47 wt%), followed by POMBA (8.12 wt%), RPFA (4.09 wt%) and CPFA (4.00 wt%). These values are in good agreement with values found in literatures of similar materials, where the LOI values for coal-derived PFA samples were reported to be lower than their bottom ash counterparts (Vassilev et al., 2005; Levandowski and Kalkreuth, 2009; Dai et al., 2010). The LOI value of the biomass-derived POMBA sample was also in good agreement with published literature of 7.3 wt% (Zainudin et al., 2005). Higher LOI values of biomass-derived ashes in comparison to that of coal-derived ash samples were also reported in published studies, where LOI values of 28 and 15 wt% for wood- and wheat straw-derived biomass ashes were reported (Thy et al., 2006).

The SiO_2 contents of the parent waste materials were of particular interest, as high concentration of SiO_2 is essential in order to ensure maximal amount of Li_4SiO_4 was generated using the waste materials, and therefore, maximising the amount of CO_2 uptake by the sorbents. As shown in Table 4.2, all waste materials contain significant amounts of SiO_2. The highest concentration of SiO_2 was found in

POMBA (66.30 wt%), followed by CPFA (55.29 wt%), RPFA (49.81 wt%) and FBA (47.77 wt%). Table 4.2 also shows that apart from SiO_2, there are considerable amounts of Al_2O_3 in all waste materials, with the highest Al_2O_3 amount found in RPFA (23.05 wt%), followed by FBA (21.55 wt%), CPFA (20.73 wt%) and the lowest amount in POMBA (1.34 wt%).

Table 4.2 Major elements analysis of the waste materials.

Element	Composition (wt%)			
	CPFA	RPFA	FBA	POMBA
LOI	4.00	4.09	8.47	8.12
SiO_2	55.3	49.8	47.8	66.3
Al_2O_3	20.7	23.1	21.6	1.34
Fe_2O_3	6.23	7.13	10.47	2.35
CaO	4.04	4.90	4.83	6.46
K_2O	2.21	2.27	1.85	6.80
MgO	1.79	2.14	2.38	3.78
P_2O_5	1.04	0.91	0.27	3.09
TiO_2	0.92	0.96	0.86	0.20
Na_2O	0.84	0.84	0.56	0.04
SO_3	0.61	1.57	0.15	0.70
MnO	0.13	0.12	0.19	0.11

In addition, relatively lower amounts of other elements such as iron, calcium, potassium, magnesium and phosphorus can also be found in all parent waste materials. Comparatively high concentrations of Fe_2O_3 were found in the coal-derived waste materials, with the highest found in FBA (10.47 wt%), followed by RPFA (7.13 wt%) and CPFA (6.23 wt%), while the biomass-derived waste material POMBA contained comparatively low Fe_2O_3 at 2.35 wt%. In contrast, highest

concentration of CaO was found in POMBA (6.46 wt%), whereas similar concentrations found in RPFA (4.90 wt%), FBA (4.83 wt%) and CPFA (4.04 wt%). Similar trends can be seen for K_2O, MgO and P_2O_5, where the highest concentrations of these elements (6.80, 3.78 and 3.09 wt%, respectively) were found in POMBA compared to the rest of the waste materials. Significant amount of potassium and phosphorus are expected in biomass, especially in oil palm-derived waste materials as these are essential elements used in fertilizers (Yin et al, 2008).

Variances in concentrations of elements across waste materials are expected, since they are highly dependent on the type and origin of the feedstock used during combustion process (Vassilev et al., 2005). However, major oxides compositions of coal-derived waste materials CPFA, RPFA and FBA are in good agreement with published values, where four of the highest amount of oxides are in the order of SiO_2>Al_2O_3>Fe_2O_3>CaO (Medina et al., 2010). In addition, major oxides compositions of biomass-derived waste material POMBA also are in good agreement with previously published studies, where SiO_2 was identified as the main component (Zainudin et al., 2005; Ooi et al., 2013). Furthermore, relatively higher concentrations of K_2O, CaO and MgO in POMBA compared to coal-derived ashes are also found in other biomass-derived ashes, where similar values reported in published studies (Thy et al., 2006; Borhan et al., 2010). Nonetheless, the key chemical compositions (SiO_2) of all waste materials were significant enough to be deemed suitable for the development of Li_4SiO_4-based sorbents at the beginning stage of this research.

While SiO_2 content in waste materials is important in order to maximize the amount of Li_4SiO_4, the unavoidable presence of other oxides in the parent waste materials is expected to affect the performance of CO_2 uptake by waste-derived Li_4SiO_4 sorbents. Gauer and Heschel (2006) reported the effect of hetero elements, such as Fe and Al doping of pure Li_4SiO_4 sorbents on CO_2 uptake performance (Gauer and Heschel, 2006). The authors adopted the concept of designing solid state ion conductors to improve ion mobility, which could be achieved by introducing defects into crystalline Li_4SiO_4 through appropriate doping of foreign elements such as Al and Fe.

Subsequently, they found that by doping Li_4SiO_4 with either Al or Fe improved the reactivity performance of Li_4SiO_4 in capturing CO_2 at temperatures above 500 °C. However, Li_4SiO_4 doped with Fe presented further improvement in releasing captured CO_2 compared to Al. The authors explained the less negative Gibbs energy of formation of Fe_2O_3 (-742 kJ/mol) compared to SiO_2 (-856 kJ/mol) might have caused the oxygen bonds in Li_4SiO_4 to be weakened and therefore the detachment of O^{2-} is eased. On the contrary, oxygen bonds might be strengthened by Al doping due to the higher negative Gibbs energy of formation of Al_2O_3 (-1582 kJ/mol) (Gauer and Heschel, 2006).

The weight percentages of dopant Al_2O_3 and Fe_2O_3 (maximum of 2.53 and 3.90 wt%, respectively) used were significantly lesser than that in most of the parent waste materials (with the exception of POMBA) used in the current research. Therefore, the CO_2 sorption reactivity performance of POMBA-derived Li_4SiO_4

sorbent is expected to be similar to the findings of Gauer and Heschel (2006). In contrast, due to the extra amount of Al_2O_3 and Fe_2O_3 found in the rest of the parent waste materials, the reactivity performance of their corresponding Li_4SiO_4 sorbents are predicted to be further improved.

In another study conducted by Mejio-Trejo et al. (2008), the authors found that CO_2 uptake improved up to 7% compared to Li_4SiO_4 sorbent by doping pure Li_4SiO_4 with Na in small quantity of up to 0.15 mol, which is equivalent to approximately 4.05 wt% of Na_2O (Mejio-Trejo et al., 2008). They also found that Na was located on the surface of Li_4SiO_4 particles, and thus, aiding the CO_2 chemisorption process and subsequently increasing the CO_2 uptake capacity of Na-doped Li_4SiO_4 sorbent. It is then expected that the CO_2 uptake performance of waste-derived Li_4SiO_4-based sorbents will be positively affected by the small amounts of Na found in the parent waste materials.

4.1.3. Phase composition analysis of waste materials

Figures 4.1 to 4.4 show the x-ray diffractograms of waste materials CPFA, RPFA, FBA and POMBA, respectively. As expected, the main crystalline phase was quartz (SiO_2) in all coal-derived waste materials (CPFA, RPFA and FBA). The identification of crystalline phase of SiO_2 as quartz contributes to produce a good high temperature Li_4SiO_4-based CO_2 sorbent, according to Seggiani et al. (2011). The authors reported that quartz produced porous and small (less than 1 μm) Li_4SiO_4 particle sizes which provide large contact area for CO_2 molecules to react

with (Seggiani et al., 2011). On the contrary, amorphous silica produced dense and larger Li_4SiO_4 particles (average of 80 μm), resulting in lower surface area (Seggiani et al., 2011). In addition to quartz, aluminosilicate crystalline phases of mullite ($Al_6Si_2O_{13}$) and sillimanite (Al_2SiO_5) were also identified in all coal-derived waste materials.

Amorphous peaks (2θ ranging from about 15 to 35° for C- and RPFA; about 15 to 25° and 55 to 65° for FBA) can also be identified in these diffractograms, indicating coexistence of amorphous constituents in the waste materials. It is thought that amorphous phase of aluminosilicate constituents was also found in the sample, as suggested by previously published study on mineral phases in coal fly ash samples (Kumar et al., 2001). Also as seen in Figures 4.1 to 4.3, there were various unidentified peaks on the diffractograms of the coal-derived waste materials. This is because coal is comprised of various other minerals such as lime and magnetite in addition to high amount of carbon (Levandowski et al., 2009; Vassilev et al., 2005), and therefore, by-products of coal combustion process are expected to contain traces of various minerals.

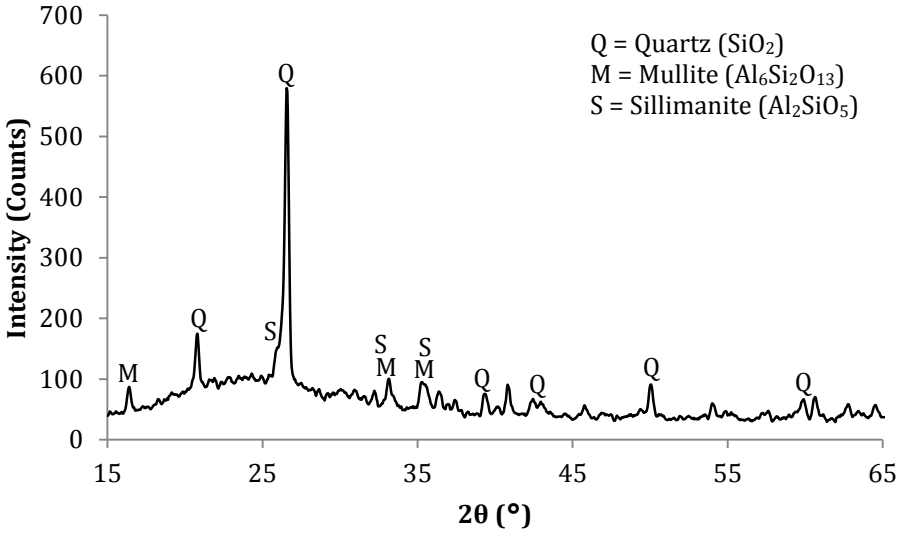

Figure 4.1 XRD diffractogram of CPFA.

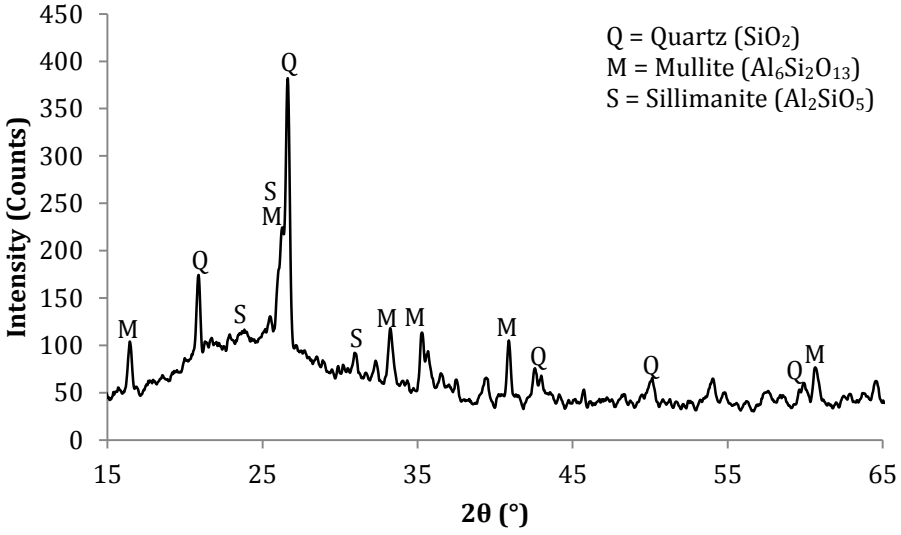

Figure 4.2 XRD diffractogram of RPFA.

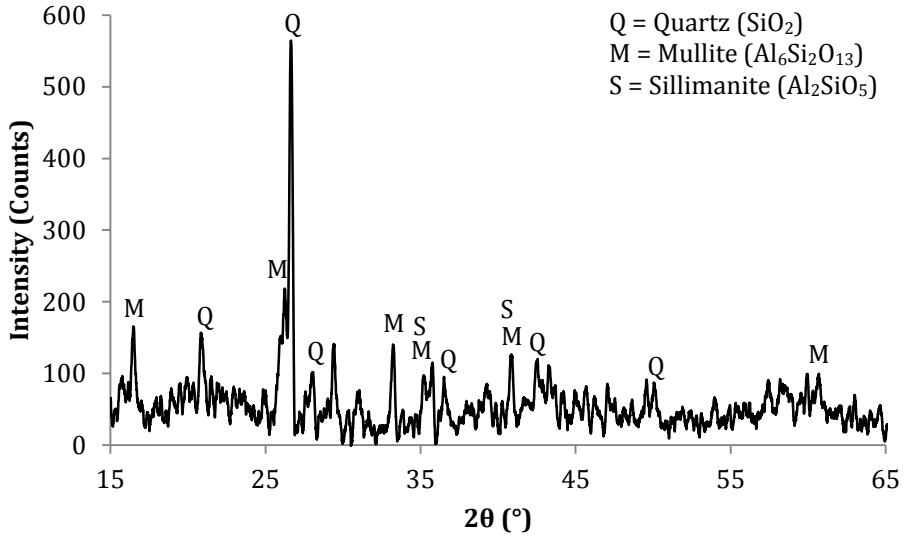

Figure 4.3 XRD diffractogram of FBA.

Similar to its coal-derived waste materials counterparts, quartz was also identified as the main crystalline phase of the biomass-derived waste material POMBA, as shown in Figure 4.4. In contrast to the coal-derived waste materials CPFA, RPFA and FBA, the absence of amorphous peak in POMBA indicates that there is no significant coexistence of amorphous constituents in the biomass-derived waste material. Consequently according to observations previously discussed by Seggiani et al. (2011), it is expected that Li_4SiO_4 sorbents deriving from this parent waste material would exhibit porous textural characteristics and smaller in particle size than the rest of the waste materials, and therefore, have the ability to capture more CO_2 (Seggiani et al., 2011). Moreover, peaks of crystalline potassium aluminium bis(tetraoxidosulphate) dodecahydrate ($KAl(SO_4)_2.12H_2O$) and jadeite ($Al_{0.52}Ca_{0.47}Fe_{0.48}Na_{0.53}Si_2O_6$) were also identified.

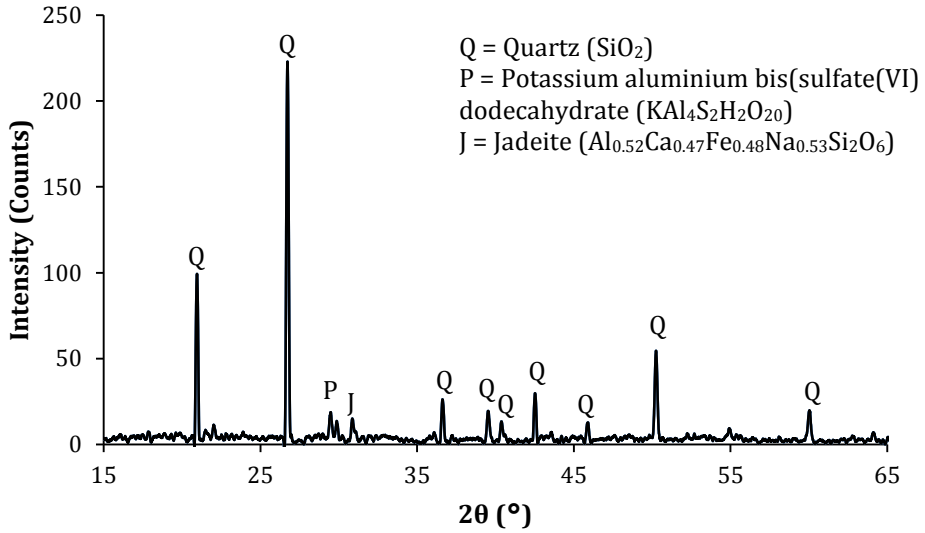

Figure 4.4 XRD diffractogram of POMBA.

4.1.4. Nitrogen adsorption/desorption isotherm profiles and surface areas

The porous texture of the parent waste materials was also analysed by nitrogen adsorption and desorption isotherms conducted at 77 K and the resulting isotherm profiles are shown in Figures 4.5 to 4.8. All of the materials exhibit similar convex isotherms to the P/P_o axis over its entire range which corresponds to type II isotherm according to the IUPAC classification (IUPAC, 1985). These type II isotherms are associated with non-porous or macroporous adsorbents with unobstructed monolayer/multilayer adsorption and indicated by a distinctive point in the isotherms labelled as Point B at the beginning of the almost linear middle section. At this point, the monolayer coverage is complete and multilayer adsorption begins (IUPAC, 1985). This textural characteristic explains the low

volume of nitrogen adsorbed by the parent waste materials, ranging from maximum volume adsorbed of 3.330 to 6.318 cm^3/g STP (Table 4.3).

In addition, all waste materials isotherm profiles exhibit hysteresis loops which are associated with capillary condensation taking place in mesopores (IUPAC, 1985). Specifically, the hysteresis loops are of type H3 according to IUPAC classification and correspond to adsorption and desorption branches almost vertical and nearly parallel over a wide range of P/P_o. Also, this type of hysteresis loop does not have limiting uptake over a range of high relative pressure P/P_o. Taking into consideration that type II isotherm profiles were exhibited by all materials, it can be deduced that all parent waste materials exhibit a combination of macroporosity and mesoporosity. Furthermore, the POMBA isotherm profile shows low pressure hysteresis which can be recognised by the extended loop to the lowest attainable pressure, as shown in Figure 4.8. This phenomenon may be related to the swelling of a non-rigid porous structure exist in the waste material (IUPAC, 1985).

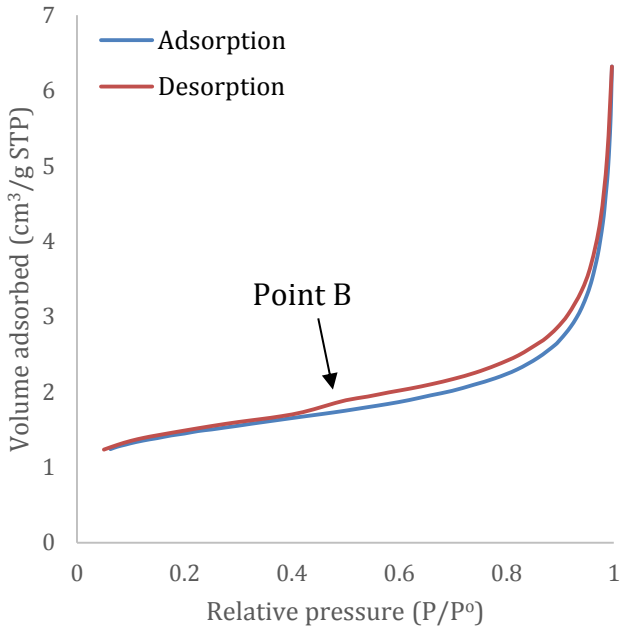

Figure 4.5 Nitrogen adsorption/desorption isotherm at 77 K of CPFA.

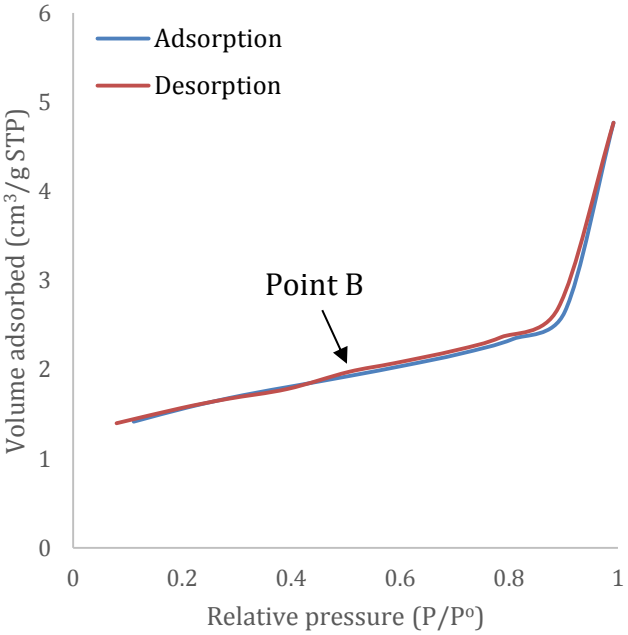

Figure 4.6 Nitrogen adsorption/desorption isotherm at 77 K of RPFA.

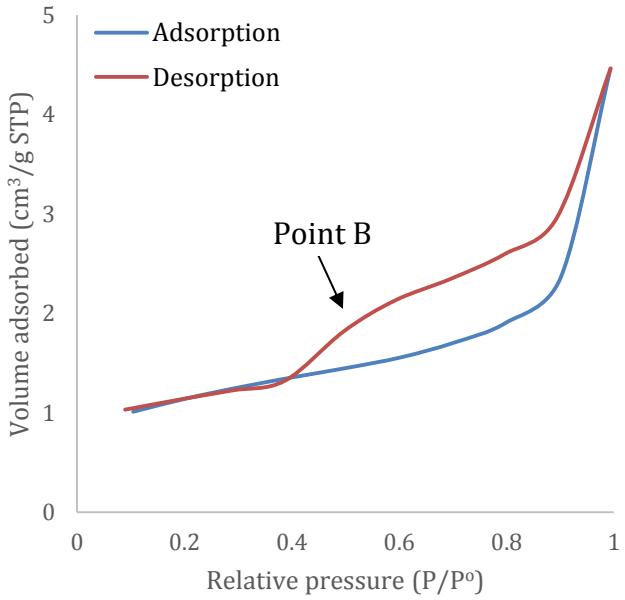

Figure 4.7 Nitrogen adsorption/desorption isotherm at 77 K of FBA.

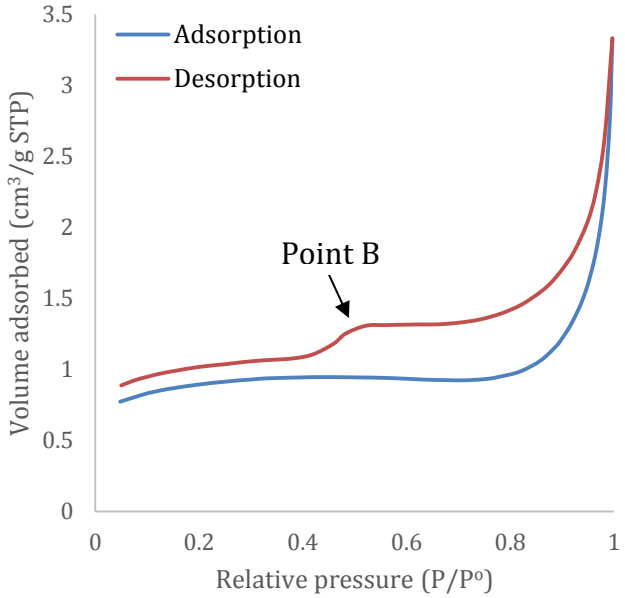

Figure 4.8 Nitrogen adsorption/desorption isotherm at 77 K of POMBA.

Surface area values of all parent waste materials can be found in Table 4.3. It is observed that surface area values of all waste materials were relatively low and follow the descending order of CPFA (4.74 m^2/g), followed by RPFA (4.10 m^2/g), FBA (3.77 m^2/g) and POMBA (2.82 m^2/g). The order of surface area values of the parent waste materials inversely correlates with that of the particle size values: CPFA>RPFA>FBA>POMBA, as presented in Table 4.1.

Comparing the surface area of parent waste materials in this study with that of published data, the surface area values of the fly ashes CPFA and RPFA are comparable to that of reported by Medina et al. (2010) (4.73 m^2/g) (Medina et al., 2010). However, there is a slight difference on BET surface area of oil palm ash reported by Zainuddin et al. (2005), where 10.2 m^2/g of surface area was obtained (Zainuddin et al., 2005). The difference could be due to different geological origins of the biomass obtained in the study, as this affects the chemical compositions of the biomass and subsequently affecting the amount of organic matter burn-off of the materials. This then affects the textural characteristics and surface area of the materials.

Table 4.3 also shows total pore volume and pore diameter of waste materials calculated using the Barrett-Joyner-Halenda (BJH) method. In general, the total pore volumes of the waste materials were relatively low and could be explained by the equally low calculated surface areas. The total pore volumes of all waste materials were highest for the fly ash samples RPFA and CPFA with volumes of 0.0079 and 0.0077cm^3/g, respectively. Total pore volume of POMBA was the

lowest value compared to other waste materials with 0.0034 cm^3/g, while FBA contained 0.0069 cm^3/g of total pore volume. All waste materials contained pore diameter larger than 2 nm but smaller than 50 nm which categorised them as having mesopore type of porosity according to the IUPAC classification (IUPAC, 1985).

Table 4.3 BET surface area, BJH total pore volume and pore diameter of waste materials.

Waste material	BET surface area (m^2/g)	BJH total pore volume x 10^{-3} (cm^3/g)	BJH pore diameter (nm)	Volume adsorbed (cm^3/g STP)
CPFA	4.74	7.71	6.02	6.32
RPFA	4.10	7.93	2.42	4.77
FBA	3.77	6.92	3.08	4.46
POMBA	2.82	3.44	20.2	3.33

4.1.5. Scanning electron microscope analysis

Figures 4.9 to 4.12 show SEM micrographs of the parent waste materials at 5000 times magnification. There are two classified differences that can be identified between the PFA (Figures 4.9 and 4.10) and bottom ash (Figures 4.11 and 4.12) samples. As seen from Figures 4.9 and 4.10, the PFA samples had no obvious porosity on the surface of the particles. Additionally, the samples consist of spherical particles and agglomerates of various particle sizes (1 – 10 μm) that correspond to inorganic constituents caused by high temperature burning of coal during combustion process (Rubio et al., 2008).

On the other hand, FBA and POMBA samples consist of polyhedral and non-porous particles as well as agglomerates, as shown in Figures 4.11 and 4.12. The particle sizes were also considerably larger than CPFA and RPFA for these samples (2 – 15 μm), considering the images were taken at the same degree of magnification as CPFA and RPFA samples. The particle sizes shown in Figures 4.11 and 4.12 are also in good agreement with the particle sizes described in subsection 4.1.1, where much larger particle sizes are observed in bottom ash samples FBA and POMBA compared to fly ash samples CPFA and RPFA.

SEM micrographs of waste materials confirm the textural analysis data discussed previously. Nitrogen adsorption/desorption isotherm profiles of waste materials exhibit type II isotherm that associated with non-porous adsorbents, as shown in Figures 4.9 to 4.12. These characteristics of waste materials contribute to the relatively low volume of nitrogen adsorbed, as reported in the previous section. They also confirm the type H3 hysteresis loop that associated with assemblage of plate-like particles which are loosely coherent that caused the aggregates to develop slit-shaped pores.

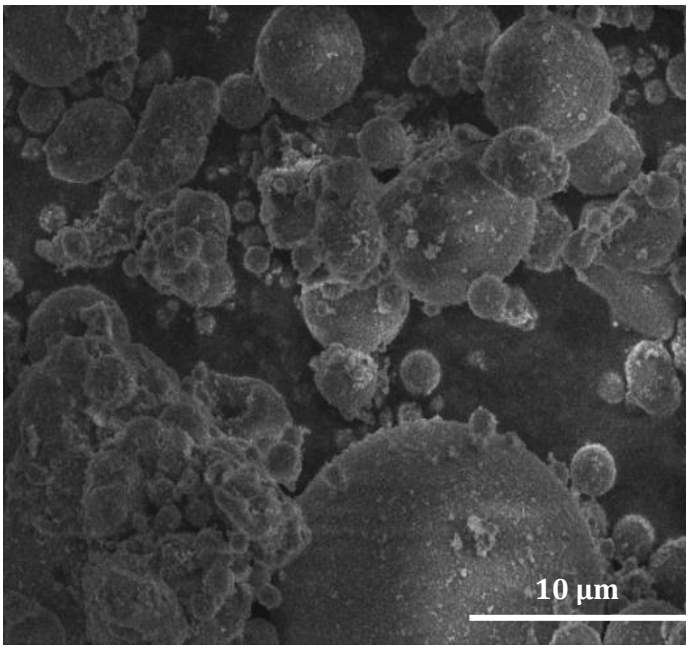

Figure 4.9 SEM micrograph of CPFA.

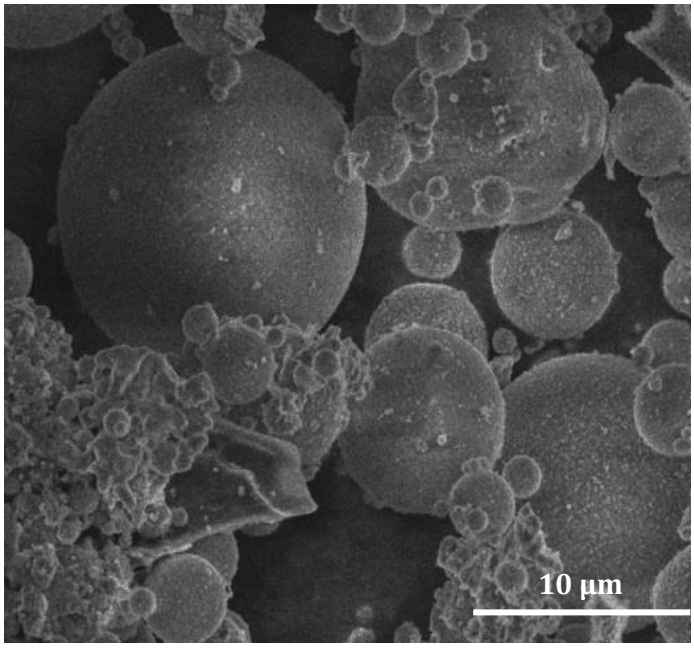

Figure 4.10 SEM micrograph of RPFA.

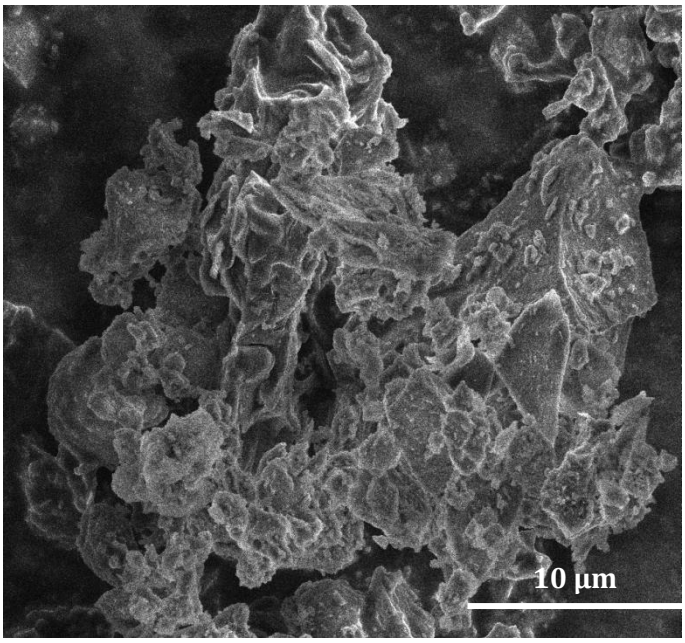

Figure 4.11 SEM micrograph of FBA.

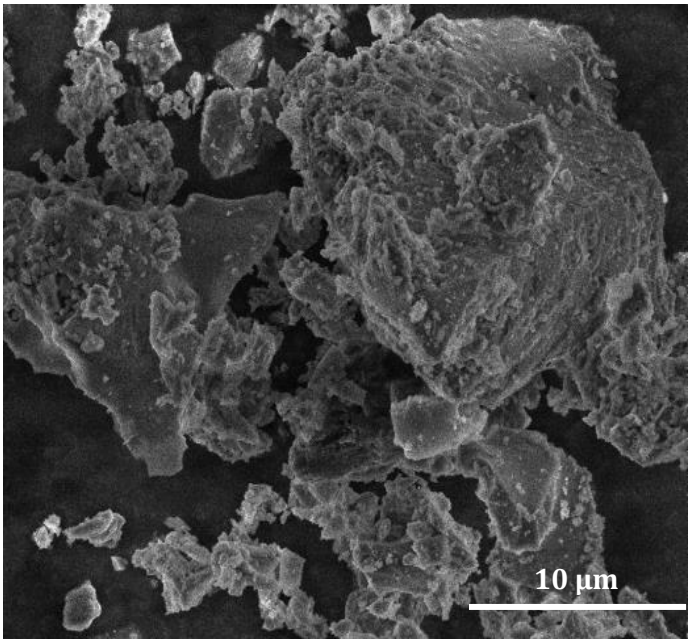

Figure 4.12 SEM micrograph of POMBA.

4.2. Characterisation of waste-derived Li_4SiO_4 sorbents

In this section, the characterisation of Li_4SiO_4-based sorbents is discussed. As described in Chapter 3, the sorbents were developed using solid state method by mixing stoichiometric amounts of the waste materials with powder Li_2CO_3 homogeneously before being subjected to heat treatment at 800 °C for 8h. It should be noted that sorbents were prepared with different amounts of excess lithium (0, 5, 10, 20 wt%).

Prepared sorbents are labelled in the form of W-X-Y-Z, where W represents preparation method of the sorbent (SS for solid state; SI for suspended impregnation), X indicates waste material that was used to develop the sorbent (C, R, F or B for CPFA, RPFA, FBA or POMBA, respectively), while Y symbolises the type of sorbent (Li_4SiO_4 in this chapter) and Z indicates the amount (in wt%) of excess lithium. For example, SS-B-Li_4SiO_4-10 denotes a POMBA-based Li_4SiO_4 sorbent prepared using solid state method with 10 wt% excess lithium.

There are five types of Li_4SiO_4-based sorbents developed in this research, deriving from CPFA, RPFA, FBA and POMBA (identified henceforward in this thesis as SS-C-Li_4SiO_4, SS-R-Li_4SiO_4, SS-F-Li_4SiO_4 and SS-B-Li_4SiO_4, respectively) samples as well as a pure-Li_4SiO_4 (SS-P-Li_4SiO_4) sorbent developed using a commercial SiO_2 powder for comparison purposes.

A series of physical and chemical characterisation analyses were carried out to examine the features of the sorbents, including X-ray diffraction (XRD) to ascertain the mineral phases present, especially that of crystalline Li_4SiO_4; Fourier transform infrared (FTIR) analysis to investigate the chemical bonds of the functional groups which could also support the outcome provided by XRD analysis; scanning electron microscope (SEM) analysis to observe the textural characteristics as well as the particle size of sorbents; and nitrogen adsorption/desorption isotherms to determine BET surface area and porous texture of sorbents.

4.2.1. Phase composition analysis of Li_4SiO_4 sorbents

Phase composition analysis was performed on all sorbents and the resulting diffractograms were compared with Joint Committee on Powder Diffraction Standards (JCPDS) database to determine the mineral phases present. Figure 4.13 shows x-ray diffractograms of SS-P-Li_4SiO_4 with different amounts of excess lithium a) SS-P-Li_4SiO_4-0; b) SS-P-Li_4SiO_4-5; c) SS-P-Li_4SiO_4-10; d) SS-P-Li_4SiO_4-20. As shown, the sorbents exhibit sharp diffraction peaks labelled by (*) attributed to Li_4SiO_4 and the variance in peak intensities can be attributed to different crystal sizes as well as the strain within the crystallites (Venegas et al., 2007). As provided by the JCPDS standard, the crystal structure of Li_4SiO_4 found in SS-P-Li_4SiO_4 sorbents were all monoclinic with space group $P2_1/m$ and lattice parameters of a = 11.532 Å, b = 6.075 Å, c = 16.678 Å, ß = 99.04 °.

Comparing across sorbents with different amounts of excess lithium, there are some SiO_2 present in SS-P-Li_4SiO_4-0, whereas no SiO_2 was detected in subsequent excess of lithium addition SS-P-Li_4SiO_4-5, SS-P-Li_4SiO_4-10 and SS-P-Li_4SiO_4-20. This suggests a more complete Li_4SiO_4 synthesis with at least 5 wt% excess lithium under synthesis conditions at 800 °C for 8h. Lithium sublimation is thought to be the reason of this occurrence, as previously reported (Antolini and Ferretti, 1995; Pfeiffer and Knowles, 2004). Loss of lithium during Li_4SiO_4 synthesis occurs as Li_2CO_3 melts and decomposes to evolve into CO_2 and Li_2O at temperature higher than 710 °C (Lu and Lee, 2000). Therefore, excess amount of lithium in Li_4SiO_4 synthesis was regarded to be a reasonable step to implement in order to increase the amount of Li_4SiO_4 produced.

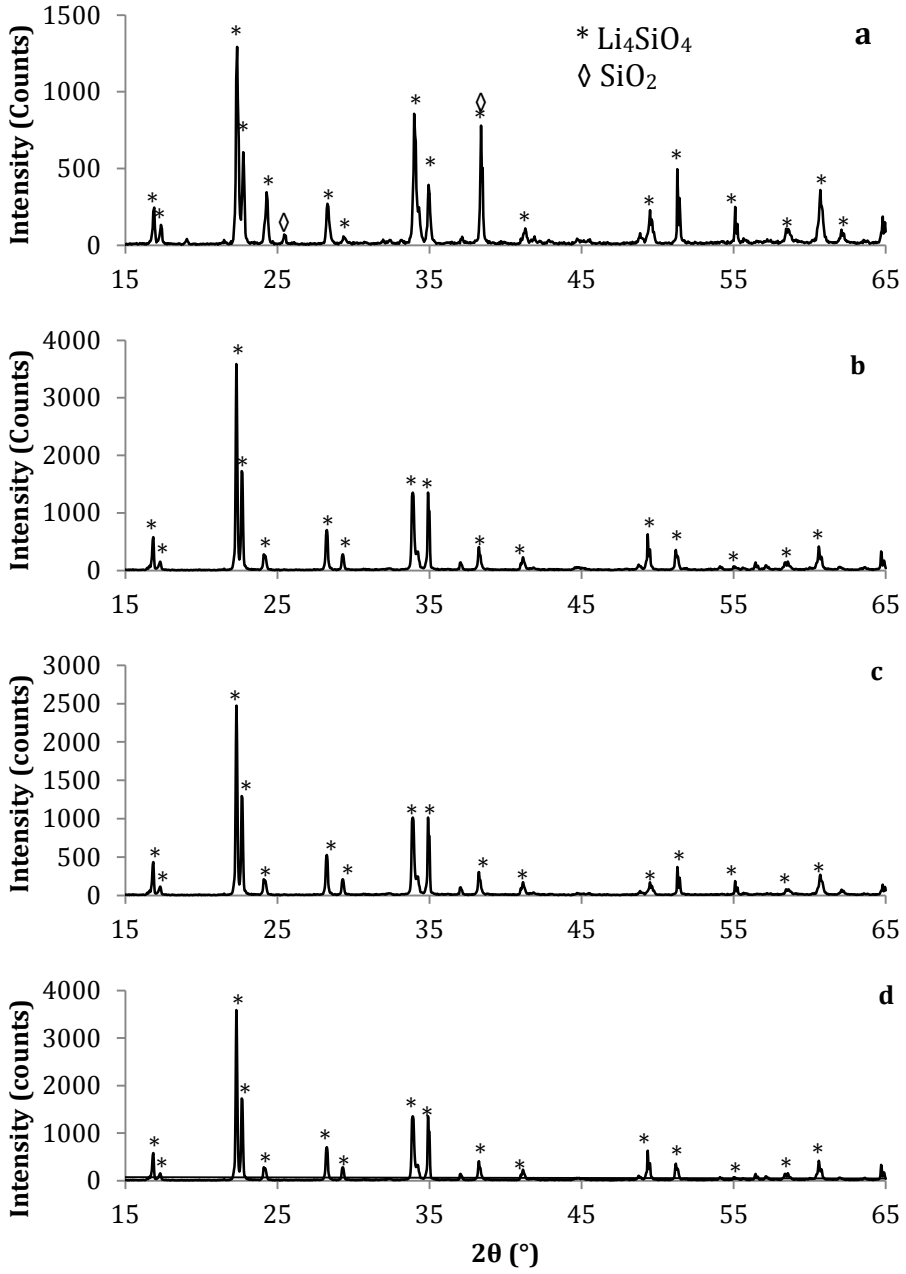

Figure 4.13 XRD diffractograms of pure Li_4SiO_4 with different amounts of excess lithium a) SS-P-Li_4SiO_4-0; b) SS-P-Li_4SiO_4-5; c) SS-P-Li_4SiO_4-10; d) SS-P-Li_4SiO_4-20.

Figure 4.14 shows the X-ray diffractograms of SS-C-Li_4SiO_4 with different amounts of excess lithium a) SS-C-Li_4SiO_4-0; b) SS-C-Li_4SiO_4-5; c) SS-C-Li_4SiO_4-10; d) SS-C-Li_4SiO_4-20. As shown, the waste-derived sorbents exhibit relatively sharp peaks compared to SS-P-Li_4SiO_4 sorbents, albeit slightly amorphous based on amorphous peaks detected at 2θ value range about 30 – 35 °. The crystal structure of Li_4SiO_4 found in SS-C-Li_4SiO_4 was also monoclinic with the same space group and lattice parameters as found in SS-P-Li_4SiO_4.

Unsurprisingly, Li_4SiO_4 was not the only crystalline phase present, as other crystal constituents were also detected in all SS-C-Li_4SiO_4 sorbents, including Li_2SiO_3, $LiAlO_2$ and $LiAlSiO_4$. The presence of crystal constituents other than Li_4SiO_4 and Li_2SiO_3 in the waste-derived sorbents was due to various compounds other than SiO_2 identified in its parent sample CPFA, as shown in Table 4.2 (Section 4.1). Since aluminosilicates like mullite ($Al_6Si_2O_{13}$) and sillimanite (Al_2SiO_5) were found in CPFA, it is expected that the resulting sorbents produced other lithium compounds deriving from these aluminosilicate crystals.

The addition of different amounts of excess lithium used in preparing the sorbents does seem to affect the intensities of Li_4SiO_4 peaks. This could be contributed by two possibilities, with one of them being due to lithium sublimation of Li_2CO_3 during synthesis, and therefore, requiring more lithium than is stoichiometrically needed. Another possibility is that, Li_2CO_3 may have reacted with other available compounds in CPFA such as the aluminosilicates, reducing the amount of Li_2CO_3 to

react with SiO_2 in the parent sample CPFA, and therefore, producing the other lithium crystals in resulting SS-C-Li_4SiO_4 sorbents.

Comparing with diffractograms of the waste material in Figure 4.1, it is expected that the chemical phase composition of CPFA has changed following the addition of Li_2CO_3 and subsequent heat treatment at 800 °C for 8h. Figure 4.8 also shows that there were no peaks that associated with Li_2CO_3 and SiO_2 in SS-C-Li_4SiO_4 sorbents, and therefore, indicating that both compounds have completely reacted during the synthesis process. The absence of peaks associated with aluminosilicates, such as mullite and sillimanite, in Figure 4.14 indicates that these mineral phases have reacted with Li_2CO_3 addition during preparation process and produced the various lithium aluminate crystals, as previously reported.

Some amorphous peaks (at approximately 2θ values of 23, 35, 45 and 50) were also detected, indicating amorphous constituents in SS-C-Li_4SiO_4 sorbents. Amorphous constituents present in the waste-derived sorbents could be advantageous to CO_2 uptake performance due to the versatility of amorphous structure to hold CO_2 molecules, and therefore, increasing the CO_2 uptake capacity of the sorbents. Furthermore, the diffusion of CO_2 molecules into amorphous structure is faster than that in crystalline due to the atomic disorder (Sadoway, 2010), and therefore, increasing the rate of CO_2 sorption of the sorbents.

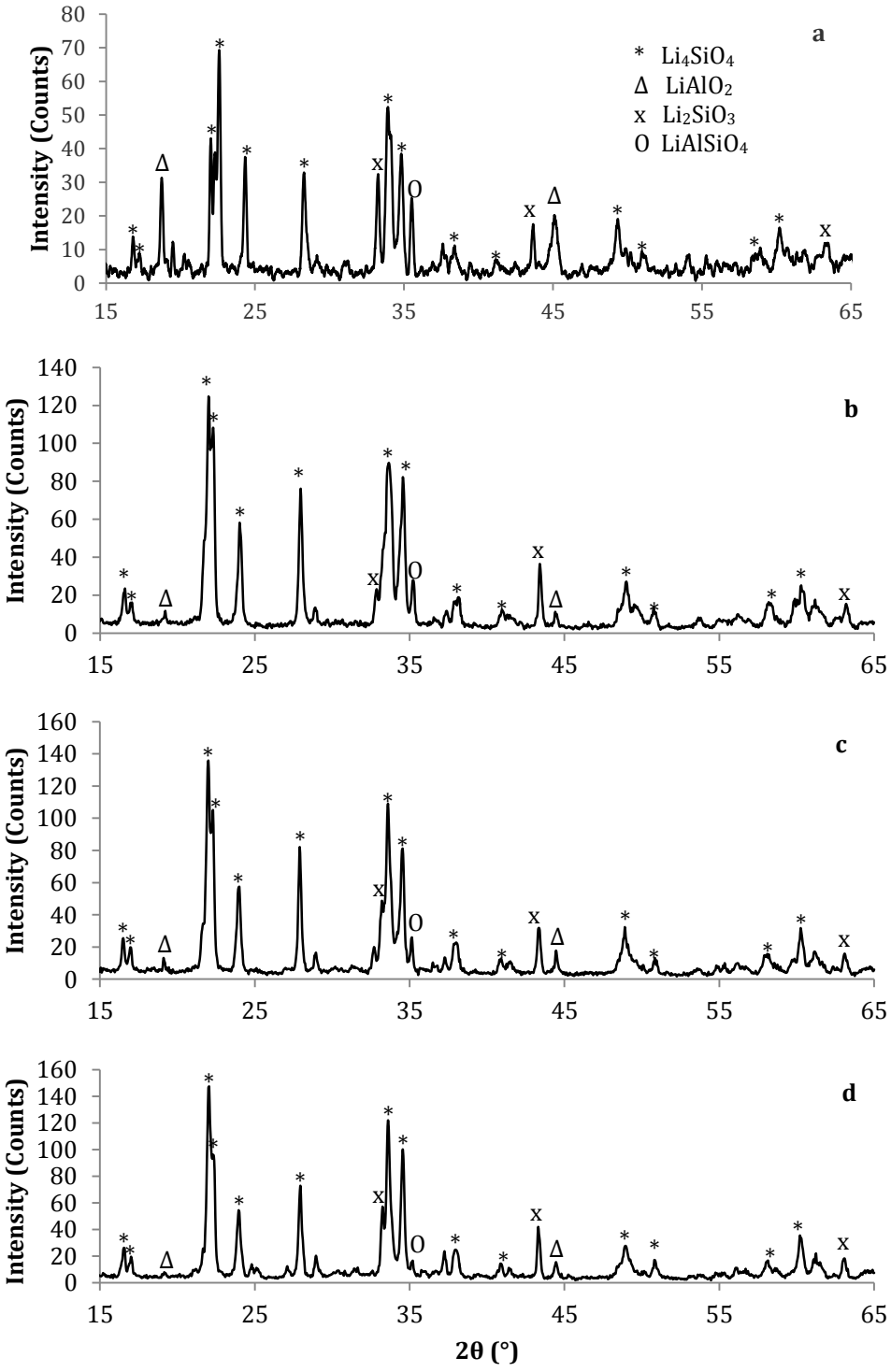

Figure 4.14 XRD diffractograms of CPFA-derived Li_4SiO_4 with different amounts of excess lithium a) SS-C-Li_4SiO_4-0; b) SS-C-Li_4SiO_4-5; c) SS-C-Li_4SiO_4-10; d) SS-C-Li_4SiO_4-20.

Similar diffractograms can also be observed for sorbents derived from RPFA and FBA waste materials, as can be seen in Figures 4.15 and 4.16. The main crystal phase present in the sorbents was Li_4SiO_4, as expected from reaction between Li_2CO_3 and significant presence of SiO_2 in the waste materials. Also, the presence of Li_2SiO_3, $LiAlO_2$ and $LiAlSiO_4$ was also detected resulting from reaction between Li_2CO_3 and other elements already exist in the parent waste materials such as the aluminosilicates. Similar observations in the diffractogram patterns of these sorbents are expected as all three parent waste materials originated from coal and have similar chemical compositions, as reported in Table 4.2.

There are also several amorphous peaks detected in SS-R-Li_4SiO_4 and SS-F-Li_4SiO_4 sorbents, as shown in Figures 4.15 and 4.16 at roughly the same 2θ values as in Figure 4.14. This indicates the coexistence of amorphous constituents, such as Li_4SiO_4 and lithium aluminosilicate derivatives, in the waste-derived sorbents. The coexistence of amorphous constituents is expected to be found in waste-derived Li_4SiO_4 sorbents, as there were amorphous peaks detected in parent waste materials RPFA and FBA. In addition, amorphous components might have existed in waste-derived Li_4SiO_4 sorbents due to the incomplete crystallisation of Li_4SiO_4.

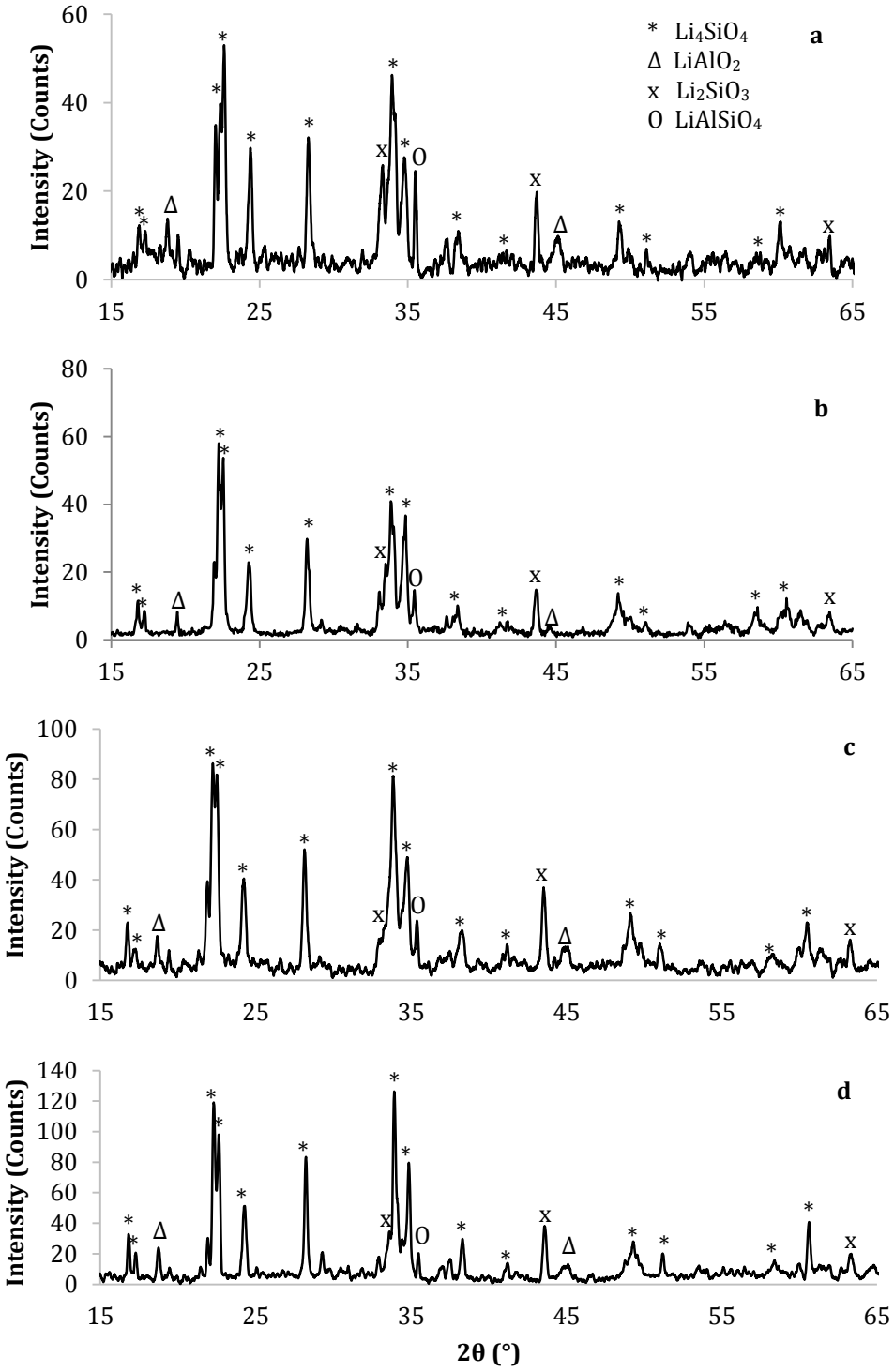

Figure 4.15 XRD diffractograms of RPFA-derived Li_4SiO_4 with different amounts of excess lithium a) SS-R-Li_4SiO_4-0; b) SS-R-Li_4SiO_4-5; c) SS-R-Li_4SiO_4-10; d) SS-R-Li_4SiO_4-20.

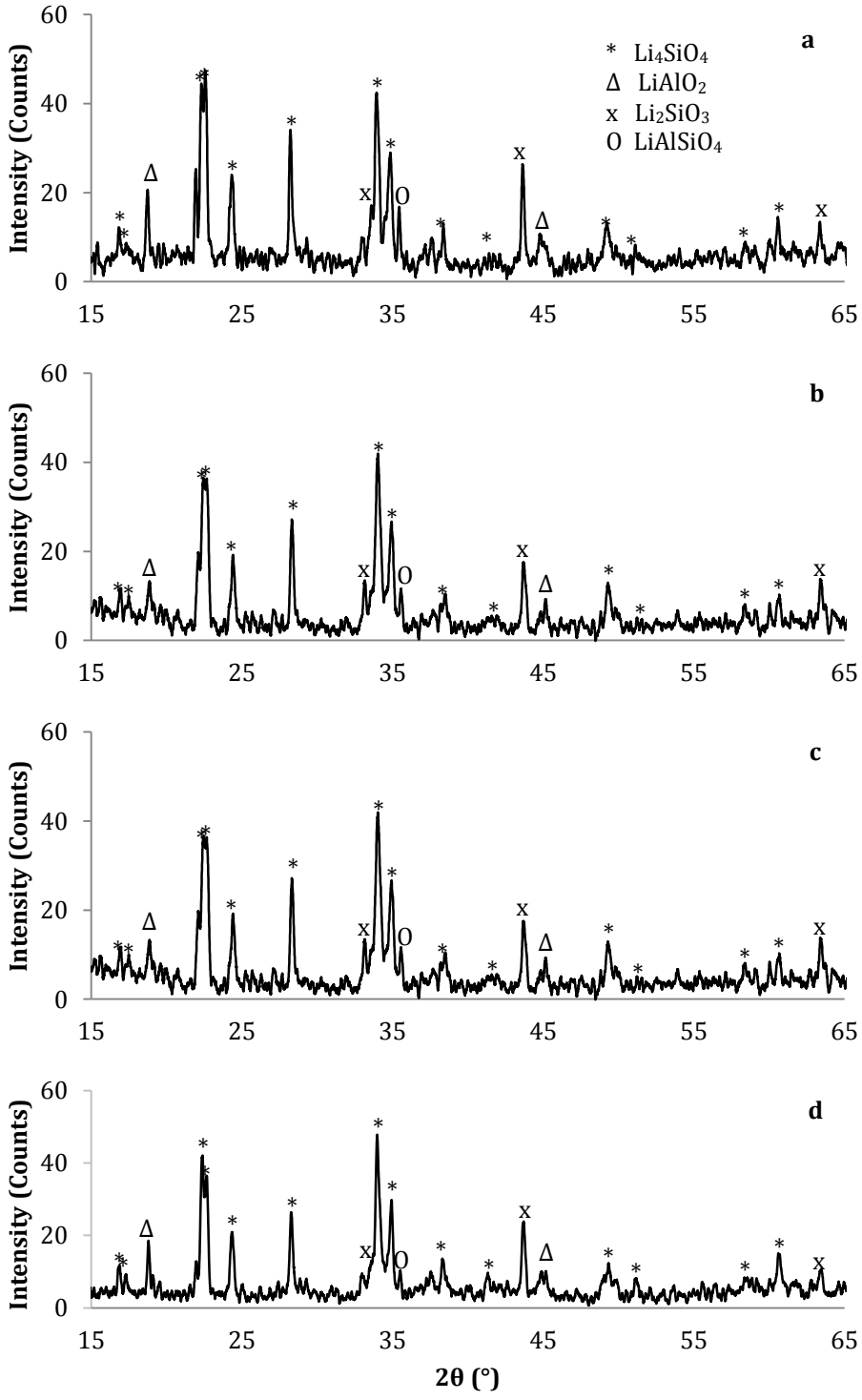

Figure 4.16 XRD diffractograms of FBA-derived Li_4SiO_4 with different amounts of excess lithium a) SS-F-Li_4SiO_4-0; b) SS-F-Li_4SiO_4-5; c) SS-F-Li_4SiO_4-10; d) SS-F-Li_4SiO_4-20.

Figure 4.17 shows the XRD diffractograms of SS-B-Li_4SiO_4 with different amounts of excess lithium a) SS-B-Li_4SiO_4-0; b) SS-B-Li_4SiO_4-5; c) SS-B-Li_4SiO_4-10; d) SS-B-Li_4SiO_4-20. The waste-derived sorbents exhibit sharp peaks comparable to SS-P-Li_4SiO_4 sorbents and more defined peaks compared to the rest of coal-derived SS-C-Li_4SiO_4, SS-R-Li_4SiO_4 and SS-F-Li_4SiO_4 sorbents. Nevertheless, the crystal structure of Li_4SiO_4 found in SS-B-Li_4SiO_4 was also monoclinic with the same space group and lattice parameters, as found in SS-P-Li_4SiO_4.

Similar to other waste-derived sorbents discussed previously, Li_4SiO_4 was not the only crystalline phase present, as other crystals were also detected in SS-B-Li_4SiO_4 sorbents including SiO_2, Li_2SiO_3 and $LiAlSiO_4$. A similar observation was seen for SS-P-Li_4SiO_4 sorbents, where the peaks associated with SiO_2 crystals in the waste-derived sorbents can also be observed (Figure 4.17), which is probably due to lithium sublimation occurred in Li_2CO_3 during synthesis process.

On the other hand, there is no SiO_2 detected in SS-B-Li_4SiO_4-5, SS-B-Li_4SiO_4-10 and SS-B-Li_4SiO_4-20 which indicates a more complete Li_4SiO_4 synthesis under synthesis conditions at 800 °C for 8h. It is thought that the already limited amount of SiO_2 present in POMBA had completely reacted with Li_2CO_3 to produce the equally limited amount of SS-B-Li_4SiO_4. Excess Li_2CO_3 is then believed to react with next available compounds in POMBA, such as calcium to produce other unidentified lithium crystals in SS-B-Li_4SiO_4, which a combination of these compounds is possible.

Comparing with the diffractogram obtained for the parent material (Figure 4.4), it is obvious that the chemical phase composition of POMBA has changed following the addition of Li_2CO_3 and heat treatment at 800 °C for 8h during synthesis of SS-B-Li_4SiO_4 sorbents. The coexistence of Li_2SiO_3 in SS-B-Li_4SiO_4 sorbents is expected, as this proved that the reaction between Li_2CO_3 and the SiO_2 in POMBA advanced according to equation 2.2 (Section 2.3.2).

Also, it should be noted that while there are more peaks associated with lithium aluminosilicate crystals detected in other waste-derived Li_4SiO_4 sorbents, there was only $LiAlSiO_4$ found in SS-B-Li_4SiO_4 sorbents. This is due to substantially low Al_2O_3 (1.34 wt%) found in the parent waste material POMBA. In addition, there was no potassium-containing crystal detected in Figure 4.17, suggesting that the potassium could be lost in some way, as it has been reported that potassium in potassium zirconates are not very stable and decompose at temperature as low as 570 up to 750 °C which are lower than synthesis temperature used in this study at 800 °C (Dash et al., 1996).

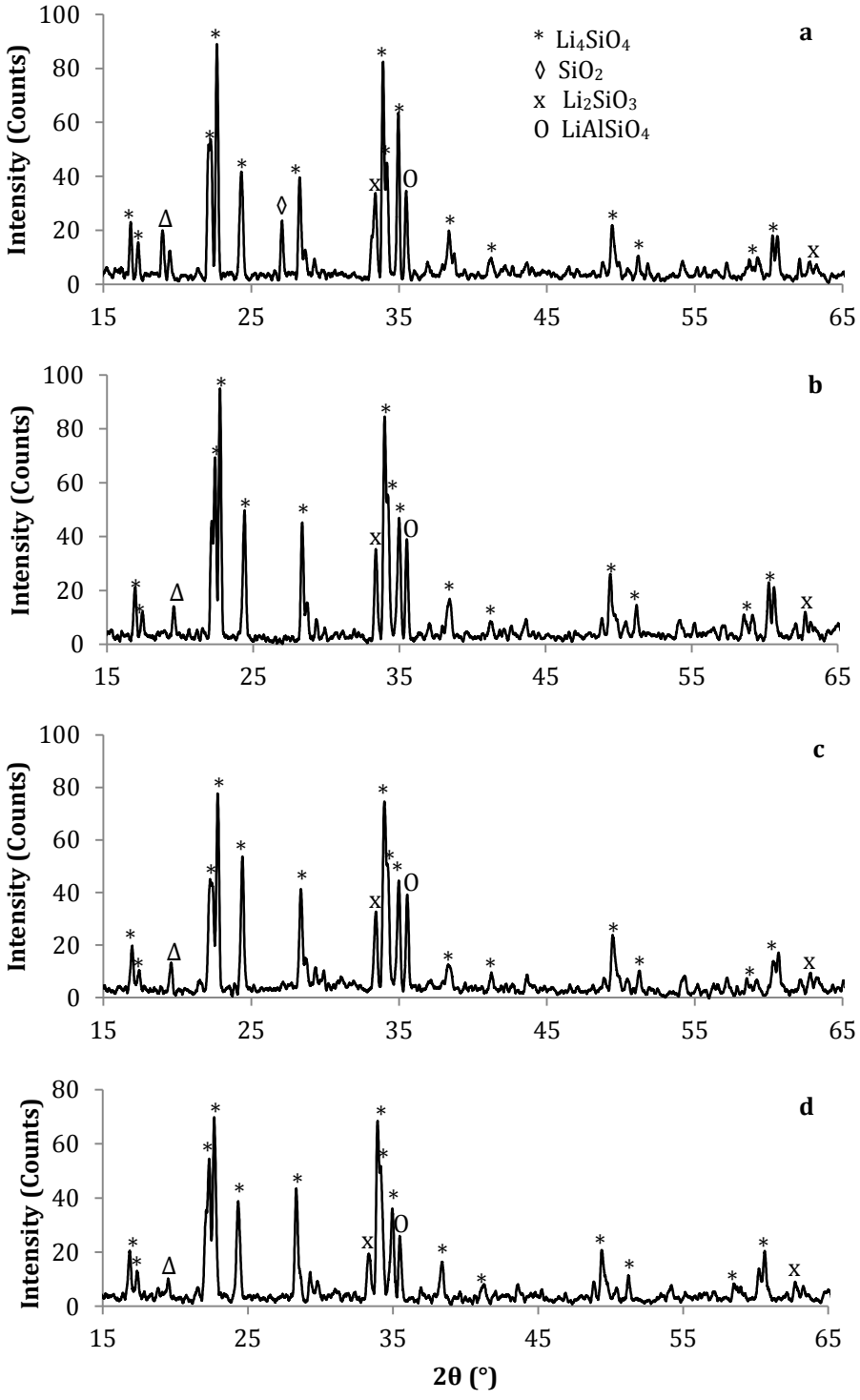

Figure 4.17 XRD diffractograms of POMBA-derived Li_4SiO_4 with different amounts of excess lithium a) SS-B-Li_4SiO_4-0; b) SS-B-Li_4SiO_4-5; c) SS-B-Li_4SiO_4-10; d) SS-B-Li_4SiO_4-20.

4.2.2. Fourier transform infrared (FTIR) analysis of Li_4SiO_4 sorbents

FTIR analyses were conducted to characterise chemical functional groups present, based on the characteristics of vibrational and rotational energies of different molecular bonds. Figure 4.18 shows the FTIR spectra of SS-P-Li_4SiO_4 sorbents with different amounts of excess lithium a) SS-P-Li_4SiO_4-0; b) SS-P-Li_4SiO_4-5; c) SS-P-Li_4SiO_4-10; d) SS-P-Li_4SiO_4-20. In general, all SS-P-Li_4SiO_4 sorbents exhibit similar spectra patterns with slight differences in the intensity of infrared absorption bands.

Upon closer observations, strong presence of absorption bands can be detected in all sorbents in the wavenumber regions between 600 and 1000 cm^{-1} as well as between 1400 and 1600 cm^{-1}. The earlier may be attributed to vibration bands of different metal-oxygen bonds, including Si-O- (807 cm^{-1}) in SiO_4 tetrahedral which exist in Li_4SiO_4 (Humphreys and Hatherly, 1995; Shokri et al., 2009) and Li-O- at 964 cm^{-1} (Ortiz-Landeros et al., 2011). However, the latter may be associated with -C=O (between 1443 and 1588 cm^{-1}) vibration bands in CO_2 of Li_2CO_3 (Hwang et al., 2007; Zhang et al., 2008). Table 4.4 summarises the absorption bands identification of SS-P-Li_4SiO_4 sorbents.

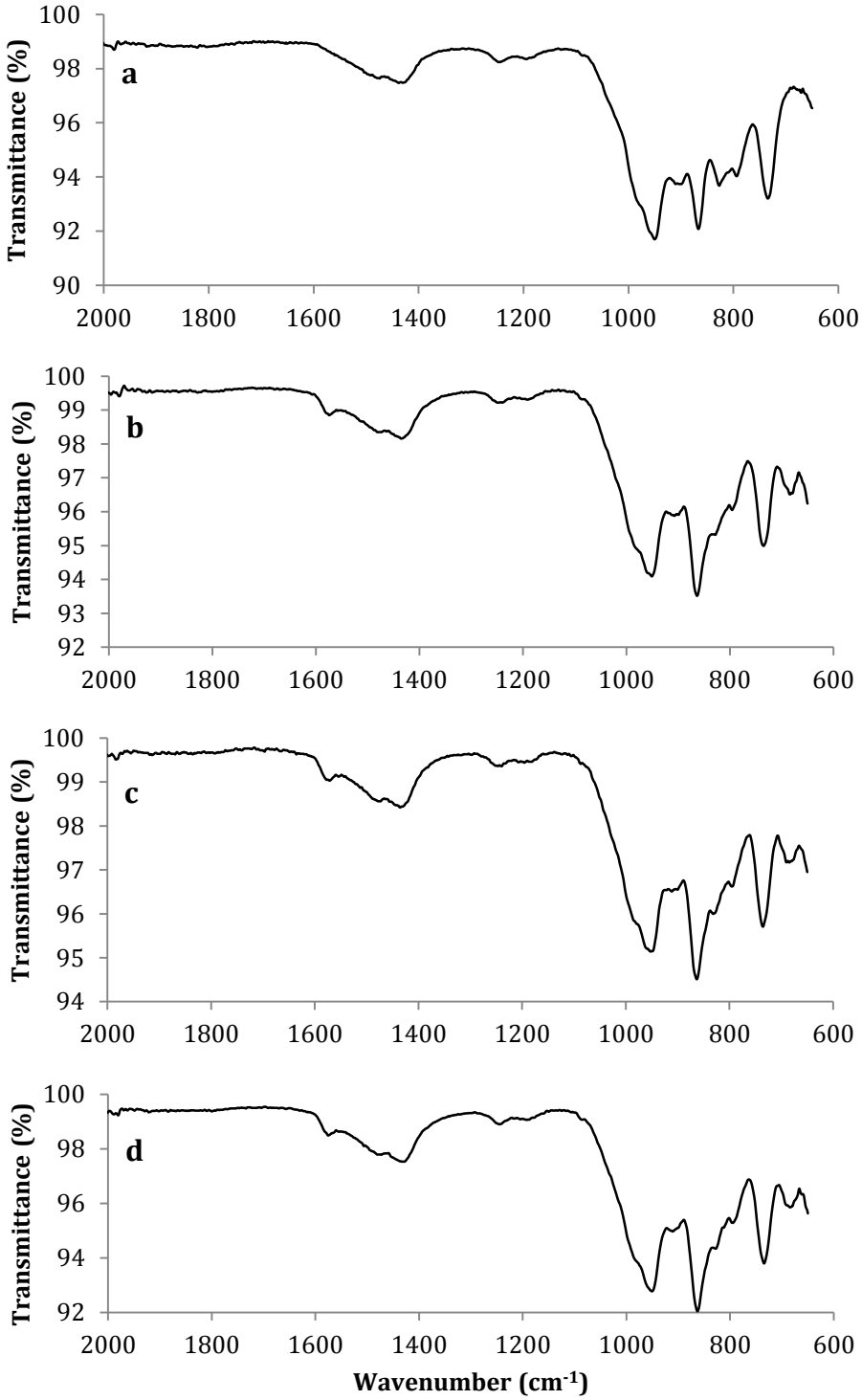

Figure 4.18 FTIR spectra of SS-P-Li_4SiO_4 sorbents with different amounts of excess lithium a) SS-P-Li_4SiO_4-0; b) SS-P-Li_4SiO_4-5; c) SS-P-Li_4SiO_4-10; d) SS-P-Li_4SiO_4-20.

Table 4.4 Absorption bands identification of SS-P-Li_4SiO_4 sorbents.

Absorption bands of sorbents (cm^{-1})				Identification
SS-P-Li_4SiO_4-0	**SS-P-Li_4SiO_4-5**	**SS-P-Li_4SiO_4-10**	**SS-P-Li_4SiO_4-20**	
	1579	1584	1584	-C=O
1475	1482	1477	1491	
1426	1434	1431	1445	
1247	1244	1247	1243	SiO_2
1194	1190	1187	1187	
986	983	986	986	
950	955	953	953	Li-O-
915	908	902	909	Si-O- in SiO_2 tetrahedral
871	864	864	862	
826	831	831	829	
806	797	795	795	
739	736	738	735	SiO_3^{2-} (metasilicate)
684	685	686	685	

Comparing spectra patterns across sorbents with different amounts of excess lithium, the absorption bands associated with carbonates in Li_2CO_3 (between 1443 and 1588 cm^{-1}) were present in all SS-P-Li_4SiO_4 sorbents. It is assumed that there are still remaining Li_2CO_3 present in all sorbents and could be a direct result of excess lithium added during the preparation process.

Figure 4.19 shows the FTIR spectra of SS-C-Li_4SiO_4 sorbents with different amounts of excess lithium a) SS-C-Li_4SiO_4-0; b) SS-C-Li_4SiO_4-5; c) SS-C-Li_4SiO_4-10; d) SS-C-Li_4SiO_4-20. In general, SS-C-Li_4SiO_4 revealed similar spectral patterns to that of SS-P-Li_4SiO_4, with absorption bands observed in two different wavenumber regions, namely 1400 and 1500 cm^{-1} and 800 and 1000 cm^{-1}. Absorption bands in the earlier region are identified to be associated with -C=O (between 1434 and 1522 cm^{-1}) vibration bands in CO_2 of Li_2CO_3, similar to the pure SS-P-Li_4SiO_4 sorbents. However, absorption bands in the latter region are slightly different, having only three distinctive and more intense absorption bands compared to that of SS-P-Li_4SiO_4 which presented substantially more in terms of quantity yet lower intensity absorption bands. Upon closer observations, absorption bands between 800 and 1000 cm^{-1} also identified to be associated with Li_4SiO_4 at wavenumbers 834, 882 and 956 cm^{-1}. Table 4.5 summarises the absorption bands identification of SS-C-Li_4SiO_4 sorbents.

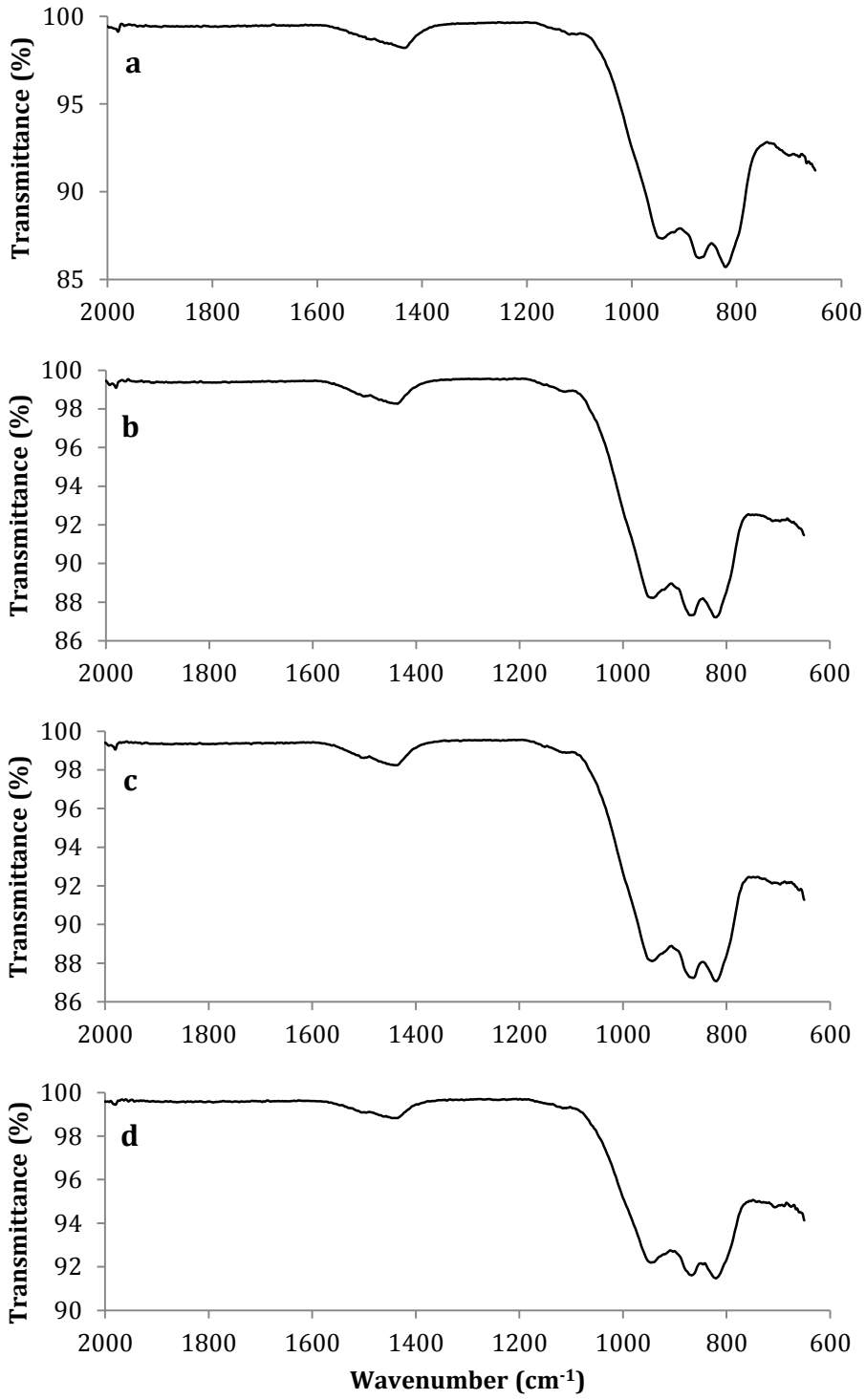

Figure 4.19 FTIR spectra of SS-C-Li_4SiO_4 sorbents with different amounts of excess lithium a) SS-C-Li_4SiO_4-0; b) SS-C-Li_4SiO_4-5; c) SS-C-Li_4SiO_4-10; d) SS-C-Li_4SiO_4-20.

Table 4.5 Absorption bands identification of SS-C-Li_4SiO_4 sorbents.

Absorption bands of sorbents (cm^{-1})				Identification
SS-C-Li_4SiO_4-0	**SS-C-Li_4SiO_4-5**	**SS-C-Li_4SiO_4-10**	**SS-C-Li_4SiO_4-20**	
	1516	1516	1516	-C=O in carbonate
1434	1443	1443	1444	
1157	1157	1155	1156	SiO_4^{4-} (orthosilicate)
1116	1115	1117	1115	
945	946	945	945	Li-O-
917	918	918	916	Si-O- in SiO_2 tetrahedral
872	872	871	871	
823	818	818	832	
701	703	702	706	SiO_3^{2-} (metasilicate)

FTIR spectra obtained for SS-R-Li_4SiO_4 and SS-F-Li_4SiO_4 sorbents showed similar patterns to that of SS-C-Li_4SiO_4 sorbents, and are included in the Appendix section at the end of this thesis (Figures A4.1 and A4.2).

Figure 4.20 shows FTIR spectra of SS-B-Li_4SiO_4 sorbents with different amounts of excess lithium a) SS-B-Li_4SiO_4-0; b) SS-B-Li_4SiO_4-5; c) SS-B-Li_4SiO_4-10; d) SS-B-Li_4SiO_4-20. Again, similar absorption bands in two different wavenumber regions can be observed in all sorbents, indicating presence of metal-oxygen bonds including Li-O- associated with Li_4SiO_4 at wavenumbers 834, 882 and 956 cm^{-1}. As

mentioned earlier, the presence of Li_2CO_3 in all sorbents could be the result of excess amounts of unreacted Li_2CO_3 added during the preparation process.

Interestingly, more intense absorption bands in the wavenumber region of 1400 and 1500 cm^{-1} are observed in SS-B-Li_4SiO_4-5, SS-B-Li_4SiO_4-10 and SS-B-Li_4SiO_4-20 sorbents (Figures 4.20b, 4.20c and 4.20d, respectively) compared to that of SS-B-Li_4SiO_4-0, as seen in Figure 4.20a. Vibration bands of -C=O (between 1443 and 1588 cm^{-1}) in CO_2 of Li_2CO_3 is thought to be the reason for the strong absorption, but Figure 4.20 also shows additional presence of other absorption bands. Table 4.6 summarises the absorption bands identification of SS-B-Li_4SiO_4 sorbents.

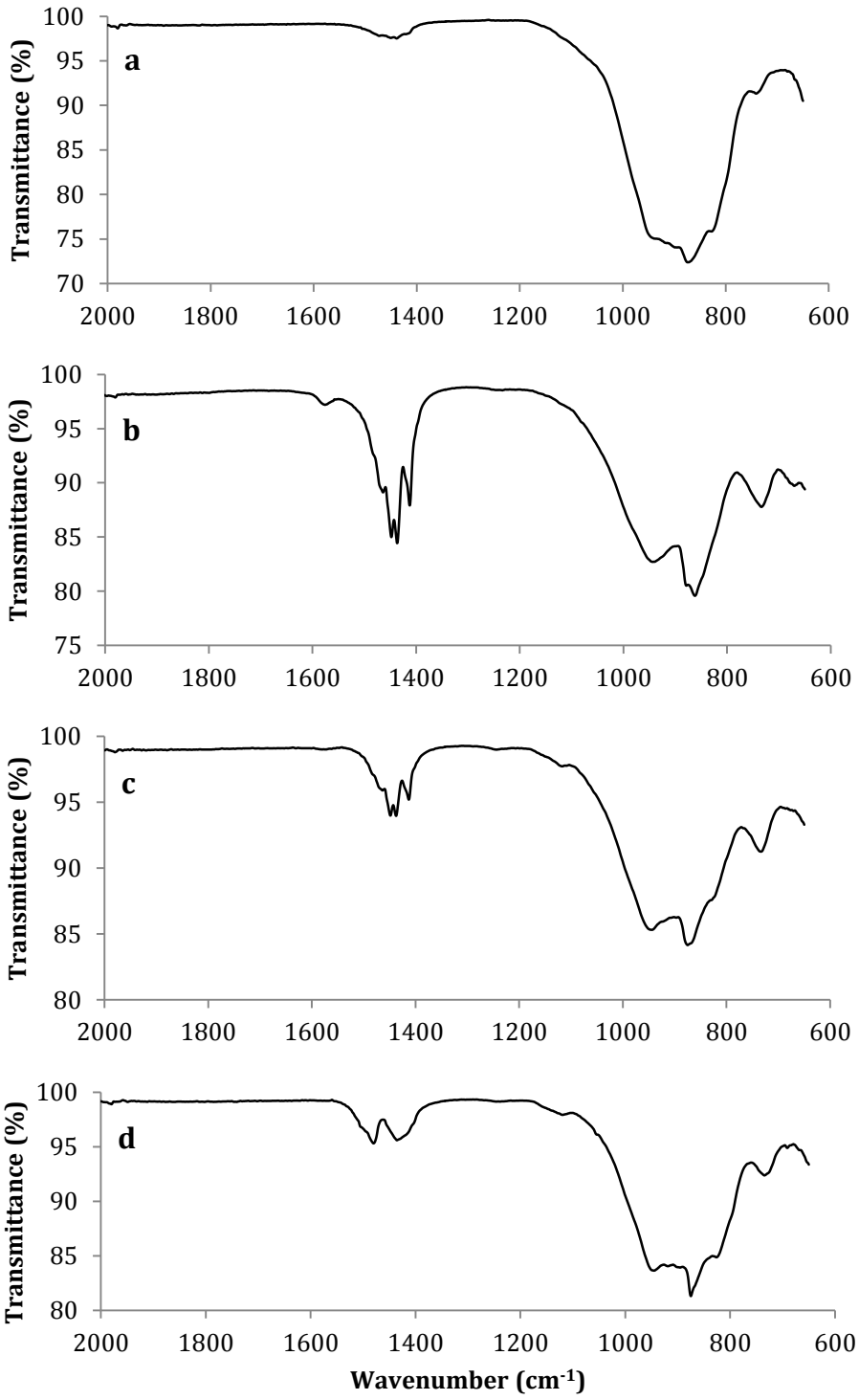

Figure 4.20 FTIR spectra of SS-B-Li_4SiO_4 sorbents with different amounts of excess lithium a) SS-B-Li_4SiO_4-0; b) SS-B-Li_4SiO_4-5; c) SS-B-Li_4SiO_4-10; d) SS-B-Li_4SiO_4-20.

Table 4.6 Absorption bands identification of SS-B-Li_4SiO_4 sorbents.

Absorption bands of sorbents (cm^{-1})				Identification
SS-B-Li_4SiO_4-0	SS-B-Li_4SiO_4-5	SS-B-Li_4SiO_4-10	SS-B-Li_4SiO_4-20	
	1573	1584	1508	-C=O
1480	1485	1487	1485	
	1457	1451	1475	
1444	1449	1449	1443	
1432	1438			
1425			1424	
1412	1414	1415	1407	
	1247	1240	1250	SiO_4^{4-} (orthosilicate)
1150	1151	1151	1152	
1117	1118	1118	1112	
			1048	
946	952	952	953	Li-O-
924	928	926	928	
881	881	880	888	Si-O- in SiO_2 tetrahedral
879	867	880	877	
835		822	822	
746	741	741	743	SiO_3^{2-} (metasilicate)
	680	682	683	CO_3^{2-} in carbonate
			674	

4.2.3. Nitrogen adsorption/desorption isotherm profiles and surface areas of Li_4SiO_4 sorbents

Figure 4.21 presents the nitrogen adsorption/desorption isotherm profiles at 77 K for a) SS-P-Li_4SiO_4-0; b) SS-P-Li_4SiO_4-5; c) SS-P-Li_4SiO_4-10 and d) SS-P-Li_4SiO_4-20. SS-P-Li_4SiO_4 sorbents exhibit isotherm profiles correlated to type II according to the IUPAC classification (IUPAC, 1985). Type II isotherm profiles are associated with non-porous or macroporous adsorbents with unobstructed monolayer/multilayer adsorption and indicated by a distinctive point in the isotherms labelled as Point B at the beginning of almost linear middle section. At this point, the monolayer coverage is complete and multilayer adsorption begins (IUPAC, 1985). The maximum volume nitrogen adsorbed by SS-P-Li_4SiO_4 sorbents ranging from 16.7 to 33.5 cm^3/g STP (Table 4.7).

The isotherm profiles of SS-P-Li_4SiO_4 also exhibit hysteresis loops type H3, which associated with assemblage of plate-like particles which are loosely coherent that caused the aggregates to develop slit-shaped pores (IUPAC, 1985). This type of hysteresis loops correspond to adsorption and desorption branches almost vertical and nearly parallel over a wide range of P/P_o and do not exhibit any limiting adsorption at high P/P_o. The resulting surface areas of the sorbents seemed to decrease with increased amounts of excess lithium, where the calculated values of BET surface areas were 8.57, 5.77, 3.14 and 1.79 m^2/g for SS-P-Li_4SiO_4-0, SS-P-Li_4SiO_4-5, SS-P-Li_4SiO_4-10 and SS-P-Li_4SiO_4-20, respectively. Similar inverse correlation between Li/Si ratio and the resulting BET surface area of sorbents has

also been reported in literature (Tang et al., 2009) and attributed to the agglomeration of individual particles causing the decrease in the overall surface area of the sorbents (Tang et al., 2009).

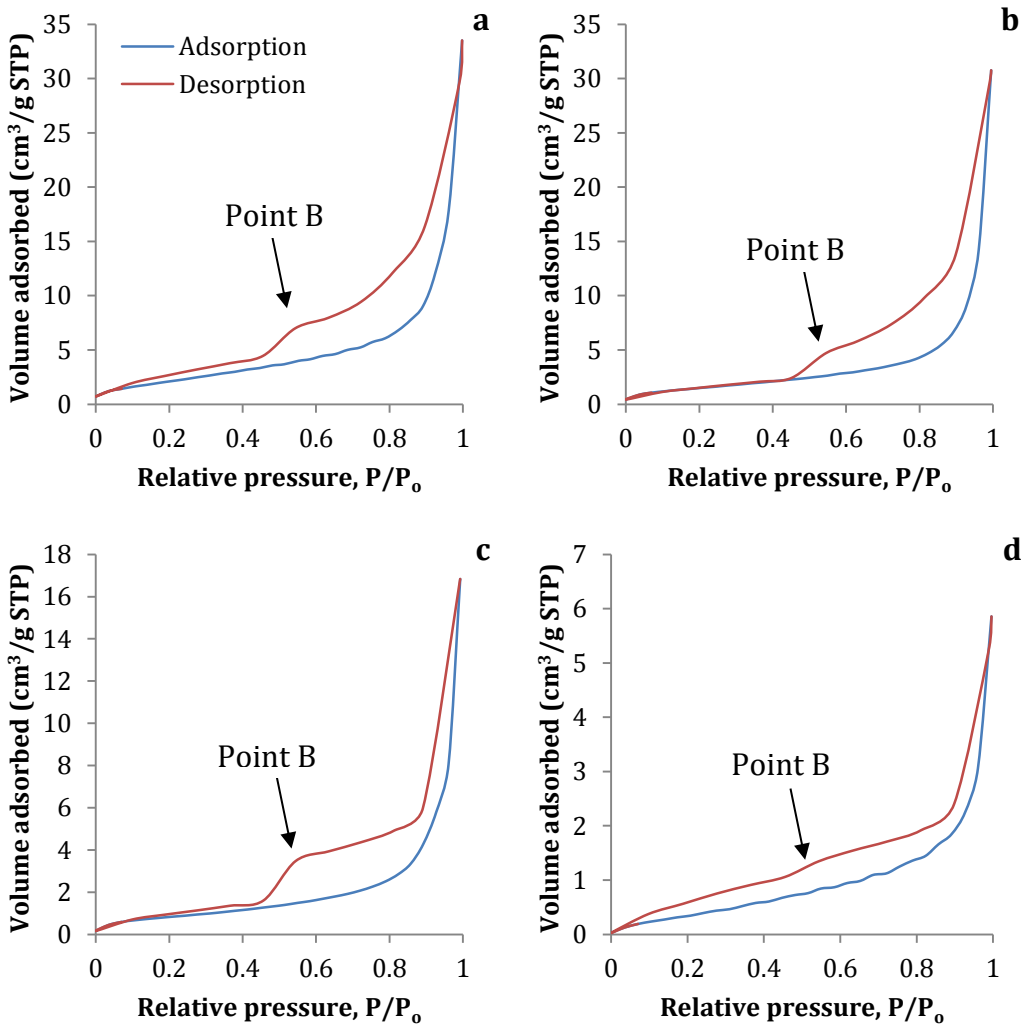

Figure 4.21 Nitrogen adsorption/desorption isotherms at 77 K for a) SS-P-Li_4SiO_4-0; b) SS-P-Li_4SiO_4-5; c) SS-P-Li_4SiO_4-10; d) SS-P-Li_4SiO_4-20.

Figure 4.22 shows the nitrogen adsorption/desorption isotherm profiles at 77 K for a) SS-C-Li_4SiO_4-0; b) SS-C-Li_4SiO_4-5; c) SS-C-Li_4SiO_4-10; d) SS-C-Li_4SiO_4-20.

Similar to SS-P-Li_4SiO_4 sorbents, SS-C-Li_4SiO_4-0 sorbent (Figure 4.22a) exhibit isotherm profile correlated to type II isotherm according to the IUPAC classification (IUPAC, 1985). Hence, it is deduced that this sorbent also is made up of non-porous or macroporous particles with unobstructed monolayer/multilayer adsorption, as indicated by a Point B at the beginning of the almost linear middle section. On the other hand, SS-C-Li_4SiO_4-5, SS-C-Li_4SiO_4-10 and SS-C-Li_4SiO_4-20 sorbents show the most prominent Point B and could indicate the least porous sorbent compared to the rest of SS-C-Li_4SiO_4 sorbents. The lack of porosity could be the reason to the low volume of nitrogen adsorbed by the sorbents, ranging from maximum volume adsorbed of 2.28 to 9.13 cm^3/g STP (Table 4.7).

The isotherm profiles of SS-C-Li_4SiO_4 sorbents also exhibit hysteresis loops type H3 which are associated with aggregates of plate-like particles developing slit-shaped pores (IUPAC, 1985). Additionally, SS-C-Li_4SiO_4-5 and SS-C-Li_4SiO_4-10 sorbents isotherm profiles show low pressure hysteresis, recognised by the extended loop to the lowest attainable pressure, as shown in Figures 4.22b and 4.22c. This phenomenon may be related to the swelling of a non-rigid porous structure exist in the waste material (IUPAC, 1985).

The resulting surface areas of the sorbents seemed to decrease with increased amounts of excess lithium, where the calculated values of surface areas were 6.2371, 0.5475, 0.9984 and 1.4558 m^2/g for SS-C-Li_4SiO_4-0, SS-C-Li_4SiO_4-5, SS-C-Li_4SiO_4-10 and SS-C-Li_4SiO_4-20, respectively (Table 4.7). As previously stated, similar inverse correlation between Li/Si ratio and the resulting surface area of

sorbents has also been reported in literature, suggesting that increase in Li/Si ratio promotes Li_4SiO_4 grain growth (Tang et al., 2009).

Contrasting SS-C-Li_4SiO_4 sorbents with the parent waste material CPFA, the textural characteristics have changed significantly following the addition of Li_2CO_3 and thermal treatment at 800 °C for 8h. Interestingly, the surface area of CPFA was temporarily improved following the addition of Li_2CO_3 and thermal treatment, but then it quickly decreased as the Li/Si ratio increased. The increase in surface area is expected, since the CPFA-Li_2CO_3 mixture was subjected to high temperature (800 °C) that may have contributed to the devolatilisation of organic constituents in CPFA that contributed to the increase in surface area. The devolatilisation of organic constituents that is believed to contribute to the increase in surface area of SS-C-Li_4SiO_4-0 sorbent supports the LOI value (4 wt%) of CPFA reported previously in section 4.1.2, confirming organic matters content in the parent waste material may cause devolatilisation.

Table 4.7 BET surface area, total pore volume and pore diameter of SS-P-Li_4SiO_4 and SS-C-Li_4SiO_4 sorbents

Sorbents	BET surface area (m^2/g)	Total pore volume x 10^{-3} (cm^3/g)	Pore diameter (nm)	Volume adsorbed (cm^3/g STP)
SS-P-Li_4SiO_4-0	8.57	50.1	13.1	33.5
SS-P-Li_4SiO_4-5	5.77	18.8	12.3	14.2
SS-P-Li_4SiO_4-10	3.14	20.9	11.2	16.8
SS-P-Li_4SiO_4-20	1.79	7.94	13.2	5.86
SS-C-Li_4SiO_4-0	6.24	8.07	4.67	5.40
SS-C-Li_4SiO_4-5	0.55	3.18	9.77	2.28
SS-C-Li_4SiO_4-10	1.00	7.19	13.8	4.80
SS-C-Li_4SiO_4-20	1.46	10.2	11.1	9.13

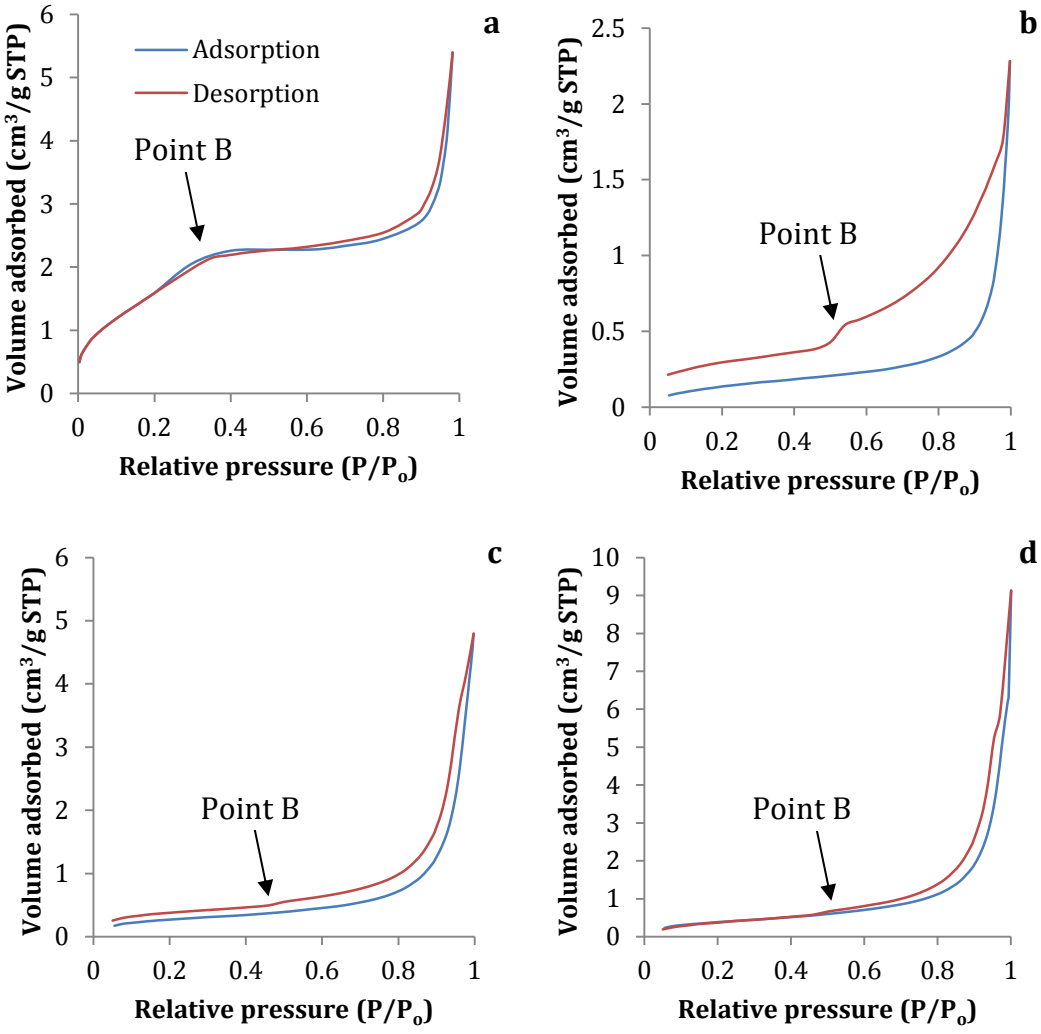

Figure 4.22 Nitrogen adsorption/desorption isotherms at 77 K for a) SS-C-Li_4SiO_4-0; b) SS-C-Li_4SiO_4-5; c) SS-C-Li_4SiO_4-10; d) SS-C-Li_4SiO_4-20.

4.2.4. Scanning electron microscope analysis of Li_4SiO_4 sorbents

Scanning electron microscope analyses were also performed to study morphological characteristics of pure and waste derived Li_4SiO_4 sorbents. Figure 4.23 shows pure SS-P-Li_4SiO_4-0 and SS-P-Li_4SiO_4-5 sorbents at 1000 and 5000 (inset figure) times magnifications. In general, the particles presented dense polyhedral morphology due to the sintering effect during the long heating process implied during preparation of the sorbents (Rodriguez-Mosqueda and Pfeiffer, 2013), having smooth surface (Figure 4.23a inset) with an average particle size of at least 5 μm, as can be observed in Figure 4.23a. These particles formed large agglomerates of around 10 μm or larger. Similar morphological descriptions of pure Li_4SiO_4 sorbents also prepared by solid state method were reported in literatures, relating the characteristics to high temperature used during the thermal treatment (Veliz-Enriquez et al., 2007; Qi et al., 2012; Seggiani et al., 2013).

Figure 4.23b shows SEM micrograph of SS-P-Li_4SiO_4-5 sorbent, in order to observe the effect of excess lithium on the texture of Li_4SiO_4 sorbent. Comparing SS-P-Li_4SiO_4-0 (Figure 4.23a) with SS-P-Li_4SiO_4-5 (Figure 4.23b), dense polyhedral particle shape can still be observed. However, the surface of pure Li_4SiO_4 sorbent with 5% excess lithium seems to exhibit surface with coarser texture than that of SS-P-Li_4SiO_4-0. This may be due to the melting of excess Li_2CO_3 with boiling point lower (628 °C) than that of synthesis temperature used in this study (800 °C).

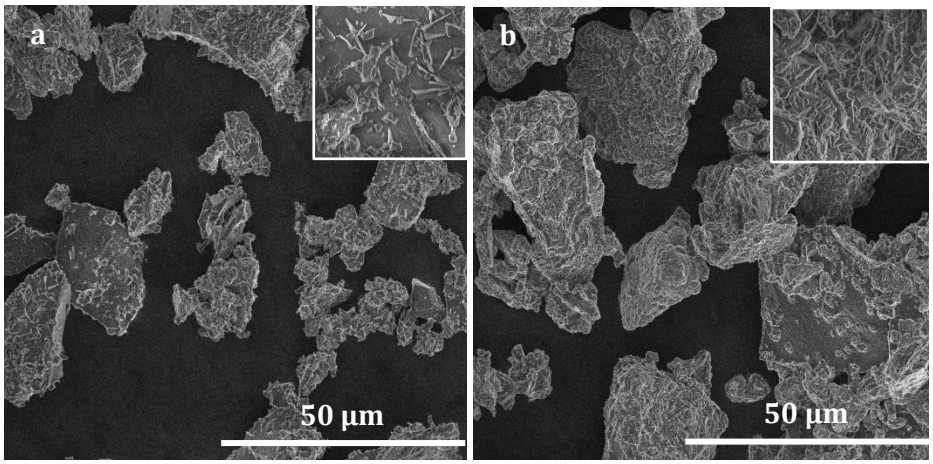

Figure 4.23 SEM micrograph of a) SS-P-Li_4SiO_4-0 and b) SS-P-Li_4SiO_4-5 sorbents.

Similar morphological characteristics to that of SS-P-Li_4SiO_4-0 sorbent can be observed in waste derived SS-C-Li_4SiO_4-0, SS-R-Li_4SiO_4-0, SS-F-Li_4SiO_4-0 and SS-B-Li_4SiO_4-0, as shown in figures 4.24a, 4.25a, 4.26a and 4.27a, respectively. All sorbents showed dense polyhedral morphology with smooth surface (insets in figures) and average particle sizes between 5 to 10 µm forming agglomerates of around 20 µm or larger. These values are larger than that of SS-P-Li_4SiO_4-0, perhaps due to the considerably smaller precursors were used in the preparation of SS-P-Li_4SiO_4-0, with SiO_2 average particle size between 5 and 15 nm.

Excess lithium added during preparation of coal-derived SS-C-Li_4SiO_4-5, SS-R-Li_4SiO_4-5 and SS-F-Li_4SiO_4-5 sorbents (Figures 4.24b, 4.25b and 4.26b, respectively) also showed coarser surface texture compared to their non-excess lithium counterparts. Again, it is believed that the excess amount of Li_2CO_3 during preparation of the sorbents melted and subsequently formed coverings of molten Li_2CO_3 on the surface of the waste-derived Li_4SiO_4 sorbents upon cooling. On the

other hand, a slightly different surface texture was observed in SS-B-Li_4SiO_4-5 sorbent (Figure 4.27b), where thread-like texture can be seen on the surface of the particles.

The particle size of resulting Li_4SiO_4 sorbents was reported to be directly related to the particle size of starting SiO_2 used in the preparation stage as SiO_2 particles remained in solid state during calcination temperature at 800 °C due to its high melting point at 1726 °C (Seggiani et al., 2013). For this reason, SiO_2 particles are strongly believed to act as cores to control the particle size of resulting Li_4SiO_4 sorbents.

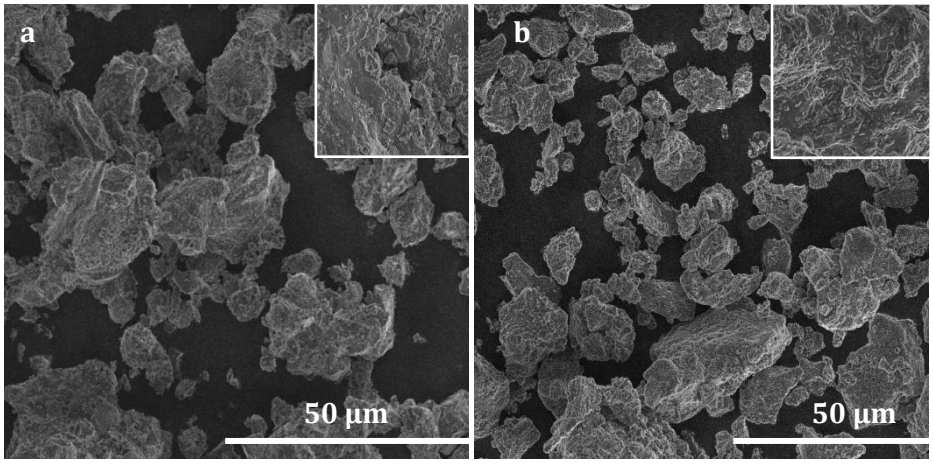

Figure 4.24 SEM micrographs of a) SS-C-Li_4SiO_4-0 and b) SS-C-Li_4SiO_4-5 sorbents.

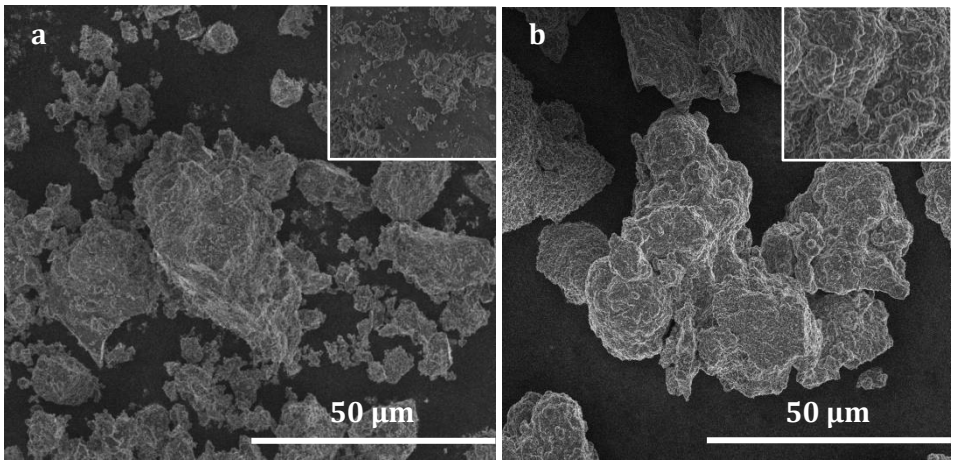

Figure 4.25 SEM micrographs of a) SS-R-Li_4SiO_4-0 and b) SS-R-Li_4SiO_4-5 sorbents.

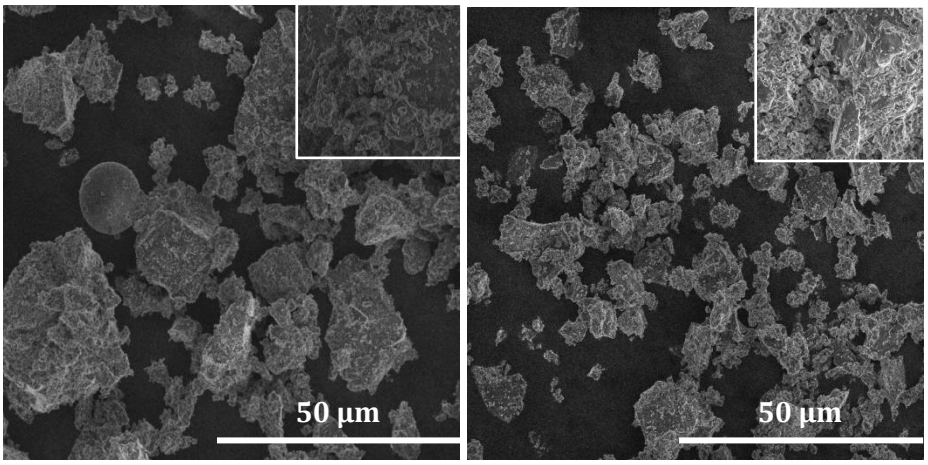

Figure 4.26 SEM micrographs of a) SS-F-Li_4SiO_4-0 and b) SS-F-Li_4SiO_4-5 sorbents.

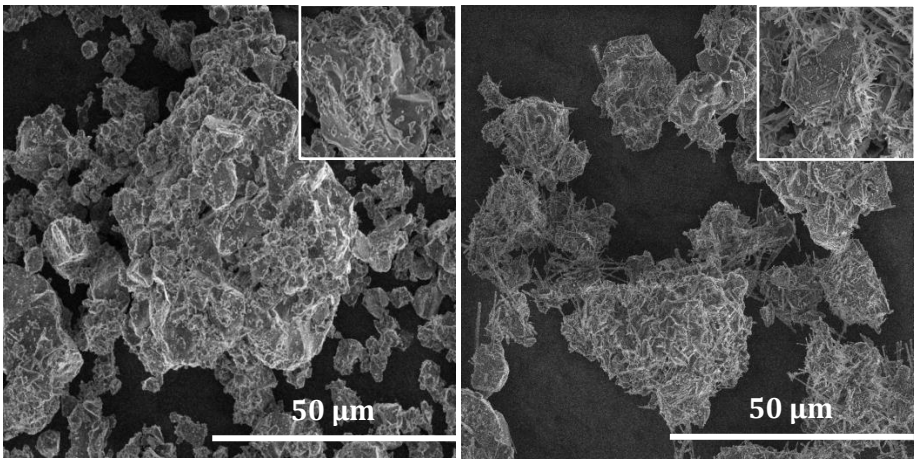

Figure 4.27 SEM micrographs of a) SS-B-Li_4SiO_4-0 and b) SS-B-Li_4SiO_4-5 sorbents.

4.3. Summary

In summary, Chapter 4 discussed the characterisation of the parent waste materials, namely, CPFA, RPFA, FBA and POMBA, used in this study (Section 4.1) and their corresponding high temperature Li_4SiO_4 sorbents (Section 4.2). A number of analytical techniques were conducted in order to study the contributing characteristics of parent waste materials and their corresponding Li_4SiO_4 sorbents that could produce high-efficient CO_2 sorbents at high sorption temperatures.

Five of these analytical techniques were conducted on four aforementioned samples of parent waste materials, including particle size distribution, major oxides composition and loss-on-ignition, phase composition, nitrogen adsorption/desorption and surface area as well as scanning electron microscopic analyses. On the other hand, four characterisation analyses were carried out on the

corresponding waste-derived Li_4SiO_4 sorbents, including mineral phase composition by XRD, Fourier transform infrared, nitrogen adsorption/desorption and surface area and scanning electron microscopic analyses.

Particle size distribution analysis of the parent waste materials revealed varying particle sizes across samples, although they can be classified according to their apparent difference in particle sizes i.e. fly ash CPFA and RPFA samples having average diameter between 13 and 41 μm, and bottom ash FBA and POMBA samples having average size (D(0.5) value) between 182 and 240 μm. Small particle sizes of parent waste materials could have an advantage over larger ones due to larger surface area can be provided for the resulting Li_4SiO_4 sorbents for the CO_2 sorption to take place.

Nevertheless, particle sizes of precursors alone cannot be used to predict CO_2 capture performance. The chemical composition and the loss-on-ignition (LOI) values of the materials also need to be taken into consideration. The samples followed decreasing order of LOI value as follows: FBA (8.47 wt%)>POMBA (8.12 wt%)>RPFA (4.09 wt%)>CPFA (4 wt%). Although the LOI values of the parent waste materials may not directly correlate with the CO_2 uptake performance of the resulting Li_4SiO_4 sorbents, they could affect the production performance of the

sorbents due to the preparation of the sorbents requires calcination at 800 °C (Section 3.2.1).

In addition, the chemical compositions of the parent waste materials also need to be taken into consideration. X-ray fluorescence analyses were carried out on all parent waste materials to identify their chemical compositions. The results showed that all materials used in this study contain significant amounts of component of interest, SiO_2, where its content exceeding 47 wt% in all samples. High amount of SiO_2 in waste materials is essential in order to ensure maximum possible content of Li_4SiO_4 was calcined using the waste materials and therefore, maximising the amount of CO_2 uptake by the sorbents. At least 47 wt% of SiO_2 content found in all parent waste materials was deemed to be suitable for a development of high temperature Li_4SiO_4-base sorbents.

The unavoidable presence of other oxides in the parent waste materials is expected to affect the performance of CO_2 uptake by waste-derived Li_4SiO_4 sorbents. As previously explained in subsection 4.1.2, the presence of other elements, such as Al, Fe and Na, into Li_4SiO_4-based sorbents could affect their CO_2 uptake performances. Based on the amounts of these elements found in their oxides form in the parent waste materials, it is expected that the reactivity

performance of CO_2 capture by the Li_4SiO_4-based sorbents developed using these materials would be improved, in comparison to the pure Li_4SiO_4 sorbents.

Phase composition analyses (subsection 4.1.3) were carried out on all parent waste materials as well as the resulting waste-derived Li_4SiO_4 sorbents. It was found that quartz was the main phase of SiO_2 in all coal-derived ash samples, in addition to aluminosilicates such as mullite and sillimanite. Moreover, there were also some amorphous phases detected in the diffractograms, indicating coexistence of amorphous constituents, such as the aluminosilicates, in parent waste materials. In the waste-derived Li_4SiO_4 sorbents (subsection 4.2.1), these crystalline and amorphous constituents were converted into mainly Li_4SiO_4 crystals, following the addition of Li_2CO_3 during calcination process. Other constituents also found in the sorbents including $LiAlO_2$, Li_2SiO_3 and $LiAlSiO_4$, resulting from the aluminosilicates discovered in the parent waste materials.

There were still some amorphous peaks detected in the waste-derived Li_4SiO_4 sorbents, compared to none found in the pure Li_4SiO_4 sorbents. The amorphous phase found in the waste-derived Li_4SiO_4 sorbents could be advantageously affecting the CO_2 uptake performance of the sorbents, due to the versatility of amorphous structure in capturing CO_2 molecules. In comparison to the more ordered structure of its crystalline counterpart which is predominantly found in pure Li_4SiO_4 sorbents, the coexistence of amorphous Li_4SiO_4 could increase the CO_2

sorption capacity of the waste-derived sorbents (Sadoway, 2010). Furthermore, the diffusion of molecules into amorphous structure is faster than that in crystalline due to the atomic disorder (Sadoway, 2010), and therefore, potentially increasing the rate of CO_2 sorption of the sorbents.

Chapter 5 CO_2 capture by waste-derived Li_4SiO_4 sorbents

This chapter discusses the CO_2 capture studies of parent waste materials and waste-derived Li_4SiO_4 sorbents at different sorption temperatures (500, 600, 700 °C). Firstly, section 5.1 examines the relative CO_2 uptake capacities by parent waste materials in pure (100 vol%) CO_2 environment. Section 5.2 discusses the CO_2 uptake capacities by waste-derived Li_4SiO_4 sorbents in pure and diluted (14 vol%, balance N_2) CO_2 environments. Subsequently, section 5.3 presents the regeneration studies of the sorbents in multiple cycles, also in pure and diluted CO_2 environments. Finally, section 5.4 summarises the CO_2 capture studies for all materials and correlates their capacities with the physico-chemical characteristics of the sorbents reported in Chapter 4.

5.1. CO_2 uptake by parent waste materials

Thermogravimetric analyses (TGA) were conducted on all as-received parent waste materials in pure (100 vol%) CO_2 environment at 500, 600 and 700 °C for 120 minutes. As previously mentioned in Chapter 3, the analysis duration of 120 minutes was conducted to allow sufficient time for CO_2 sorption to take place. It is also worthy to note that the parent waste materials were not subjected to any pre-treatment method before the CO_2 uptake analysis. This provides 'raw' CO_2 uptake capacity of waste materials prior to calcination process and also serves as the benchmark values for the progress of subsequent modification of the materials.

Figure 5.1 shows TGA weight change profiles of CPFA at 500, 600 and 700 °C in CO_2 environment. In general, the weight of the parent waste material CPFA is observed to be progressively increasing with temperature, depending on the residence time. At 500 °C, the weight gradually increased until it reached the end of analysis. On the other hand at 600 °C, the weight change profile presents a peak at approximately between 50 and 90 minutes into the analysis, before rapidly decreasing afterwards. Similar trend can be observed at 700 °C, where a sharper peak is observed at about 55th minute of analysis duration and the decrease is faster than that observed at 600 °C.

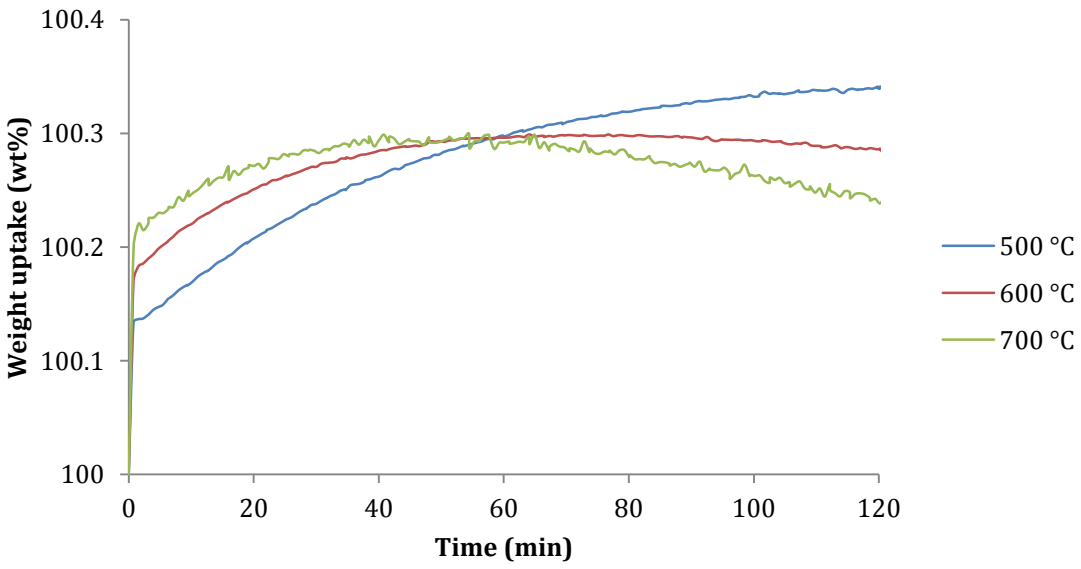

Figure 5.1 Isothermal weight uptake profiles of CPFA at 500, 600 and 700 °C in pure CO_2 environment.

The peaking behaviour shown by CPFA is believed to be caused by the instability of the material when it is being subjected to high sorption temperatures, as shown in

Figure 5.1. In order to verify this theory, additional experiments were carried out under N_2 flow in isothermal conditions at 500, 600 and 700 °C (Figure 5.2). It is apparent that the decrease in weight percentage of the material became more pronounced as the temperature increased. This indicates that the degree of instability of the material is strongly affected by the temperatures investigated in this study. This observation corroborates the peaking behaviour (Figure 5.1), where the weight of CPFA was observed to have the most prominent decrease at 700 °C.

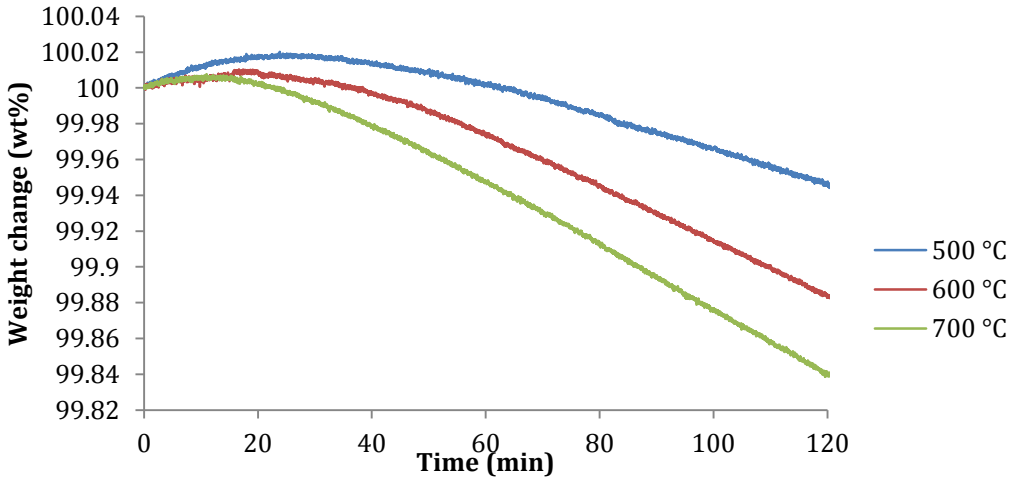

Figure 5.2 Thermal stability of CPFA in N_2 environment at isothermal conditions (500, 600 and 700 °C).

Figure 5.3 shows TGA weight change profiles of RPFA at 500, 600 and 700 °C in CO_2 environment. It is observed that the weight change profiles of RPFA progressively increasing with temperature throughout the analysis duration. At 500 °C, the weight gradually increased until it reached the end of analysis. Similar trend is observed at 600 °C with an increased in overall weight change. However

at 700 °C, a mild peaking behaviour is detected approximately between 50 and 75 minutes into the analysis.

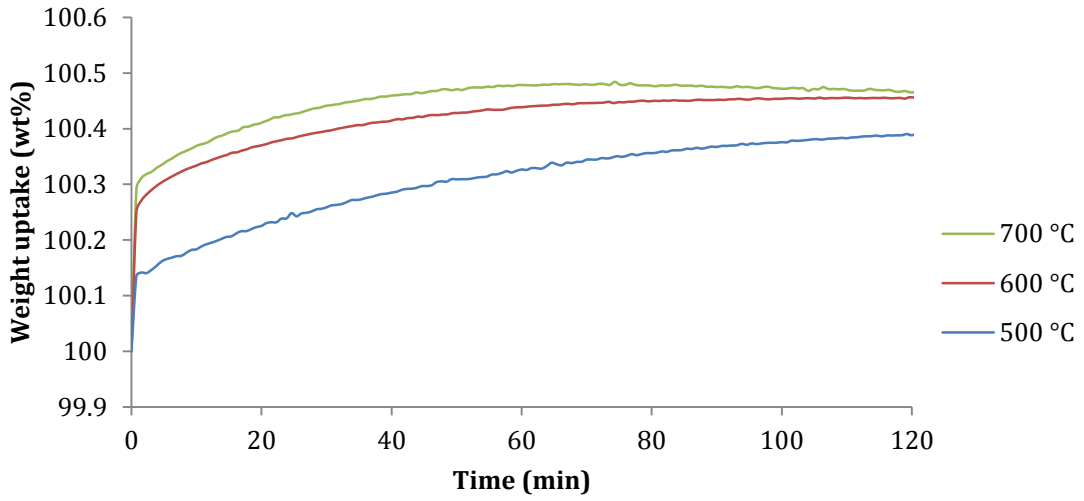

Figure 5.3 Isothermal weight change profiles of RPFA at 500, 600 and 700 °C in pure CO_2 environment.

Again, it is believed that the peaking behaviour was caused by the instability of the material at high temperatures. Therefore, additional experiments were carried out under N_2 flow in isothermal conditions at 500, 600 and 700 °C (Figure 5.4). A similar profile to CPFA (Figure 5.2) was also observed in RPFA (Figure 5.4), where the weight of the parent waste material decreased as the temperature increased. This observation corroborates the peaking behaviour (Figure 5.3), where the weight of RPFA was observed to have the most prominent decrease at 700 °C.

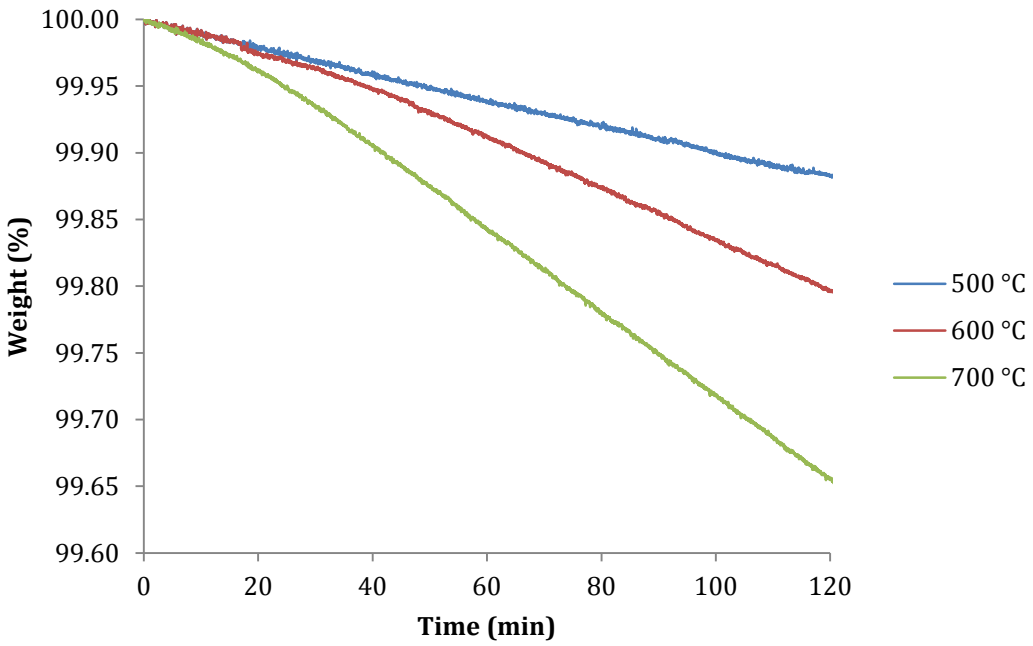

Figure 5.4 Thermal stability of RPFA in N_2 environment at isothermal conditions (500, 600 and 700 °C).

In order to determine the overall amount of CO_2 uptake by the parent waste materials, weight change due to the instability of the material needs to be accounted for by subtracting the weight change of the material under N_2 flow from that of CO_2 analysis. The overall amount of CO_2 uptake by all parent waste materials at isothermal conditions are summarised in Table 5.1.

Table 5.1 Weight changes in pure CO_2 and N_2, as well as overall CO_2 sorption of parent waste materials at 500, 600 and 700 °C. The overall CO_2 sorption was calculated by subtracting the weight decrease in N_2 from the weight uptake in pure CO_2. The overall CO_2 uptake values are also converted into mg/g for ease of comparison in later discussions.

Waste material	Temperature (°C)	Weight uptake in CO_2 (wt%)	Weight decrease in N_2 (wt%)	Overall CO_2 uptake	
				(wt%)	(mg/g)
CPFA	500	0.34	0.07	0.27	2.70
	600	0.30	0.13	0.17	1.70
	700	0.29	0.16	0.13	1.30
RPFA	500	0.39	0.12	0.27	2.70
	600	0.46	0.19	0.27	2.70
	700	0.48	0.34	0.14	1.40
FBA	500	0.30	0.21	0.09	0.90
	600	0.52	0.27	0.25	2.50
	700	0.66	0.29	0.37	3.70
POMBA	500	0.32	0.23	0.08	0.80
	600	0.53	0.27	0.26	2.60
	700	0.58	0.26	0.32	3.20

In general, overall CO_2 uptake capacities are all less than 4 mg CO_2/g sorbent. The CO_2 uptake values by waste materials are significantly lower than that of commercially available solvents (approximately 176 mg CO_2/g sorbent) (Samanta et al., 2012). This proves unsuitability of the waste materials as CO_2 sorbents if they were to be used without any treatment.

Most of the parent waste materials (RPFA, FBA and POMBA) show an increasing uptake with increased sorption temperatures during the 120 minutes of analysis. After taking into account the instability factor of the parent waste materials, FBA

showed the highest overall CO_2 uptake capacity of 3.70 mg CO_2/g sorbent at 700 °C. This is then followed by POMBA, with maximum overall CO_2 uptake capacity of 3.20 mg CO_2/g sorbent, also at 700 °C. RPFA showed similar trend of increasing weight uptake capacity in CO_2 environment, analogous to FBA and POMBA. However, the trend changed after taking into account the instability factor of the parent waste material in N_2 environment. The maximum overall CO_2 uptake capacity of RPFA was calculated to be 2.70 mg CO_2/g sorbent at 500 °C.

On the other hand, CPFA shows inverse correlations between CO_2 uptake capacity and sorption temperature before and after taking into account the instability factor, with highest overall CO_2 uptake capacity of 2.70 mg CO_2/g sorbent at 500 °C. The maximum CO_2 uptake capacities of parent waste materials exhibited a direct correlation with LOI values, as showed previously in Table 4.2 (8.47 wt% for FBA, 8.12 wt% for POMBA, 4.09 wt% for RPFA and 4.00 wt% for CPFA). The amounts of maximum CO_2 capacities decreased with decreasing LOI values of the materials, according to descending order of LOI values: FBA>POMBA>RPFA>CPFA.

Analysing the results from a wider point of view, several factors could contribute to the generally low CO_2 uptake by parent waste materials. These include low surface area due to dense textural characteristics, as discussed in Chapter 4. There is also the possibility that the CO_2 uptake capacity of parent waste materials is contributed by the reaction between CO_2 molecules and metal oxides present on the surface of the waste materials. Pure metal oxides such as MgO and CaO are known to chemically absorb CO_2 at elevated temperatures of higher than 400 °C

(Martavaltzi and Lemonidou, 2008; Hassanzadeh and Abbasian, 2010) producing $MgCO_3$ and $CaCO_3$, respectively. Significantly low concentrations (<10 wt%) of these metal oxides in waste materials, also as reported in Chapter 4, is deemed to be key reason for the low CO_2 uptake.

Table 5.2 shows the correlations between the maximum CO_2 uptake capacities by waste materials and their total concentrations of CaO and MgO at 500, 600 and 700 °C. At 500 °C, the CO_2 uptake capacities of fly ashes CPFA and RPFA decreased with decreasing amounts of CaO and MgO. Interestingly, it does not seem to be the case for the bottom ashes FBA and POMBA, where the CO_2 uptake capacities decreased with increasing amounts of CaO and MgO. While it is expected that the CO_2 uptake capacities of the waste materials to have a direct correlation with the amount of CaO and MgO because of their ability to chemically absorb CO_2 at high temperatures, it is not expected for these two parameters to have an inverse correlation. A possible explanation for this observation could be contributed by the significantly larger particle sizes of the bottom ash waste materials compared to the fly ash ones, causing less CO_2 captured by FBA and POMBA within the same analysis duration of 120 minutes. Higher sorption temperature could improve CO_2 uptake by FBA and POMBA, since CO_2 sorption of CaO and MgO chemically motivate on thermal energy.

However at 600 °C, an increasing trend of this correlation is observed, where the CO_2 uptake capacity increased as a function of MgO and CaO concentrations in the waste materials. The descending order of CO_2 uptake capacities by the waste

materials corresponds well with the descending order of CaO and MgO amounts, to follow POMBA>FBA>RPFA>CPFA order. It is also observed that the amount of CO_2 captured by waste materials increased compared to that at 500 °C. This observation seems to verify the suggestion that an increase in sorption temperature was needed to further promote the chemical sorption of CO_2 by the waste materials.

This is particularly valid when there is a significant amount of unburnt carbon present in the waste materials. Activation process is performed on waste materials to further increase their surface areas in order to provide more areas for CO_2 capture via physical adsorption, while the surface of the sorbents is chemically modified to increase the attraction of the surface of the sorbents to the CO_2 molecules, and therefore, improving the overall uptake. These low temperature sorbents are known to have higher (69.5 mg CO_2/g sorbent) CO_2 uptake at much lower sorption temperatures (30 °C) (Maroto-Valer et al., 2008). This is heavily influenced by their ability to perform physical adsorption at lower temperature rather than chemical absorption at higher temperatures.

Table 5.2 Correlations between the amounts of CaO + MgO and CO_2 uptake capacities by waste materials at 500, 600 and 700 °C.

500 °C	Maximum CO_2 uptake capacity (mg CO_2/g sorbent)	3.94 > 3.41 > 2.98 > 2.31
	CaO + MgO (wt%)	7.04 > 5.83 < 7.21 < 10.24
	Waste materials	RPFA > CPFA < FBA < POMBA
	LOI values (wt%)	(4.09) (4.00) (8.47) (8.12)
600 °C	Maximum CO_2 uptake capacity (mg CO_2/g sorbent)	5.26 > 5.18 > 4.60 > 3.00
	CaO + MgO (wt%)	10.24 > 7.21 > 7.04 > 5.83
	Waste materials	POMBA > FBA > RPFA > CPFA
	LOI values (wt%)	(8.12) (8.47) (4.09) (4.00)
700 °C	Maximum CO_2 uptake capacity (mg CO_2/g sorbent)	6.61 > 5.76 > 4.79 > 2.96
	CaO + MgO (wt%)	7.21 < 10.24 > 7.04 > 5.83
	Waste materials	FBA < POMBA > RPFA > CPFA
	LOI values (wt%)	(8.47) (8.12) (4.09) (4.00)

5.2. CO_2 uptake by waste-derived Li_4SiO_4 sorbents

This section investigates the CO_2 uptake capacities by sorbents under pure and diluted CO_2 environments by studying the weight change of the sorbents in a thermogravimetric analyser. CO_2 uptake capacities by sorbents are presented as curves of weight of CO_2 captured in mg per unit g of sorbent versus the analysis duration of 120 minutes. As mentioned in Section 3.2, all of waste-derived Li_4SiO_4 sorbents were prepared with excess amount of lithium due to the tendency of lithium to sublimate at temperatures higher than 710 °C during calcination of the sorbents (Lu and Wei-Cheng, 2000).

However, there is no published study on the specific amount of excess lithium recommended, as well as the effect of excess lithium on CO_2 uptake capacity of Li_4SiO_4 sorbents. Therefore, all sorbents synthesised in this research were prepared with different amounts of excess lithium (5%, 10%, and 20%) in order to study its effect on CO_2 uptake capacities of sorbents. Excess lithium is the amount of additional lithium added to the stoichiometric ratio of Li_4SiO_4. Li_4SiO_4 sorbents with no excess lithium (0%) were also prepared to establish benchmark sorption performance of the sorbents for comparison purposes.

5.2.2. CO_2 uptake by sorbents in pure CO_2 environment

Figure 5.5 shows the isothermal CO_2 uptake profiles of a) SS-P-Li_4SiO_4-0; b) SS-P-Li_4SiO_4-5; c) SS-P-Li_4SiO_4-10; d) SS-P-Li_4SiO_4-20 sorbents in pure CO_2 environment. There appears to be a direct correlation between the CO_2 uptake performance by the sorbents and the sorption temperatures throughout the duration of analysis. All sorbents captured the lowest amount of CO_2 at 500 °C and the highest at 700 °C, with intermediate amount of captured CO_2 at 600 °C.

The direct correlation between the amount of CO_2 uptake and sorption temperature can be explained using the double shell mechanism (Figure 5.6), whereby superficial chemical sorption occurs between CO_2 and Li^+ and O^{2-} ions to form external Li_2CO_3 and Li_2SiO_3 shells over Li_4SiO_4 particles at lower temperature (500 °C) (Essaki et al., 2005; Duran-Munoz et al., 2013). Diffusion is then promoted as the sorption temperature increases, allowing Li^+ and O^{2-} ions on the

bulk of Li_4SiO_4 particle to diffuse through the double shells and react with more CO_2 molecules (Essaki et al., 2005; Duran-Munoz et al., 2013). The direct correlation between CO_2 uptake capacity of waste-derived Li_4SiO_4 sorbents and sorption temperature is also in good agreement with previous studies which reported similar trend (Olivares-Marin et al., 2010; Wang et al., 2011).

Figure 5.5 also shows an increase in sorption rate as the sorption temperature increased, as indicated by the slope of the CO_2 uptake capacity at the beginning of analysis duration. This could be explained again due to increased diffusion, resulting in faster sorption rate compared to that at lower sorption temperature. The CO_2 uptake capacity of SS-P-Li_4SiO_4 sorbents did not reach sorption equilibrium in all cases, indicating substantially longer sorption time (>120 minutes) is needed by SS-P-Li_4SiO_4 sorbents to achieve sorption equilibrium.

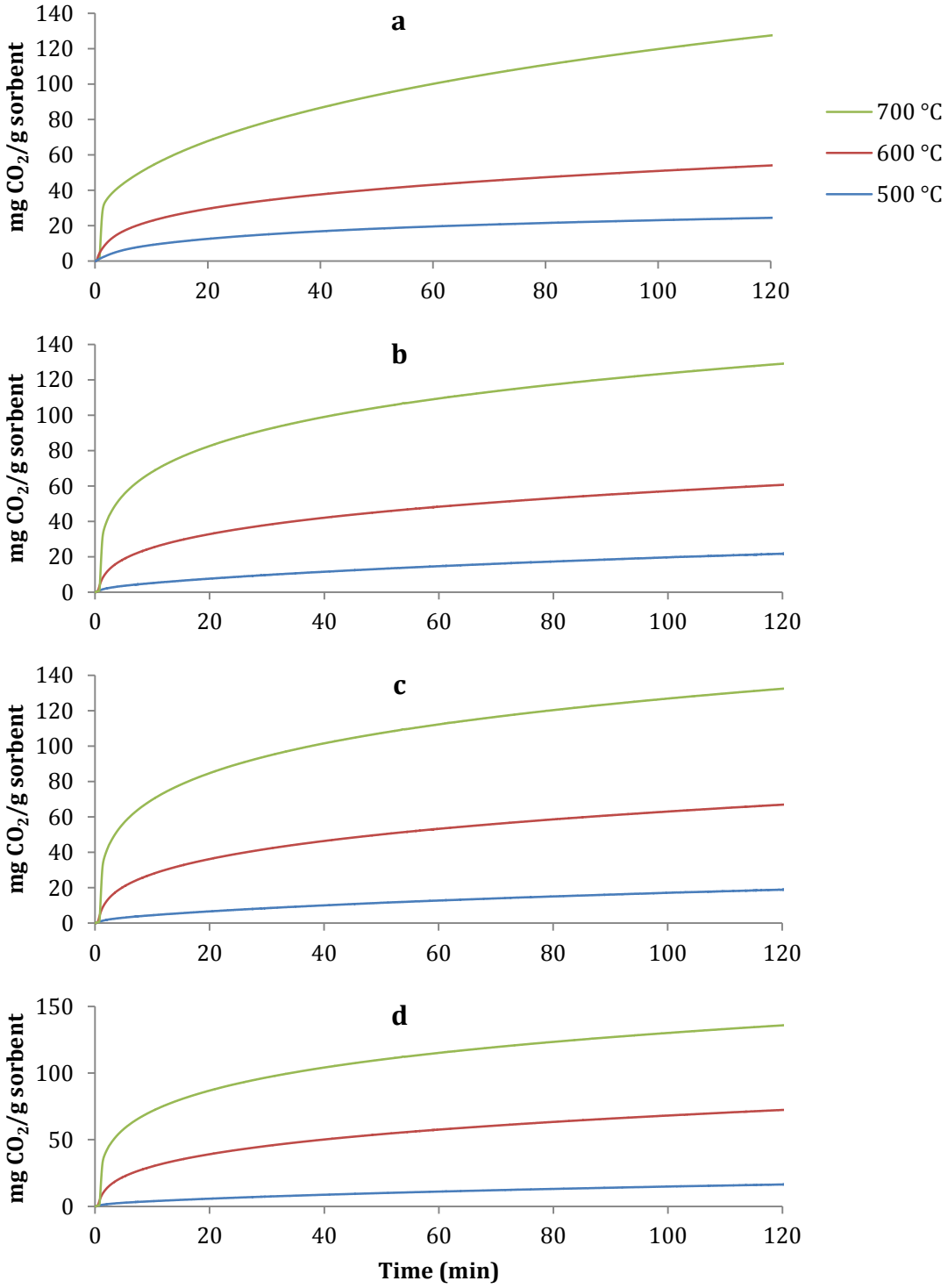

Figure 5.5 Isothermal CO_2 uptake profiles of a) SS-P-Li_4SiO_4-0; b) SS-P-Li_4SiO_4-5; c) SS-P-Li_4SiO_4-10; d)SS-P-Li_4SiO_4-20 sorbents in pure CO_2 environment.

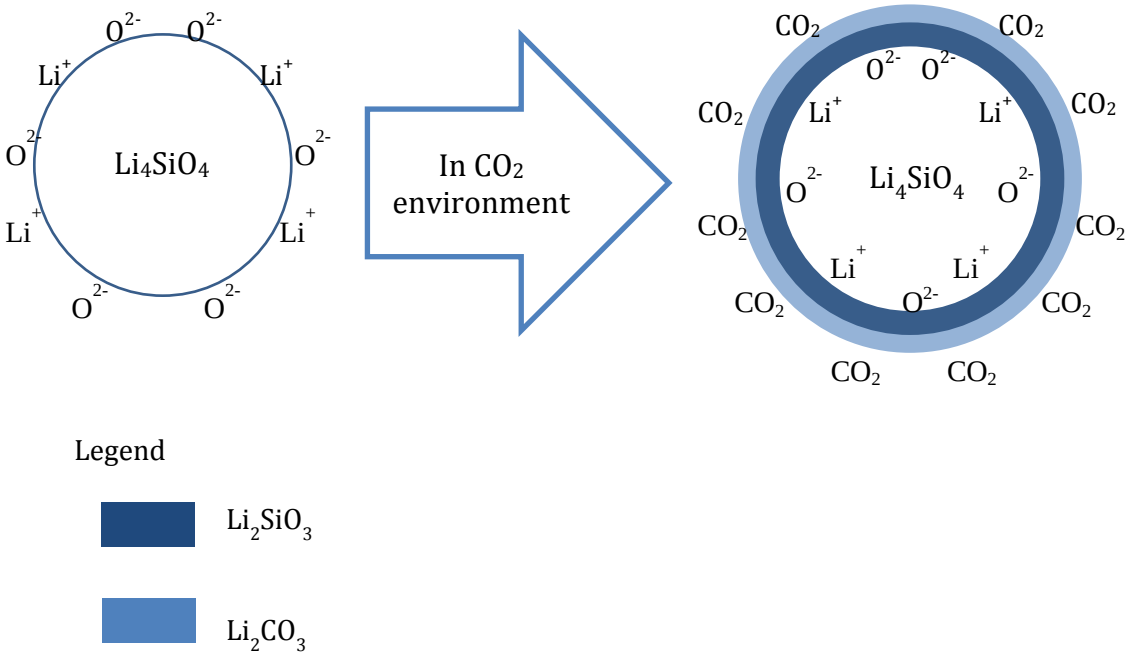

Figure 5.6 Li_4SiO_4 double shell mechanism, adapted from Essaki et al. (2005).

Table 5.3 shows the CO_2 uptake capacity of SS-P-Li_4SiO_4 sorbents with different amounts of excess lithium at sorption temperatures 500, 600 and 700 °C in pure CO_2 environment at different times (30 and 120 minutes) during the analysis. It is observed that the CO_2 uptake capacity of SS-P-Li_4SiO_4 sorbents peaks at sorption temperature of 700 °C (135.8 mg CO_2/g sorbent) by SS-P-Li_4SiO_4-20 sorbent, while the lowest uptake capacity was observed by SS-P-Li_4SiO_4-0 sorbent at 500 °C with 24.47 mg CO_2/g sorbent captured. At 500 °C, the CO_2 uptake capacity of SS-P-Li_4SiO_4 sorbents decreased with increasing amounts of excess lithium. However at 600°C, an increasing trend of overall maximum CO_2 uptake capacity of sorbents

can be observed. Similarly, increased amount of maximum CO_2 uptake capacity as a function of amounts of excess lithium is observed at 700 °C.

The addition of excess amounts of lithium seems to inhibit CO_2 uptake by SS-P-Li_4SiO_4-0 sorbent at lower sorption temperature (500 °C) (Table 5.3). It is assumed that there is insufficient thermal energy provided at this temperature to fully activate the diffusion of CO_2 through the bulk of Li_4SiO_4 particles, and therefore, the addition of excess lithium inhibits the overall sorption process. A chemical reaction can be determined if it is thermodynamically favourable by obtaining the Gibbs free energy change (ΔG) of that particular process. ΔG of a reaction is factored in by the heat of reaction (ΔH) and the multiplication product of temperature and entropy (ΔS) in the following relationship $\Delta G = \Delta H - T\Delta S$. This shows that the temperature directly affects the thermodynamic spontaneity of that chemical reaction, which is measured by the negativity of ΔG value. Essaki et al. (2006) reported ΔG value for CO_2 absorption by Li_4SiO_4 sorbent to have negative values up to 720 °C, when ΔG values start to show positive values, indicating desorption of CO_2 occurs (Essaki et al., 2006).

Hence, additional thermal energy provided at sorption temperature higher than 500 °C causes the ΔG value of CO_2 sorption on Li_4SiO_4 to be smaller (more negative) than at 500 °C, and therefore, permitting Li_4SiO_4 to capture more CO_2. As the sorption temperature increased to 600 and 700 °C, it is assumed that there is enough thermal energy to completely activate the diffusion process. The subsequent addition of excess amounts of lithium that previously acted as inhibitor

now facilitates the sorption process instead, resulting in an increase in CO_2 uptake capacities by sorbents.

Comparing the amount of CO_2 uptake by SS-P-Li_4SiO_4 sorbents with that of published studies, Olivares-Marin et al, (2010) reported higher capacity of a pure Li_4SiO_4 sorbent. For example at 500 °C, a pure Li_4SiO_4 sorbent captured approximately 50 mg CO_2/g sorbent in analysis duration of 60 minutes (Olivares-Marin et al., 2010). It is worthy to note that although solid-state reaction was applied, excess amount of lithium was not added during the preparation of pure Li_4SiO_4 sorbent in that study (Olivares-Marin et al., 2010). The CO_2 uptake capacity obtained in that study was two times higher than the amount of CO_2 captured by SS-P-Li_4SiO_4-0 sorbent at the same sorption temperature in longer sorption time (120 minutes). In addition, the sorbent was calcined at 950 °C for 8h (Olivares-Marin et al., 2010), as opposed to 800 °C for 8h in this study. Hence, the difference in sorbent calcination conditions and preparation method was believed to be the reason for the discrepancy in the amount of CO_2 uptake capacities of pure Li_4SiO_4 sorbents in both studies.

Table 5.3 CO_2 uptake capacity by SS-P-Li_4SiO_4 sorbents with different amounts of excess lithium at isothermal sorption conditions in pure CO_2 environment.

Amount of excess lithium (%)	Sorption temperature (°C)	CO_2 uptake capacity (mg CO_2/g sorbent)	
		30 min	120 min
0	500	14.99	24.47
5		9.694	21.68
10		8.441	18.87
20		7.325	16.38
0	600	34.13	54.02
5		37.99	60.59
10		41.92	66.87
20		45.32	72.29
0	700	78.11	127.4
5		91.98	129.1
10		94.34	132.4
20		96.76	135.8

Figure 5.7 presents the isothermal CO_2 uptake profiles of a) SS-C-Li_4SiO_4-0; b) SS-C-Li_4SiO_4-5; c) SS-C-Li_4SiO_4-10 and d) SS-C-Li_4SiO_4-20 sorbents in pure CO_2 environment. Generally, CO_2 uptake profiles of SS-C-Li_4SiO_4 exhibit similar trend as that of SS-P-Li_4SiO_4, where the uptake capacity increased as a function of sorption temperature. All sorbents captured the lowest amount of CO_2 at 500 °C and the highest at 700 °C, with intermediate amount of captured CO_2 at 600 °C.

The CO_2 uptake profile of SS-C-Li_4SiO_4-0 at 700 °C displays a horizontal line of uptake from minute 15 until the end of analysis duration, indicating that the sorbent is saturated with CO_2 and has reached sorption equilibrium. CO_2 uptake capacities by other SS-C-Li_4SiO_4 sorbents did not display sorption equilibrium

during analysis duration, probably due to the incomplete diffusion process, as indicated by the slower sorption rate towards the end of the analysis duration. Therefore, longer time is needed for the sorbents to reach saturation. Also similar to SS-P-Li_4SiO_4 sorbents, different amounts of excess lithium added during preparation stage did not seem to affect the sorption temperature at which the CO_2 uptake capacity of SS-C-Li_4SiO_4 sorbents is optimal i.e. at 700 °C.

Comparing the CO_2 uptake trend of the waste-derived SS-C-Li_4SiO_4 sorbents prepared in this study with that published by Wang et al. (2011), it can be seen that the samples presented a similar trend, where the CO_2 uptake of a rice husk-derived RHA1-Li_4SiO_4 sorbent increased with sorption temperatures (Wang et al., 2011). It is worthy to note that during preparation of the sorbent, excess amount of lithium (10%) was added in the solid-state reaction preparation method before being subjected to thermal treatment at 800 °C for 4h. Evaluating the CO_2 uptake trend by SS-C-Li_4SiO_4-10 with that of RHA1-Li_4SiO_4 sorbent, a similar trend is observed, where no sorption equilibrium was achieved at sorption temperatures of 500 and 600 °C (Wang et al., 2011). CO_2 uptake capacity analysis by RHA1-Li_4SiO_4 sorbent was not reported isothermally at 700 °C, and therefore, the uptake trend could not be compared with that of SS-C-Li_4SiO_4-10 sorbent in this study.

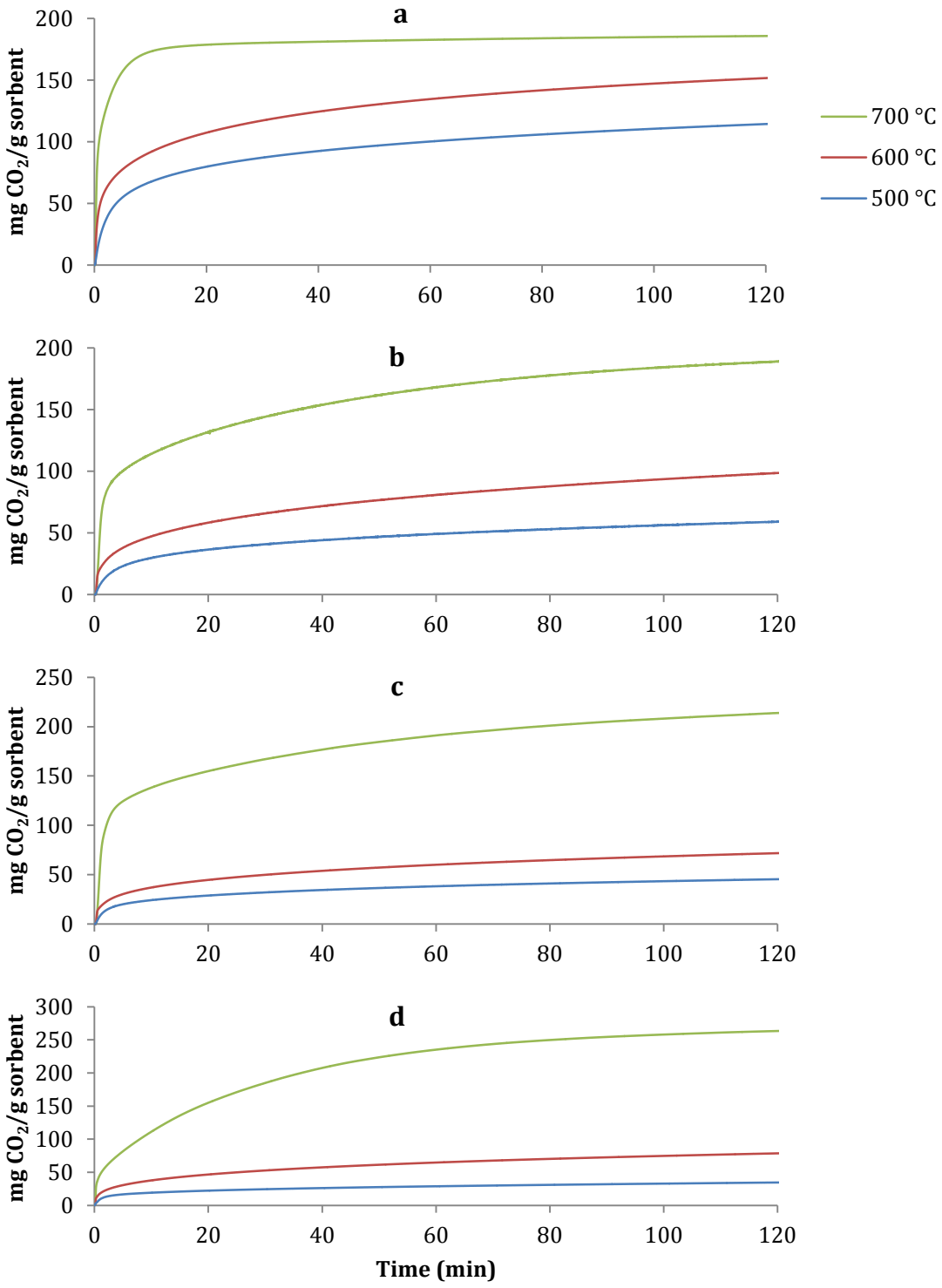

Figure 5.7 Isothermal CO_2 uptake profiles by a) SS-C-Li_4SiO_4-0; b) SS-C-Li_4SiO_4-5; c) SS-C-Li_4SiO_4-10; d) SS-C-Li_4SiO_4-20 sorbents in pure CO_2 environment.

The CO_2 uptake capacity of SS-C-Li_4SiO_4 sorbents with different amounts of excess lithium at isothermal sorption conditions are shown in Table 5.4. In general, the CO_2 uptake capacity of sorbents increased with sorption temperature, with the highest CO_2 uptake capacity of 263.4 mg CO_2/g sorbent at 700 °C, while the lowest 34.52 mg CO_2/g sorbent at 500 °C. In addition, sorption rate of the sorbents also increased with sorption temperature. This is indicated by the increased amount of CO_2 captured by sorbents at 30 minutes into the analysis at each sorption temperature.

Evidently, there are two different uptake trends of the sorbents with different amounts of excess lithium, where one (at 700 °C) shows increased CO_2 uptake capacity, while the others (at 500 and 600 °C) show the opposite trend of decreasing amount of CO_2 captured with increasing amount of excess lithium. Similar to previously observed in SS-P-Li_4SiO_4 sorbents, it is thought that the addition of excess lithium inhibits SS-C-Li_4SiO_4 sorbents at lower sorption temperatures (500 and 600 °C) are due to insufficient thermal energy to encourage the reaction between the sorbents and CO_2 molecules, resulting in decreasing amount of CO_2 uptake capacity with increasing amount of excess lithium.

At 700 °C, the thermal energy is supposed to be more than enough to contribute to the negativity of ΔG value and causing the sorbents to capture more CO_2 even with increasing amount of excess lithium. Therefore, the reaction only completely activated at 700 °C for SS-C-Li_4SiO_4 sorbents, as opposed to 600 °C for SS-P-Li_4SiO_4 sorbents. Other impurities found in the parent waste material CPFA could be the

reason for the inhibition of the overall reaction process by SS-C-Li_4SiO_4 sorbents. This will be further discussed at the end of this section.

Table 5.4 Table CO_2 uptake capacity of SS-C-Li_4SiO_4 sorbents with different amounts of excess lithium at isothermal sorption conditions in pure CO_2 environment.

Amount of excess lithium (%)	Sorption temperature (°C)	CO_2 uptake capacity (mg CO_2/g sorbent)	
		30 min	120 min
0	500	87.12	114.4
5		40.79	59.04
10		32.06	45.40
20		24.40	34.52
0	600	117.2	151.6
5		65.80	98.54
10		49.90	71.81
20		52.70	78.57
0	700	180.1	185.7
5		144.1	188.9
10		167.0	213.8
20		184.9	263.4

Figure 5.8 presents the isothermal CO_2 uptake profiles of a) SS-R-Li_4SiO_4-0; b) SS-R-Li_4SiO_4-5; c) SS-R-Li_4SiO_4-10 and d) SS-R-Li_4SiO_4-20 in pure CO_2 environment. It is observed that the uptake profile of the sorbents increased as a function of sorption temperature, similar to SS-P-Li_4SiO_4 and SS-C-Li_4SiO_4 sorbents. In addition, CO_2 uptake profile of all SS-R-Li_4SiO_4 sorbents reached sorption equilibrium during the duration of analysis at 700 °C.

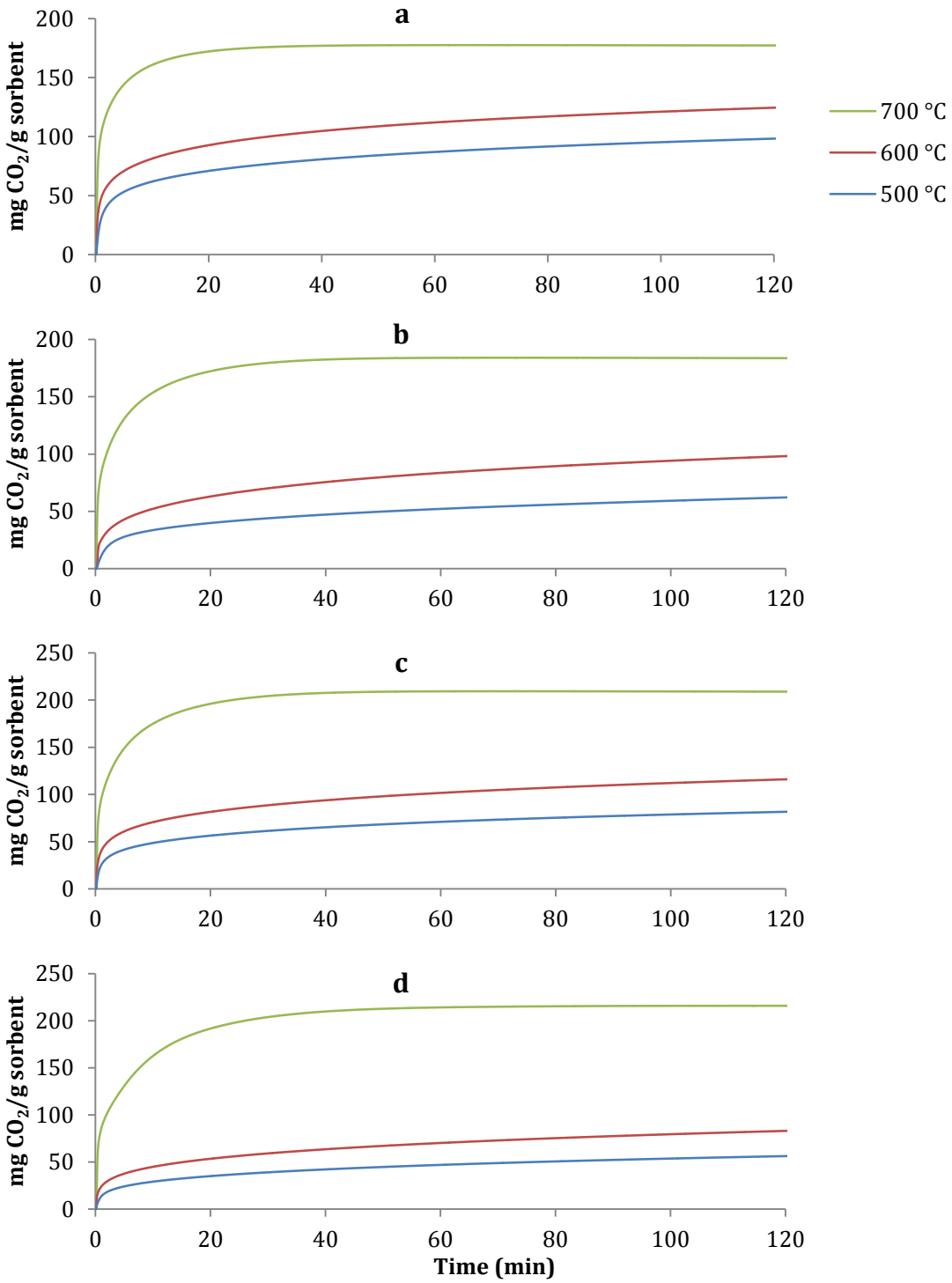

Figure 5.8 Isothermal CO_2 uptake profiles of a) SS-R-Li_4SiO_4-0; b) SS-R-Li_4SiO_4-5; c) SS-R-Li_4SiO_4-10 and d) SS-R-Li_4SiO_4-20 in pure CO_2 environment.

The CO_2 uptake capacity of SS-R-Li_4SiO_4 sorbents with different amounts of excess lithium at isothermal sorption conditions are tabulated in Table 5.5. In general, the CO_2 uptake capacity of sorbents increased with sorption temperature. It is observed that the highest CO_2 uptake capacity for the entire duration of analysis was 215.8 mg CO_2/g sorbent by SS-R-Li_4SiO_4-20 sorbent at 700 °C, while the lowest 56.33 mg CO_2/g sorbent by the same sorbent at 500 °C. Furthermore, sorption rate of the sorbents also increased with sorption temperature. This is indicated by the increased amount of CO_2 captured by sorbents at 30 minutes into the analysis at each sorption temperature.

Comparing the CO_2 uptake capacity of sorbents with increasing amounts of excess lithium at 500 and 600 °C, a familiar decreasing trend to the SS-C-Li_4SiO_4 sorbents can be observed. On one hand, the highest CO_2 uptakes by the initial SS-R-Li_4SiO_4-0 sorbent were 98.27 and 124.5 mg CO_2/g sorbent at 500 and 600 °C, respectively. As the amount of excess of lithium increased, the CO_2 uptake capacity by SS-R-Li_4SiO_4-20 sorbent decreased at 56.33 and 83.09 mg CO_2/g at 500 and 600 °C, respectively. On the other hand, maximum CO_2 uptake by SS-R-Li_4SiO_4-0 sorbent at 700 °C was found to be 177.2 mg CO_2/g sorbent and keeps increasing with the addition of excess amount of lithium until eventually, the maximum CO_2 uptake by SS-R-Li_4SiO_4-20 sorbent reached 215.8 mg CO_2/g sorbent. The presence of other elements in the parent waste material R-PFA is also thought to affect the degree of inhibition of the reaction between SS-R-Li_4SiO_4 sorbents and CO_2 molecules. Further discussion on this can be found at the end of this section.

Table 5.5 Maximum CO_2 uptake capacity of SS-R-Li_4SiO_4 sorbents with different amounts of excess lithium at isothermal sorption conditions in pure CO_2 environment.

Amount of excess lithium (%)	Sorption temperature (°C)	CO_2 uptake capacity (mg CO_2/g sorbent)	
		30 min	120 min
0	500	76.55	98.27
5		43.99	62.17
10		61.44	81.65
20		39.11	56.33
0	600	99.68	124.5
5		70.15	98.17
10		88.59	116.0
20		59.20	83.09
0	700	175.7	177.2
5		183.6	183.9
10		204.2	208.9
20		203.9	215.8

Figure 5.9 presents CO_2 uptake profiles of a) SS-F-Li_4SiO_4-0; b) SS-F-Li_4SiO_4-5; c) SS-F-Li_4SiO_4-10 and d) SS-F-Li_4SiO_4-20 in pure CO_2 environment. Similar to previously discussed sorbents, the CO_2 uptake capacity of SS-F-Li_4SiO_4 sorbents increased as a function of sorption temperature in pure CO_2 environment. The lowest, intermediate and highest amount of CO_2 captured are at 500, 600 and 700 °C, respectively. Interestingly, all SS-F-Li_4SiO_4 sorbents reached sorption equilibrium within 20 minutes of analysis duration at 700 °C. In relation to this, it is assumed that the diffusion of ions in Li_4SiO_4 were completely activated at 700 °C for all SS-F-Li_4SiO_4 sorbents. The addition of excess lithium on each sorbent did not seem to affect the dependency of CO_2 uptake capacity on sorption temperatures, although the excess amount of lithium slightly improved the overall CO_2 uptake capacity of the sorbent.

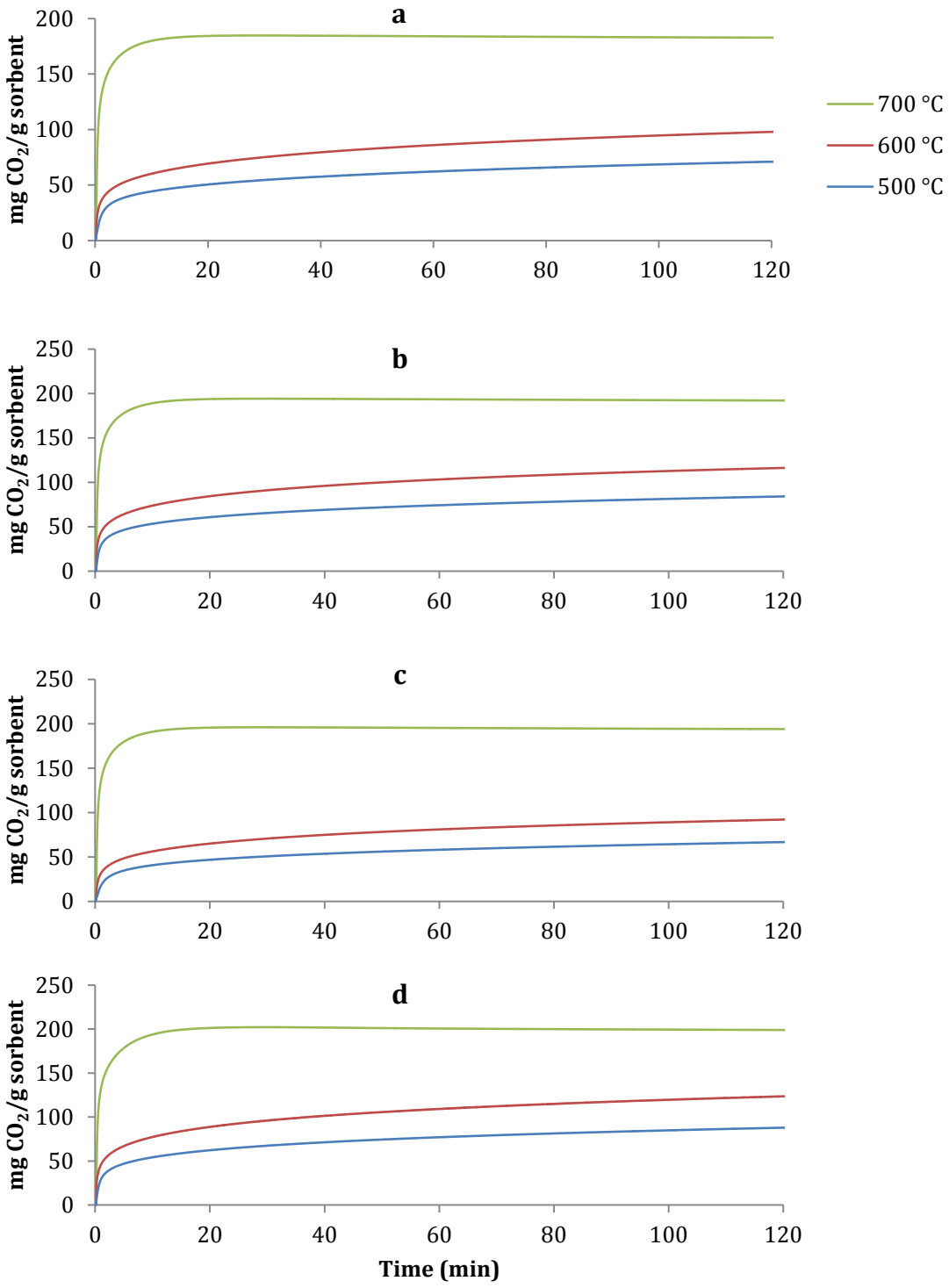

Figure 5.9 Isothermal CO_2 uptake profiles of a) SS-F-Li_4SiO_4-0; b) SS-F-Li_4SiO_4-5; c) SS-F-Li_4SiO_4-10 and d) SS-F-Li_4SiO_4-20 in pure CO_2 environment.

The CO_2 uptake capacity of SS-F-Li_4SiO_4 sorbents with different amounts of excess lithium at isothermal sorption conditions are shown in Table 5.6. The highest CO_2 uptake for the complete duration of analysis is captured by SS-F-Li_4SiO_4-20 at 700 °C (199 mg CO_2/g sorbent), while the lowest CO_2 uptake by SS-F-Li_4SiO_4-10 (66.68 mg CO_2/g sorbent) at 500 °C. The highest and lowest amounts of CO_2 captured by SS-F-Li_4SiO_4 sorbents present a direct correlation between the CO_2 uptake capacity and sorption temperature. In addition, an increasing uptake trend as a function of amount of excess lithium is observed at all sorption temperatures. Moreover, sorption rate of sorbents also increased as a function of temperature, as indicated by the increasing amount of CO_2 captured at 30 minutes into the analysis duration.

Table 5.6 CO_2 uptake capacity of SS-F-Li_4SiO_4 sorbents with different amounts of excess lithium at isothermal sorption conditions in pure CO_2 environment.

Amount of excess lithium (%)	Sorption temperature (°C)	CO_2 uptake capacity (mg CO_2/g sorbent)	
		30 min	120 min
0	500	54.55	71.02
5		65.39	84.04
10		50.67	66.68
20		67.52	87.91
0	600	75.10	97.87
5		90.96	116.2
10		70.63	92.04
20		96.03	123.5
0	700	182.8	182.8
5		192.1	192.1
10		190.9	190.9
20		199.0	199.0

Figure 5.10 shows the isothermal CO_2 uptake profiles of a) SS-B-Li_4SiO_4-0; b) SS-B-Li_4SiO_4-5; c) SS-B-Li_4SiO_4-10 and d) SS-B-Li_4SiO_4-20 in pure CO_2 environment. Evidently, all CO_2 uptake profiles of SS-B-Li_4SiO_4 sorbents exhibit sorption equilibrium within 15 minutes of analysis duration at 700 °C. Also observed in Figure 5.10 is the continuing trend of increased CO_2 uptake capacity with sorption temperature, where the amount of CO_2 uptake peaks at 700 °C and the lowest at 500 °C. In addition, the CO_2 uptake capacity increased as a function of the amount of excess lithium. Furthermore, the addition of excess lithium during preparation method of sorbents seems to enhance the CO_2 uptake capacity, as can be seen from the increased upper limit of sorption equilibrium with the amount of excess lithium.

Wang et al. (2011) stated that potassium and sodium contents in parent waste materials contributed to the improvement of CO_2 uptake capacities in the resulting waste-derived Li_4SiO_4 sorbents (Wang et al., 2011). The authors pointed out that these impurities in the parent waste materials followed reactions represented by equation 5.1, where M represents sodium or potassium and $Li_{2-x}M_{x/2}CO_3$ denotes a mixture of Li_2CO_3, K_2CO_3 and Na_2CO_3.

$$Li_{4-x}M_xSiO_4 + CO_2 \leftrightarrow Li_{2-x}M_{x/2}CO_3 + Li_{2-x}M_{x/2}SiO_3 \quad (5.1)$$

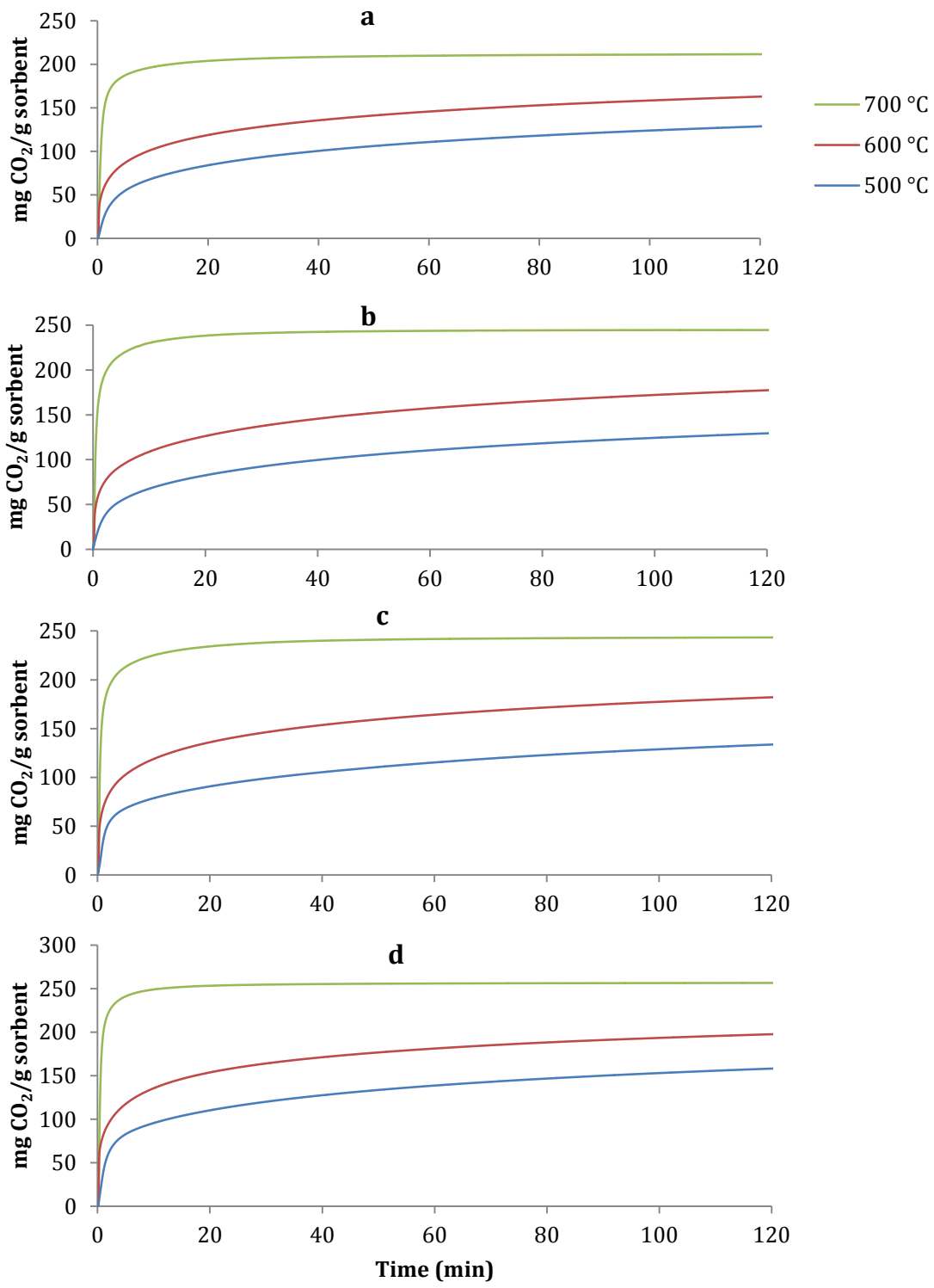

Figure 5.10 Isothermal CO_2 uptake profiles of a) SS-B-Li_4SiO_4-0; b) SS-B-Li_4SiO_4-5; c) SS-B-Li_4SiO_4-10 and d) SS-B-Li_4SiO_4-20 in pure CO_2 environment.

Although there was significantly higher content of K_2O in POMBA (6.80 wt%) compared to the rest of parent waste materials (<2.27 wt%), there was particularly lower content of Na_2O in POMBA (0.03 wt%) compared to other waste materials (up to 0.84 wt%) (Table 4.2). Therefore, it could be concluded that only high content of potassium in POMBA contributed to the significant improvement of CO_2 uptake capacity of SS-B-Li_4SiO_4 sorbents compared to SS-P-Li_4SiO_4 and other waste derived Li_4SiO_4 sorbents. Sodium content in parent waste material did not seem to affect CO_2 uptake capacity of the resulting waste-derived Li_4SiO_4 sorbents in current study.

Table 5.7 presents the CO_2 uptake capacity of SS-B-Li_4SiO_4 sorbents with different amounts of excess lithium at isothermal sorption conditions and different times (30 and 120 minutes) into the analysis. In general, it is observed that SS-B-Li_4SiO_4 sorbents exhibit an increase in CO_2 uptake capacity as a function of excess lithium addition. The lowest CO_2 uptake was obtained by SS-B-Li_4SiO_4-0 sorbent (128.6 mg CO_2/g sorbent) at 500 °C, while the highest was obtained by SS-B-Li_4SiO_4-20 (256.5 mg CO_2/g sorbent) at 700 °C. Similar to other waste-derived Li_4SiO_4 sorbents, the sorption rate of sorbents increased with sorption temperatures. This is indicated by the amount of CO_2 captured by sorbents at 30 minutes into the duration of analysis.

Table 5.7 CO_2 uptake capacity of SS-B-Li_4SiO_4 sorbents with different amounts of excess lithium at isothermal sorption conditions in pure CO_2 environment at 30 and 120 minutes into the analysis.

Amount of excess lithium (%)	Sorption temperature (°C)	CO_2 uptake capacity (mg CO_2/g sorbent)	
		30 min	120 min
0	500	93.45	128.6
5		92.40	129.4
10		98.93	133.6
20		114.0	158.1
0	600	128.5	162.8
5		137.5	177.4
10		146.2	182.1
20		164.0	197.5
0	700	211.5	211.5
5		244.5	244.5
10		243.4	243.4
20		256.5	256.5

As stated in previous studies, the CO_2 sorption mechanism by Li_4SiO_4 sorbents can be explained by two processes i.e. surface chemisorption of CO_2 and diffusion of Li^+ and O^{2-} ions through the double shells that formed over the bulk of Li_4SiO_4 particle (Essaki et al., 2005; Duran-Munoz et al., 2013). The diffusion rate is believed to be the limiting step due to the slower reaction rate towards the end of analysis duration, in comparison to the chemisorption step indicated by significantly steeper slope at the beginning of sorption isotherms. If this is the case, then the CO_2 sorption by sorbents can be simulated by a double exponential model, as represented by equation (5.2), where y (mg CO_2/g sorbent) is the sorption capacity at time t. k_1 and k_2 (s^{-1}) represent the exponential rate constants for chemisorption

and diffusion, respectively, while A and B are the pre-exponential constants and C is the y-intercept.

$$y = Ae^{(-k_1 t)} + Be^{(-k_2 t)} + C \qquad (5.2)$$

In an attempt to corroborate this hypothesis with the data obtained in this study, kinetic analyses were performed on the sorbents with the highest CO_2 sorption capacity (SS-B-Li_4SiO_4). Table 5.8 shows the kinetic parameters obtained from SS-B-Li_4SiO_4 isotherms for chemisorption and diffusion i.e. k_1 and k_2, respectively, as well as the R^2 values indicating the goodness of fit. Generally, k_1 values are at least 1 order of magnitude higher than those of k_2 for all SS-B-Li_4SiO_4 sorbents. This confirms that the diffusion step kinetically limits the overall CO_2 sorption process at sorption temperatures 500, 600 and 700 °C for all SS-B-Li_4SiO_4 sorbents. It is also observed that both k_1 and k_2 values increased with sorption temperatures, confirming that the rate of sorption improved with an increase in sorption temperature. k_1 and k_2 values obtained in this study were also found to be in good agreement with published studies. Olivares-Marin et al. (2010) reported similar findings, where k_1 values were at least 1 magnitude higher than those of k_2 for fly ash-derived Li_4SiO_4 sorbents.

Table 5.8 Kinetic parameters and R^2 values obtained from SS-B-Li_4SiO_4 isotherms.

Sorbents	Sorption temperature (°C)	k_1 (s^{-1})	k_2 (s^{-1})	R^2
SS-B-Li_4SiO_4-0	500	5.28×10^{-3}	3.14×10^{-4}	0.999
	600	6.66×10^{-3}	3.70×10^{-4}	0.995
	700	2.52×10^{-2}	1.35×10^{-3}	0.995
SS-B-Li_4SiO_4-5	500	7.12×10^{-3}	4.07×10^{-4}	0.999
	600	1.03×10^{-2}	3.87×10^{-4}	0.995
	700	2.85×10^{-2}	1.93×10^{-3}	0.992
SS-B-Li_4SiO_4-10	500	1.05×10^{-2}	2.95×10^{-4}	0.998
	600	1.07×10^{-2}	4.16×10^{-4}	0.993
	700	3.03×10^{-2}	1.47×10^{-3}	0.990
SS-B-Li_4SiO_4-20	500	9.60×10^{-3}	3.31×10^{-4}	0.999
	600	1.14×10^{-2}	4.73×10^{-4}	0.989
	700	3.17×10^{-2}	2.27×10^{-3}	0.986

The k values were then used to generate the Arrhenius plot, in order to determine the temperature dependence of the reaction rates by obtaining the activation energy (E_a) of the reactions. The E_a values were obtained by plotting natural logarithm of the reaction rates, i.e. ln k_1 and ln k_2, versus the inverse of the sorption temperatures in degree Kelvin (1/T). The slope of the plot equals to E_a/RT, from which E_a value can be calculated (Equation 5.2). Note that R is the gas constant and ln A is the y-intercept.

$$\ln k = \ln A - \frac{E_a}{RT} \tag{5.2}$$

Figures 5.11 to 5.14 show Arrhenius plots of SS-B-Li_4SiO_4 sorbents with the calculated values of E_a corresponding to k_1 and k_2 values. Note that E_{ac} represents the activation energy of the chemisorption step, while E_{ad} corresponds to

activation energy of the diffusion step. High activation energy denotes reaction rate that is strongly affected by temperature, while low activation energy corresponds to a reaction rate that slightly changes with temperature.

It is found that almost all E_{ac} values of SS-B-Li_4SiO_4 sorbents were lower (42.4, 31.9, 36.1 kJ/mol for SS-B-Li_4SiO_4-5, SS-B-Li_4SiO_4-10 and SS-B-Li_4SiO_4-20, respectively) than those of E_{ad} (46.5, 49.0, 58.5 kJ/mol for SS-B-Li_4SiO_4-5, SS-B-Li_4SiO_4-10 and SS-B-Li_4SiO_4-20, respectively), with the exception of SS-B-Li_4SiO_4-0, where the E_{ac} value was higher (47.3 kJ/mol) than E_{ad} (44.2 kJ/mol). This indicates that the diffusion step of the CO_2 sorption process on SS-B-Li_4SiO_4-0 sorbents was slightly affected by sorption temperatures 500, 600 and 700 °C, in comparison to the rest of SS-B-Li_4SiO_4 sorbents. Furthermore, E_{ac} values decreased with increasing excess lithium, but at the same time E_{ad} values increased with the addition of excess lithium. This suggests that the excess lithium enhanced the chemisorption step of CO_2 sorption, but inhibited the diffusion step with addition of excess lithium.

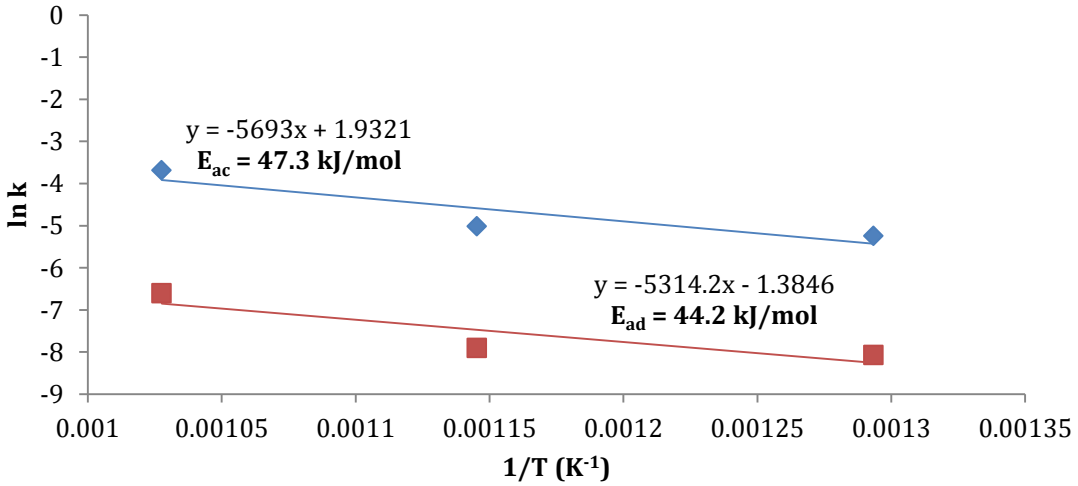

Figure 5.11 Arrhenius plot with E_a values of SS-B-Li_4SiO_4-0 sorbent at 500, 600 and 700 °C.

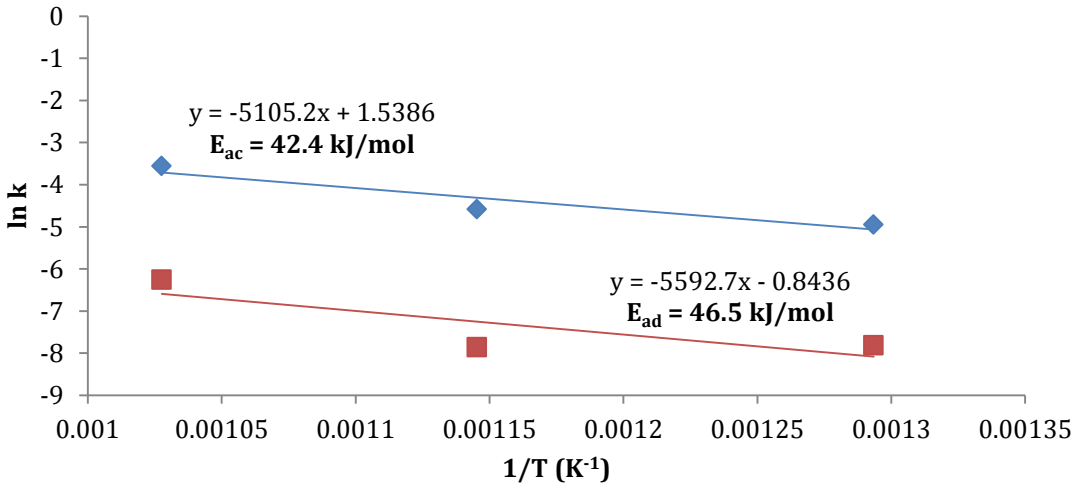

Figure 5.12 Arrhenius plot with E_a values of SS-B-Li_4SiO_4-5 sorbent at 500, 600 and 700 °C.

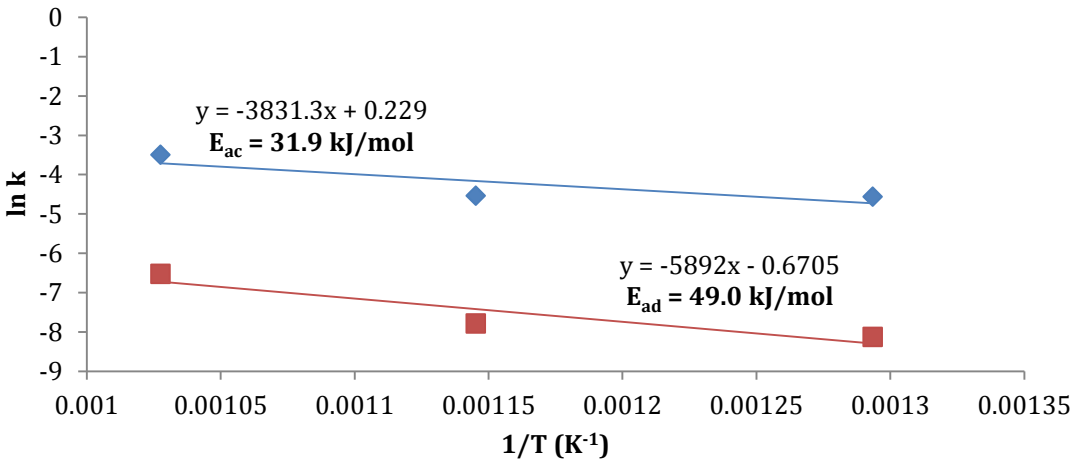

Figure 5.13 Arrhenius plot with E_a values of SS-B-Li_4SiO_4-10 sorbent at 500, 600 and 700 °C.

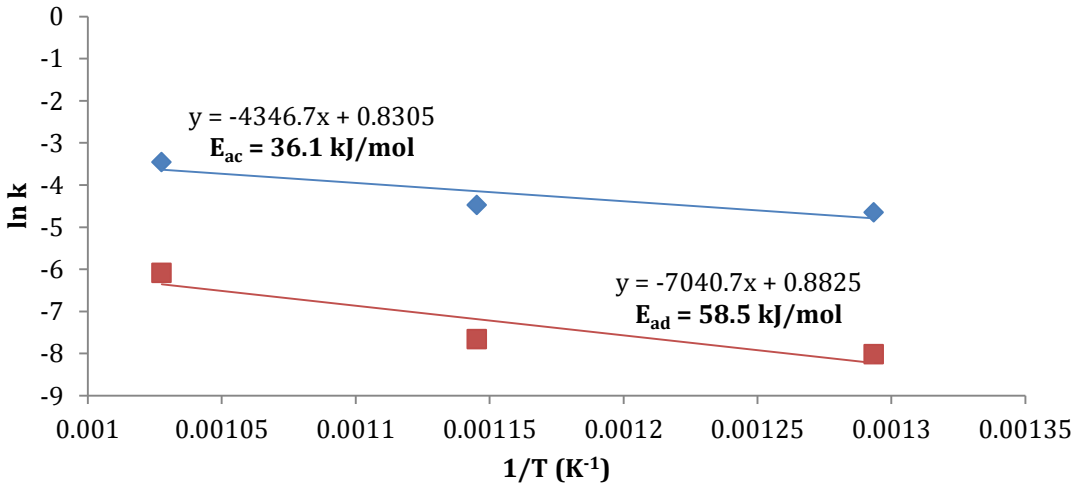

Figure 5.14 Arrhenius plot with E_a values of SS-B-Li_4SiO_4-20 sorbent at 500, 600 and 700 °C.

Comparing the CO_2 uptake profiles across all five sorbents with various percentages of excess lithium at 500 °C revealed that the CO_2 uptake profiles did not reach equilibrium by the end of the 120-minute analysis time. Interestingly, pure SS-P-Li_4SiO_4 sorbents captured significantly less CO_2 compared to its waste-derived sorbent counterparts, despite pure SiO_2 was used in the preparation of the sorbent.

As discussed in Section 4.3, the amorphous phase found in the waste-derived Li_4SiO_4 sorbents could be contributing to the enhanced CO_2 uptake performance of the sorbents due to the versatility of amorphous structure in capturing CO_2 molecules. In comparison to the more ordered structure of its crystalline counterpart which is predominantly found in SS-P-Li_4SiO_4 sorbents, the coexistence of amorphous Li_4SiO_4 is thought to contribute to the increase in CO_2 sorption capacity of the waste-derived sorbents. Faster diffusion of molecules into amorphous structure than that in crystalline due to the atomic disorder (Sadoway, 2010) is also believed to increase the rate of CO_2 sorption of the sorbents.

All five sorbents did not exhibit sorption equilibrium at 600 °C, although the overall CO_2 uptake capacities by all sorbents appeared to be improved with increased sorption temperature by 100 °C except for SS-C-Li_4SiO_4 and SS-R-Li_4SiO_4 which showed the opposite trend. This indicates that the increment in sorption temperature has provided enough thermal energy to increase the diffusion of ions in the bulk of Li_4SiO_4 particles to react with CO_2 molecules, but at the same time not enough for the diffusion to be completely activated that would lead to sorption

equilibrium of sorbents (Duran-Munoz et al., 2013). The overall sorption rate of all sorbents also improved following the increment of sorption temperature from 500 to 600 °C, as indicated by the increase in amount of CO_2 captured by sorbents during the first 30 minutes of analysis.

In addition, SS-P-Li_4SiO_4 sorbents still showed the lowest amount of CO_2 captured compared to the waste-derived sorbents even at an increased sorption temperature. Among the waste-derived Li_4SiO_4 sorbents, the highest CO_2 uptake capacity was obtained by SS-B-Li_4SiO_4 sorbents at all amounts of excess lithium with highest capacity of up to approximately 197 mg CO_2/g sorbent by SS-B-Li_4SiO_4-20 sorbent. On the other hand, the lowest CO_2 uptake capacity of waste-derived Li_4SiO_4 sorbents was obtained by either SS-R-Li_4SiO_4 or SS-F-Li_4SiO_4 sorbent, depending on the amount of excess lithium. SS-F-Li_4SiO_4 sorbents captured more CO_2 (up to 124 mg CO_2/g sorbent) with the addition of excess lithium, while SS-R-Li_4SiO_4 sorbents captured more CO_2 (up to 124 mg CO_2/g sorbent) with less amounts of excess lithium.

Evidently, the CO_2 uptake capacity profiles at 700 °C exhibit a different trend compared to that at 600 °C. Sorption equilibrium was attained at some point depending on the amount of excess lithium by almost all Li_4SiO_4 sorbents, with the exception of SS-P-Li_4SiO_4. Overall CO_2 uptake capacities by all sorbents appeared to be improved at 700 °C. This indicates that the increment in sorption temperature has provided enough thermal energy to completely activate the diffusion of ions in the bulk of Li_4SiO_4 particles to react with CO_2 molecules that in

turn, lead to sorption equilibrium of sorbents (Duran-Munoz et al., 2013). The overall sorption rate of all sorbents has also substantially improved following the increment of sorption temperature from 600 to 700 °C.

In addition, SS-P-Li_4SiO_4 sorbents still showed the lowest amount of CO_2 captured compared to the waste-derived sorbents even at an increased sorption temperature. It is believed that the impurities in the starting waste materials, e.g. K_2O, contributed to the improvement of CO_2 uptake capacities of waste-derived Li_4SiO_4 sorbents, in particular the SS-B-Li_4SiO_4 sorbents. However, the CO_2 uptake capacities of SS-P-Li_4SiO_4 sorbents have improved significantly at 700 °C of up to 136 mg CO_2/g sorbent by SS-P-Li_4SiO_4-20. Among the waste-derived Li_4SiO_4 sorbents, the highest CO_2 uptake capacity was also obtained by SS-B-Li_4SiO_4 sorbents at all amounts of excess lithium with highest capacity of up to approximately 257 mg CO_2/g sorbent by SS-B-Li_4SiO_4-20 sorbent at the same sorption temperature. On the other hand, the lowest CO_2 uptake capacity of waste-derived Li_4SiO_4 sorbents was obtained by SS-F-Li_4SiO_4 sorbent of up to 199 mg CO_2/g sorbent by SS-F-Li_4SiO_4-20.

5.2.3. CO_2 uptake by sorbents in diluted CO_2 environment

The CO_2 uptake capacities for all prepared Li_4SiO_4 sorbents were determined using diluted CO_2 (14 vol% CO_2, balance N_2) environment. The diluted CO_2 concentration is selected specifically at 14 vol% to simulate the CO_2 concentration in a flue gas stream exiting the combustion chamber in a coal-fired power plant, containing

from 10 to 15 vol% of CO_2 (GCCSI, 2012). It is worthy to note that apart from the concentration of CO_2 used in the analysis, other experimental conditions such as sorption temperatures (500, 600 and 700 °C) and duration of analysis (120 minutes) remained constant to that of conditions reported in the previous section.

Isothermal CO_2 uptake profiles of SS-P-Li_4SiO_4 sorbents with different amounts of excess lithium are presented in Figure 5.15. Similar to the outcome reported in previous section (Figure 5.5), the profiles do not exhibit sorption equilibrium at the end of the analysis. Also, the amount of CO_2 uptake capacity by sorbents decreased significantly in diluted CO_2 environment compared to that in pure one. This observation is in good agreement with a study by Essaki et al. (2005) which reported the CO_2 uptake capacity of pure Li_4SiO_4 pellets decreased significantly (from 27 wt% in 15 vol% CO_2 at 600 °C to 2 wt% in 5 vol% CO_2) as the partial pressure of CO_2 decreased (Essaki et al., 2005).

Additionally, there is a distinctive trend of CO_2 uptake profiles in diluted CO_2 environment, where the amount of CO_2 uptake increased with sorption temperature up to 600 °C before decreasing significantly at 700 °C. The decrease in CO_2 uptake capacity is expected due to the substantially low CO_2 partial pressure making it harder for the sorbents to capture CO_2 efficiently. Seggiani et al. (2013) explained this occurrence to be attributed to the Gibbs free energy changes (ΔG) of the sorption reaction between CO_2 and Li_4SiO_4 (Seggiani et al., 2013). As the CO_2 sorption is an exothermic reversible gas-solid reaction with equilibrium constant equivalent to an inverse of CO_2 partial pressure, the lower the CO_2 concentration

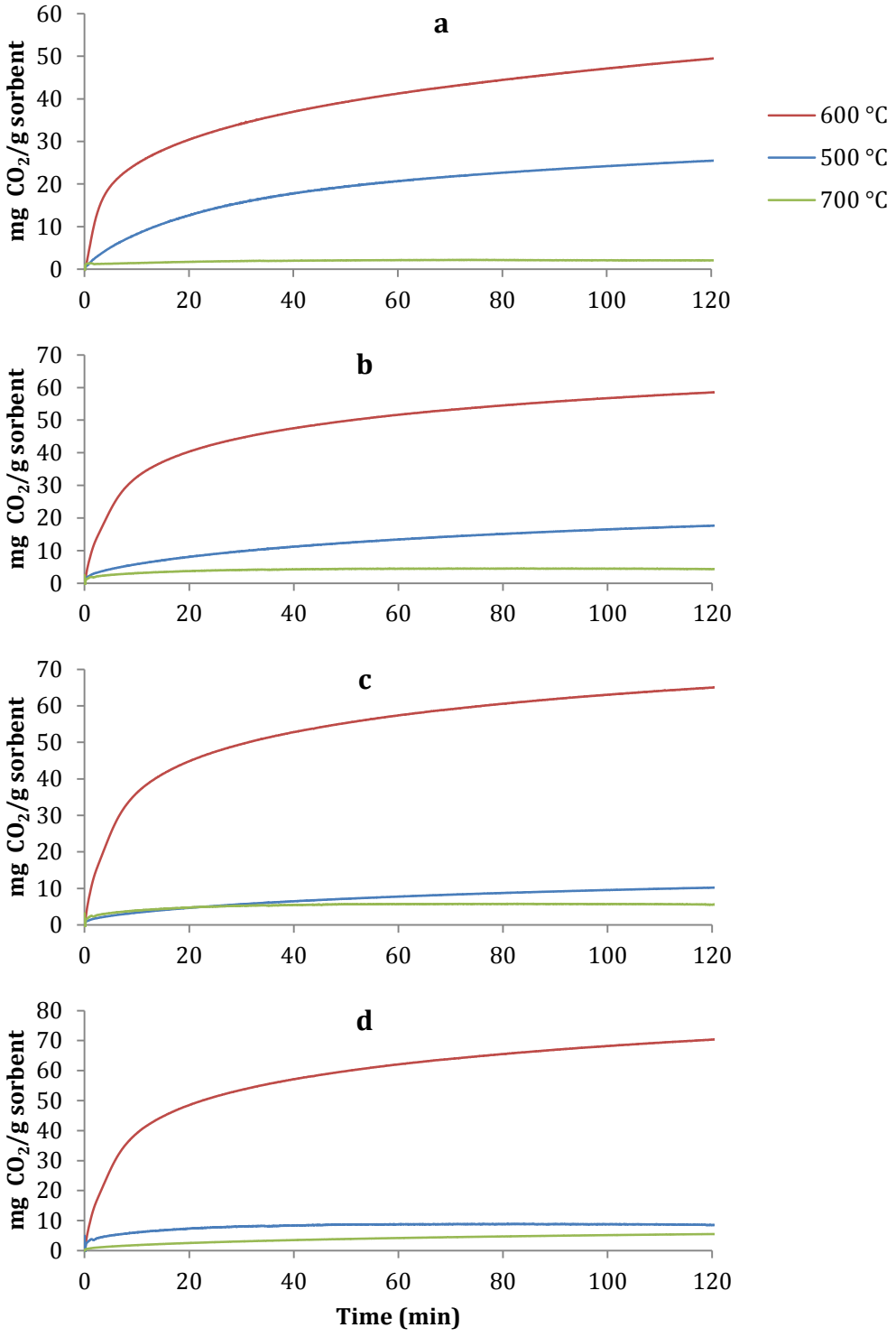

Figure 5.15 Isothermal CO_2 uptake profiles of a) SS-P-Li_4SiO_4-0; b) SS-P-Li_4SiO_4-5; c) SS-P-Li_4SiO_4-10 and d) SS-P-Li_4SiO_4-20 in diluted CO_2 (14 vol%) environment.

the lower the equilibrium emission temperature, which is the temperature where CO_2 sorption and regeneration both share the same temperature. Consequently, desorption process was initiated at lower temperature (600 °C) in diluted CO_2 sorption environment compared to the pure one, i.e. at 700 °C (Seggiani et al., 2013).

The CO_2 uptake capacities of SS-P-Li_4SiO_4 sorbents with different amounts of excess lithium at isothermal sorption conditions in diluted CO_2 environment are presented in Table 5.9. It is observed that CO_2 uptake capacity by SS-P-Li_4SiO_4 sorbents in diluted CO_2 environment peaked at sorption temperature of 600 °C with 20 wt% excess lithium (70.32 mg CO_2/g sorbent), while the lowest uptake capacity was observed by SS-P-Li_4SiO_4-0 with 2.08 mg CO_2/g sorbent captured at 700 °C. In addition, the sorption rate of SS-P-Li_4SiO_4 sorbents is observed to increase as a function of sorption temperature of up to 600 °C before it dropped abruptly at 700 °C. This is indicated by the amounts of CO_2 captured at 30 minutes into the analysis duration compared to at the end of the analysis (120 min).

Analysing the CO_2 uptake capacity isothermally and according to increasing amount of excess lithium, SS-P-Li_4SiO_4 sorbents captured less CO_2 with more addition of excess lithium at 500 °C. However at 600 °C, an increasing trend of uptake capacity is observed as the amount of excess lithium is increased. Similar trend was identified at 700 °C despite the sharp decrease in overall CO_2 uptake capacity. The same trend was also observed in pure CO_2 environment (Table 5.3), deducing the same assumption that the excess amounts of lithium inhibits CO_2

uptake by sorbents at lower sorption temperature (500 °C) but not at higher temperatures (600, 700 °C).

Table 5.9 CO_2 uptake capacity of SS-P-Li_4SiO_4 sorbents with different amounts of excess lithium at isothermal sorption conditions in diluted CO_2 environment.

Amount of excess lithium (%)	Sorption temperature (°C)	CO_2 uptake capacity (mg CO_2/g sorbent)	
		30 min	120 min
0	500	15.5716	25.46
5		9.7643	17.64
10		5.6585	10.22
20		3.0474	8.494
0	600	34.19	49.40
5		44.58	58.50
10		49.54	65.01
20		53.59	70.32
0	700	1.9285	2.078
5		4.0859	4.311
10		5.2617	5.551
20		8.0507	5.504

Figure 5.16 shows the isothermal CO_2 uptake profiles of a) SS-C-Li_4SiO_4-0; b) SS-C-Li_4SiO_4-5; c) SS-C-Li_4SiO_4-10 and d) SS-C-Li_4SiO_4-20 in diluted CO_2 environment. CO_2 uptake capacity profiles by SS-C-Li_4SiO_4 sorbent do not exhibit sorption equilibrium during the 120-minute analysis, similarly to the profiles in pure CO_2 environment. Moreover, the CO_2 uptake profiles trend presented in Figure 5.16 is analogous to that of SS-P-Li_4SiO_4 sorbents in previously discussed Figure 5.15, whereby shifted equilibrium emission temperature to 600 °C in diluted CO_2 environment is observed.

The rate of CO_2 sorption by SS-C-Li_4SiO_4 sorbents increased as the sorption temperature increased from 500 to 600 °C. However, the sorption rate declined abruptly at 700 °C. Additionally, the sorption rate is also noticeably higher than that of SS-P-Li_4SiO_4. Furthermore, the amount of excess lithium added during sorbent preparation also seemed to improve the sorption rate, as seen in Figure 5.16.

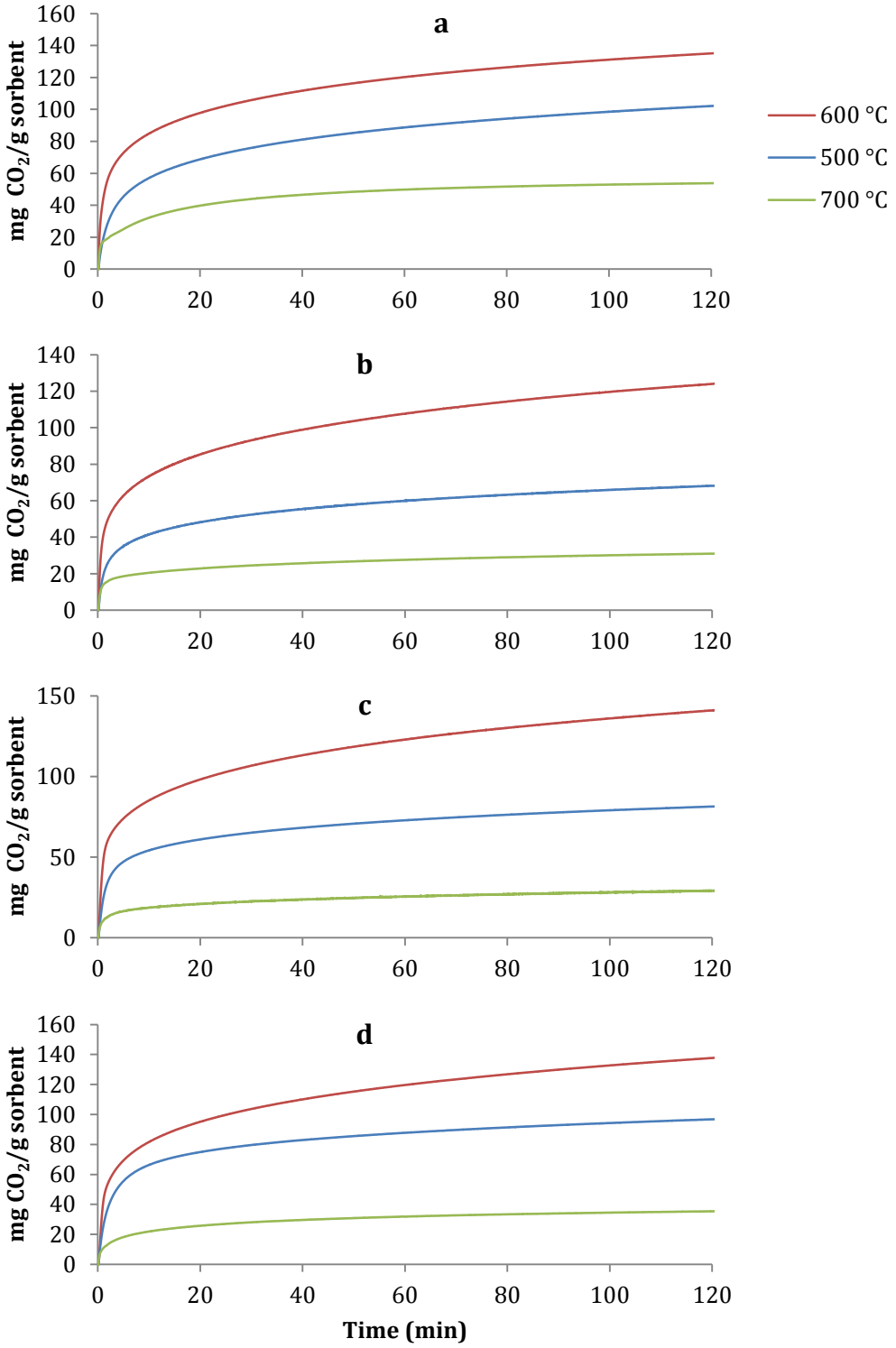

Figure 5.16 Isothermal CO_2 uptake profiles of a) SS-C-Li_4SiO_4-0; b) SS-C-Li_4SiO_4-5; c) SS-C-Li_4SiO_4-10 and d) SS-C-Li_4SiO_4-20 in diluted CO_2 (14 vol%) environment.

Table 5.10 presents maximum CO_2 uptake capacity of waste-derived SS-C-Li_4SiO_4 sorbents with different amounts of excess lithium at isothermal sorption conditions in diluted CO_2 environment. At 500 °C sorption temperature, the overall CO_2 uptake exhibits decreasing trend with increasing amount of excess lithium. On the other hand, increasing trend in CO_2 uptake as a function of excess lithium at 600 °C was observed, also with slight drop in CO_2 uptake by SS-C-Li_4SiO_4-5 and SS-C-Li_4SiO_4-20 sorbents. At 700 °C, similar increasing overall trend of CO_2 uptake by sorbents with amounts of excess lithium is observed.

Comparing with CO_2 uptake in pure environment, there is a change in uptake/amount of excess lithium trend. The highest CO_2 uptake was 140.9 mg CO_2/g sorbent at 600 °C by SS-C-Li_4SiO_4-10, whereas the lowest amount of CO_2 also captured by SS-C-Li_4SiO_4-10 sorbent at 700 °C (29.18 mg CO_2/g sorbent). The sorption rate of sorbents was also increased up until 600 °C before plummeted at 700 °C, based on the amount of CO_2 uptake capacity of sorbents at 30 minutes into the analysis compared to the amount at 120 minutes.

Table 5.10 CO_2 uptake capacity of SS-C-Li_4SiO_4 sorbents with different amounts of excess lithium at isothermal sorption conditions in diluted CO_2 environment.

Amount of excess lithium (%)	Sorption temperature (°C)	CO_2 uptake capacity (mg CO_2/g sorbent)	
		30 min	120 min
0	500	75.90	102.1
5		52.38	68.17
10		65.15	81.37
20		79.63	96.77
0	600	105.79	135.1
5		93.11	124.0
10		106.68	140.9
20		103.68	137.7
0	700	43.90	53.77
5		24.51	30.99
10		22.31	29.18
20		28.07	35.41

Isothermal CO_2 uptake profiles of SS-R-Li_4SiO_4, SS-F-Li_4SiO_4 and SS-B-Li_4SiO_4 sorbents in diluted CO_2 environment exhibit similar trend to that of SS-C-Li_4SiO_4 sorbents and therefore, are presented in the Appendix section (Figures A5.3, A5.4 and A5.5) at the end of this thesis.

Table 5.11 lists the CO_2 uptake capacity of waste-derived Li_4SiO_4 sorbents with different amounts of excess lithium at isothermal sorption conditions in diluted CO_2 environment at the end of analysis duration. At 500 and 600 °C, overall CO_2 uptake trend by SS-R-Li_4SiO_4 sorbents decreased with increasing amount of excess lithium. However, an inverse trend of CO_2 uptake is observed at 700 °C. On the

other hand, a direct correlation between amount of excess lithium and CO_2 uptake was observed by both SS-F-Li_4SiO_4 and SS-B-Li_4SiO_4 sorbents. There is no apparent change when comparing CO_2 uptake trend by all three SS-R-Li_4SiO_4, SS-F-Li_4SiO_4 and SS-B-Li_4SiO_4 sorbents in pure CO_2 environment, although the overall amounts of CO_2 uptake decreased significantly. The decrease in amounts of CO_2 uptake captured by sorbents in diluted CO_2 environment is expected as there is substantially less CO_2 molecules available to react with sorbents.

As mentioned previously, the amount of excess lithium strongly affects the amount of CO_2 uptake by sorbents. In the case of SS-R-Li_4SiO_4 sorbents, the absence of excess lithium produced a sorbent with maximum CO_2 uptake in diluted CO_2 environment at 600 °C (110.1 mg CO_2/g sorbent), while SS-R-Li_4SiO_4-5 captured the lowest amount of CO_2 (27.21 mg CO_2/g sorbent). For both SS-F-Li_4SiO_4 and SS-B-Li_4SiO_4 sorbents, 20% excess lithium enhanced the CO_2 uptake up to 117.3 and 186.1 mg CO_2/g sorbent at 600 °C, respectively. However, the least CO_2 uptake by SS-F-Li_4SiO_4 and SS-B-Li_4SiO_4 sorbents observed by SS-F-Li_4SiO_4-10 (33.73 mg CO_2/g sorbent) and SS-B-Li_4SiO_4-5 (16.35 mg CO_2/g sorbent) at 700 °C despite the direct correlation between amount of excess lithium and CO_2 uptake by the sorbents.

Table 5.11 CO_2 uptake capacity of waste-derived Li_4SiO_4 sorbents with different amounts of excess lithium at isothermal sorption conditions in diluted CO_2 environment at the end of analysis duration.

Sorbent	Amount of excess lithium (%)	CO_2 uptake at different sorption temperatures (mg CO_2/g sorbent)		
		500 ℃	600 ℃	700 ℃
SS-R-Li_4SiO_4	0	94.22	110.1	47.91
	5	51.75	86.39	27.21
	10	73.72	102.8	57.23
	20	54.55	78.38	47.37
SS-F-Li_4SiO_4	0	64.33	105.7	43.00
	5	78.36	106.3	39.19
	10	62.18	88.80	33.73
	20	81.13	117.3	53.27
SS-B-Li_4SiO_4	0	111.5	152.6	34.41
	5	82.78	142.5	16.35
	10	111.2	162.1	25.90
	20	126.1	186.1	28.24

5.3. Regeneration of waste-derived Li_4SiO_4 sorbents

Following the CO_2 uptake analysis, regeneration performance of waste-derived Li_4SiO_4 sorbents in both pure and diluted CO_2 environments are discussed in this section. Regeneration performance analyses were carried out in cyclic isothermal sorption conditions at which the sorbents captured the highest amount of CO_2 i.e. at 700 ℃. Regeneration of sorbents at 600 ℃ was also carried out for comparison purposes. The sorption time was held for 30 minutes in CO_2 environment (pure or diluted) before being regenerated in an inert environment (N_2) for 30 minutes.

The sorption/regeneration cycle was then repeated for 10 times in order to establish preliminary study of the stability of the sorbents in cyclic conditions.

5.3.1. Regeneration of waste-derived sorbents in pure CO_2 environment

Figure 5.17 shows the multiple cycles regeneration profiles of SS-P-Li_4SiO_4 sorbents with 0, 5, 10 and 20% excess lithium at a) 600 ℃ and b) 700 ℃. While the addition of excess lithium improved the overall CO_2 uptake capacity in a single cycle at 600 ℃ (Table 5.3), it did not seem to affect the stability of the sorbents in multiple cycles regeneration process at the same temperature (Figure 5.17a). In addition, the amount of CO_2 uptake capacity of sorbents did not reach sorption equilibrium. This is expected as the CO_2 uptake analysis of the same sorbents also did not attain sorption equilibrium during 120 minutes of analysis duration, as shown in Figure 5.5.

Moreover, it is evident in Figure 5.17a that the amount of CO_2 uptake capacity of sorbents progressively increasing despite the decreasing sorption rate with each regeneration cycle. This suggests that the sorbents were continuously capturing more CO_2 as the analysis advances until sorption equilibrium is reached. At 700 °C (Figure 5.17b), the CO_2 uptake capacity no longer increased with regeneration cycles as it was observed at 600 °C. The regeneration cycles now are observed to be more stabilised after the first two cycles and continued performing in this manner until the end of analysis duration. There is, however, a slight degradation

in the amount of CO_2 uptake (approximately 2 mg CO_2/g sorbent) by SS-P-Li_4SiO_4 sorbents between the first and the 10th regeneration cycle.

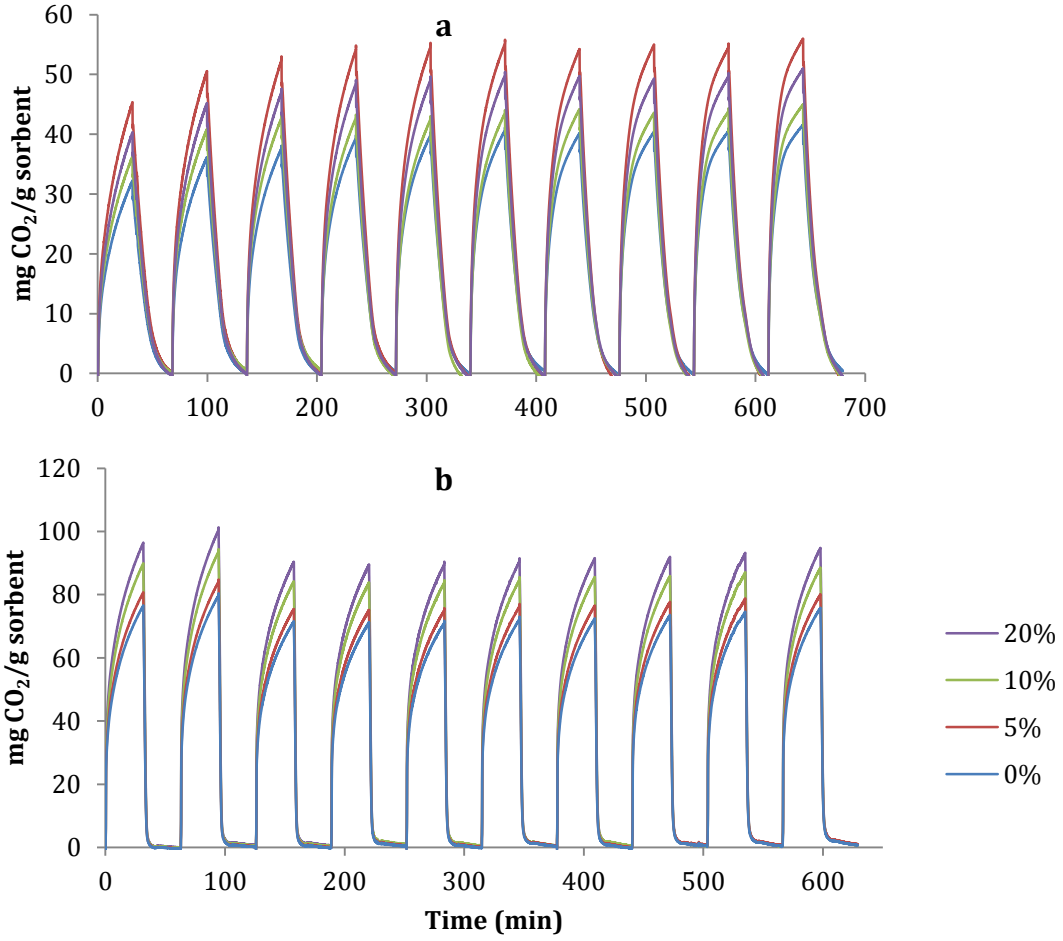

Figure 5.17 Regeneration profiles of SS-P-Li_4SiO_4 sorbents at a) 600 ℃ and b) 700 ℃ with different amounts of excess lithium.

Similar to the performance in single cycle at 700 °C, the CO_2 uptake capacity by SS-P-Li_4SiO_4 sorbents increased with the addition of excess lithium. However, the difference of CO_2 uptake capacity and the amount of excess lithium was not significantly improved, considering the amount of excess lithium that needs to be

added to achieve a small degree of improvement in the amount of CO_2 captured. For example, 20% of excess lithium will only improve approximately 20 mg CO_2/g sorbent throughout the regeneration cycles. From the perspective of potential industrial application, it might not be worth adding an excess amount of lithium if this would not significantly improve the CO_2 uptake capacity performance of the sorbent. Comparing the amount of CO_2 uptake between the regeneration cycles at 600 and 700 °C, it is evident that the latter performed better with cumulative amount of CO_2 captured by SS-P-Li_4SiO_4 sorbents of approximately 850 mg CO_2/g sorbent after 10 cycles. On the other hand, the same sorbents captured about 580 mg CO_2/g sorbent at 600 °C throughout the analysis.

Figure 5.18 shows the regeneration profiles of SS-C-Li_4SiO_4 sorbents at a) 600 °C and b) 700 °C with different amounts of excess lithium. In general, there was no sorption equilibrium attained at 600 °C, as can be expected from the CO_2 uptake analysis of the same sorbents at the same sorption temperatures in Figure 5.7. It is also observed in Figure 5.18a the familiar increment of CO_2 uptake capacity of sorbents as the analysis advances. As explained in the previous paragraphs, this suggests that the sorbents were progressively capturing more CO_2 as the analysis progresses until sorption equilibrium is eventually reached.

It is observed that the CO_2 uptake capacity of sorbents decreased as a function of excess lithium. This is expected as similar trend was detected during the CO_2 uptake analysis of the same sorbent (Table 5.4). Sorbents with no excess lithium captured significantly higher amount of CO_2 (up to 170 mg CO_2/g sorbent) than

sorbents with 20% of excess lithium (up to 85 mg CO_2/g sorbent) in multiple regeneration cycles. This brings to a deduction that apart from the CO_2 uptake capacity of sorbents, the addition of excess lithium seems to have neither a positive nor a negative effect to the performance of CO_2 regeneration by SS-C-Li_4SiO_4 sorbents at 600 °C in pure CO_2 environment.

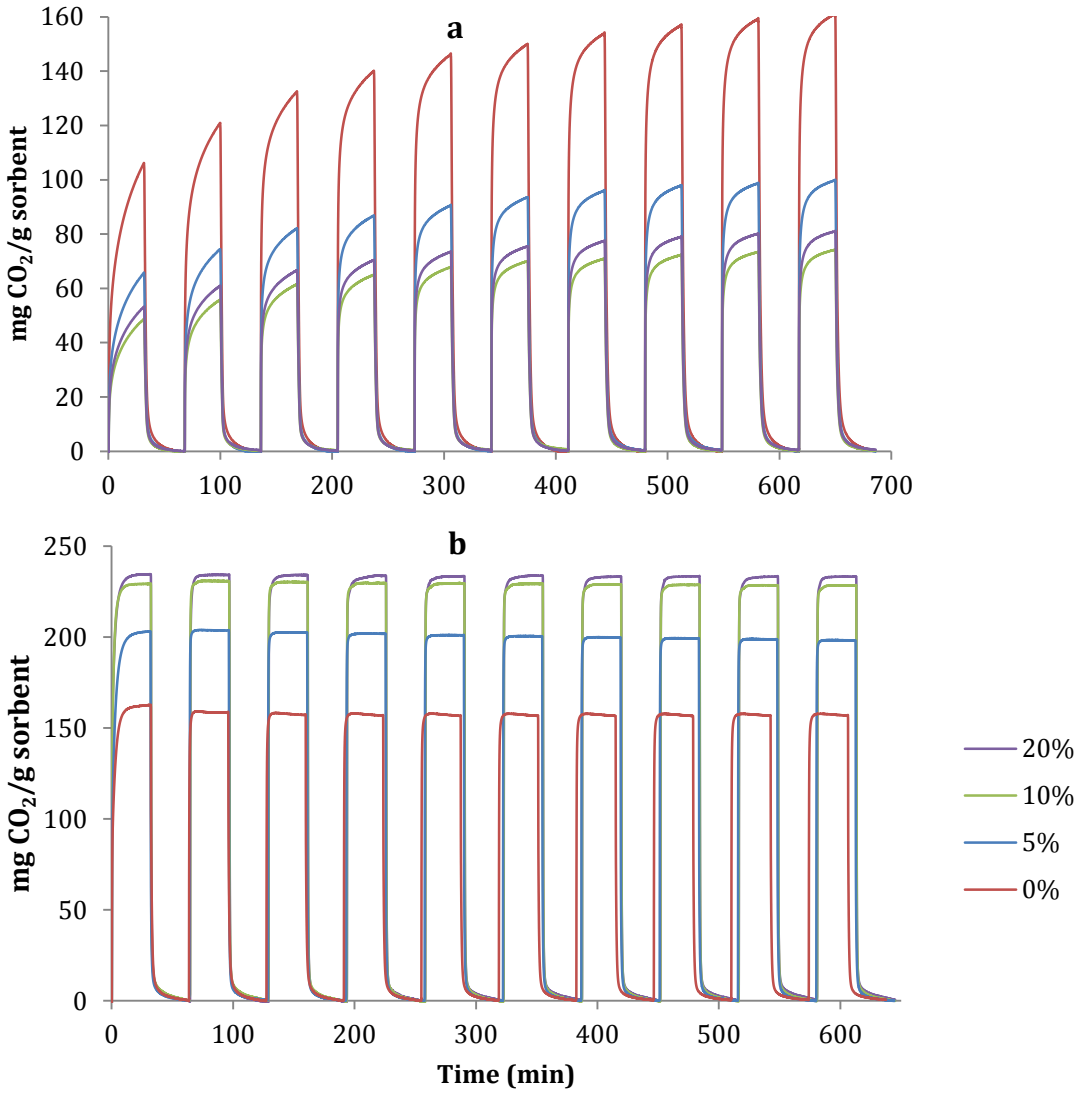

Figure 5.18 Regeneration profiles of SS-C-Li_4SiO_4 sorbents at a) 600 °C and b) 700 °C with different amounts of excess lithium in pure CO_2 environment.

The regeneration profiles of SS-C-Li_4SiO_4 sorbents at 700 °C in Figure 5.18b seemingly exhibit a different trend compared to at 600 °C, where all SS-C-Li_4SiO_4 sorbents attained sorption equilibrium throughout the analysis. As a result of this, the profiles showed a more stabilised sorption/regeneration cycles compared to at 600 °C. In addition, the CO_2 uptake capacity increased as a function of excess lithium, as can be expected from the single cycle analysis shown in Table 5.4.

Figure 5.19 shows the regeneration profiles of SS-B-Li_4SiO_4 sorbents at a) 600 °C and b) 700 °C with different amounts of excess lithium. In general, Figure 5.19 presents similar regeneration profiles to that of SS-C-Li_4SiO_4 sorbents in Figure 5.18. The effect of excess lithium on CO_2 uptake performance of both SS-C-Li_4SiO_4 and SS-B-Li_4SiO_4 sorbents are to be expected, as similar trend was also observed in their respective single cycle CO_2 uptake performances in Figures 5.7 and 5.10. Also, it is evident that no sorption equilibrium was reached at 600 °C, as shown in Figure 5.18a. This is to be expected from previous observations, where no sorption equilibrium was reached at sorption temperatures lower than 700 °C. Despite showing similar regeneration performances, SS-B-Li_4SiO_4 sorbents seemed to have higher CO_2 uptake capacities than SS-C-Li_4SiO_4 sorbents. For example, SS-B-Li_4SiO_4-20 captured cumulatively 2540 mg CO_2/g sorbent at 700 °C, while SS-C-Li_4SiO_4-20 captured about 2300 mg CO_2/g sorbent at the same temperature.

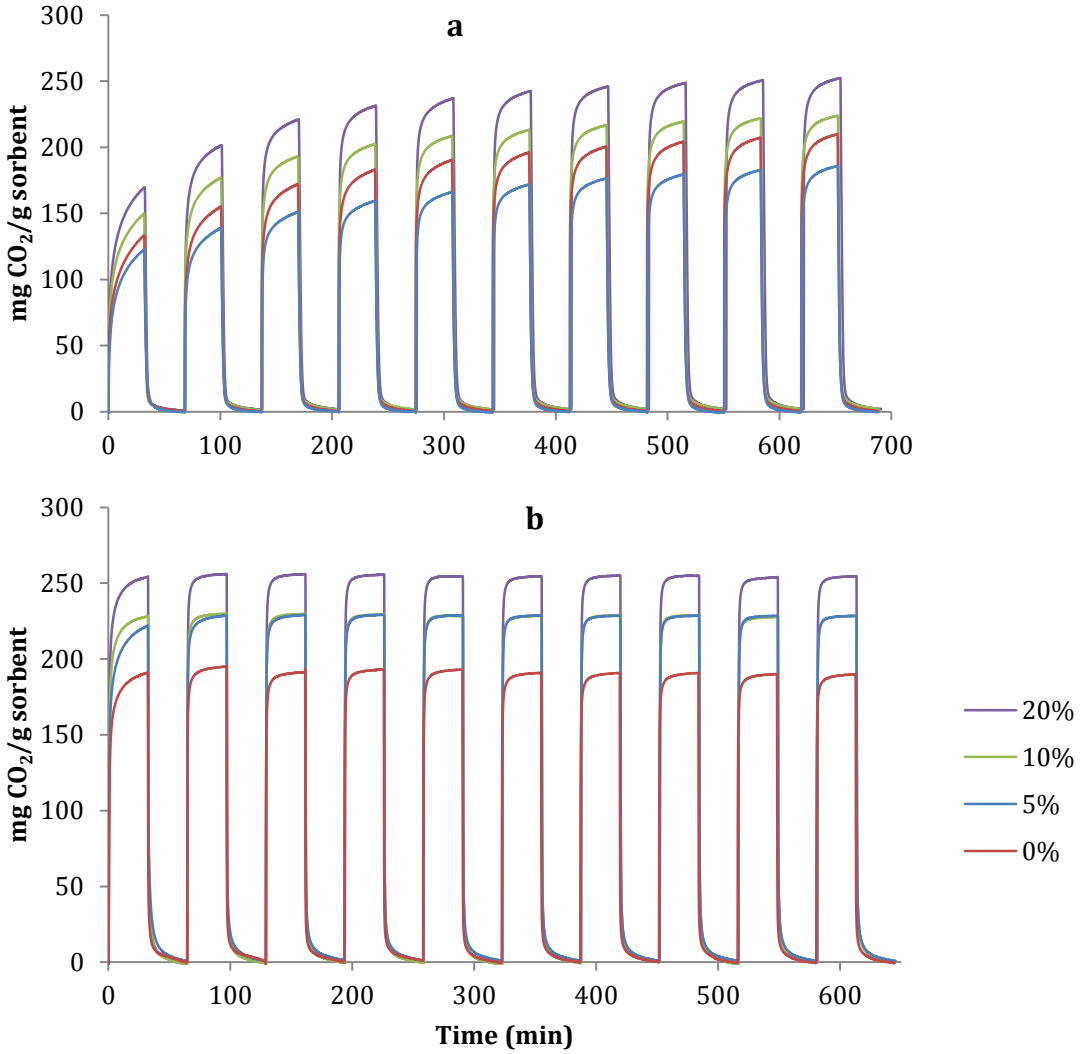

Figure 5.19 Regeneration profiles of SS-B-Li_4SiO_4 sorbents at a) 600 ℃ and b) 700 ℃ with different amounts of excess lithium in pure CO_2 environment.

5.3.2. Regeneration of waste-derived sorbents in diluted CO_2 environment

SS-C-Li_4SiO_4 and SS-B-Li_4SiO_4 sorbents were also studied for their multiple cycles regeneration performance in diluted CO_2 environment. It is worthy to note that apart from the concentration of CO_2 used in the analysis, other experimental

conditions such as regeneration temperatures (600 and 700 °C) and duration of regeneration cycles (30 minutes sorption, 30 minutes regeneration) remain unchanged to that of conditions reported in the previous section, so that meaningful comparisons can be established.

Figures 5.20a and 5.20b represent the regeneration profiles of SS-C-Li_4SiO_4 at 600 and 700 °C, respectively, with different amounts of excess lithium in diluted CO_2 environment. As expected at 600 °C, no sorption equilibrium was attained during the sorption step of the regeneration cycle by the sorbents. As the analysis progresses, the CO_2 uptake capacity of sorbents gradually increased, a similar trend that was also observed in pure CO_2 environment (Figure 5.18).

The CO_2 uptake capacity trend in multiple cycles as a function of excess lithium corresponds to that of CO_2 uptake analysis of the same sorbents in diluted CO_2 environment in section 5.2.2 (Table 5.10). Sorbents with no excess lithium captured significantly higher amount of CO_2 (up to 160 mg CO_2/g sorbent) than sorbents with 20% of excess lithium (up to 112 mg CO_2/g sorbent) in multiple regeneration cycles.

It is observed that the same sorbents performed differently at 700 °C. Evidently, the overall CO_2 uptake capacity of sorbents decreased substantially (Figure 5.20b) compared to the performance of the same sorbents in pure CO_2 environment (Figure 5.18b). As discussed in section 5.2.2, the considerable change in CO_2 uptake of sorbents in a significantly reduced CO_2 partial pressure has changed the

ΔG of the sorption reaction between CO_2 and Li_4SiO_4 particles and thus, decreasing the CO_2 uptake of sorbents (Seggiani et al., 2013). For this reason, it is expected that the sorbents performed in a similar trend in multiple regeneration cycles as they did during the CO_2 uptake analysis.

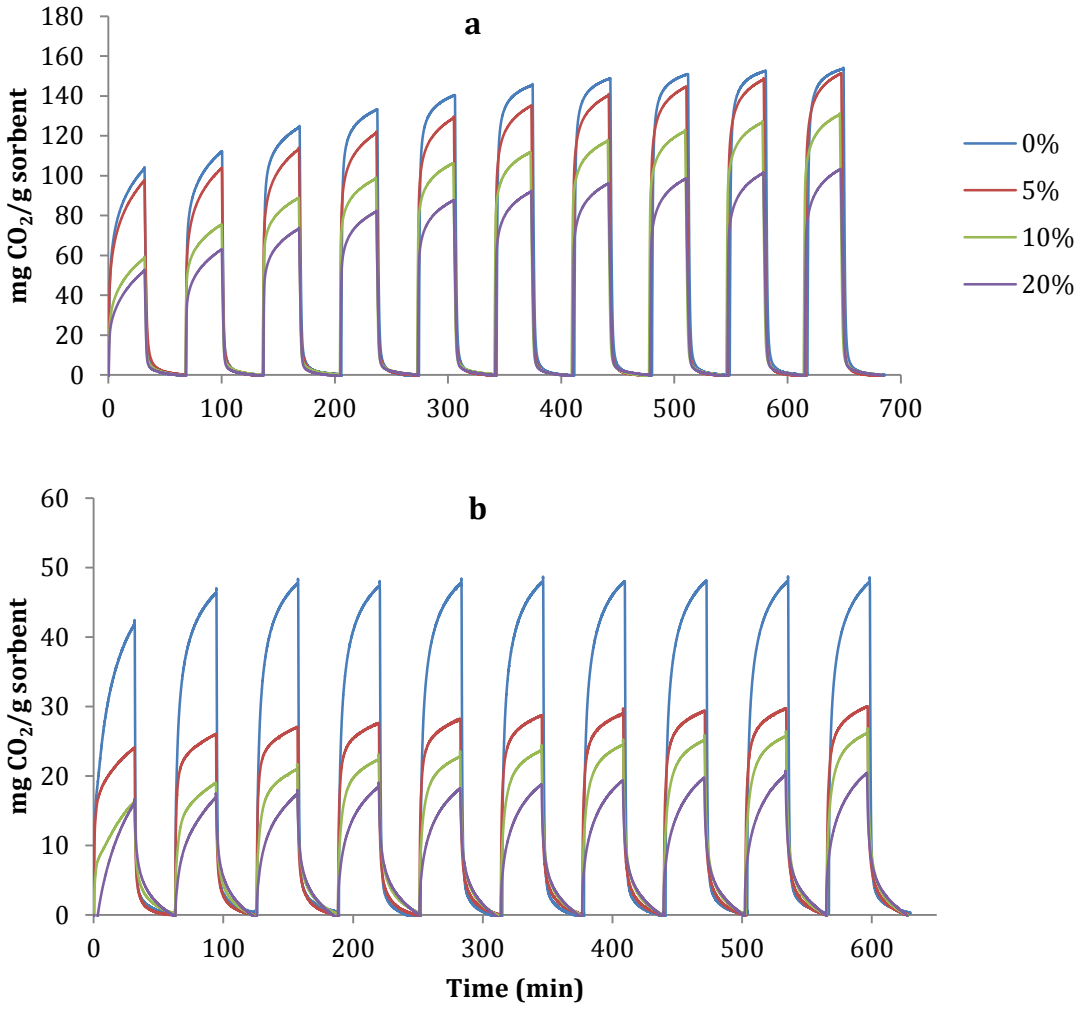

Figure 5.20 Regeneration profiles of SS-C-Li_4SiO_4 sorbents at a) 600 ℃ and b) 700 ℃ with different amounts of excess lithium in diluted CO_2 environment.

Analysing the effect of excess lithium in sorbents, it is observed that the sorbents maintained the familiar decreasing trend of CO_2 uptake capacity as a function of excess lithium. However, the downward tendency of CO_2 uptake capacity was not as obvious in SS-C-Li_4SiO_4-0 compared to the rest of the SS-C-Li_4SiO_4 sorbents. Additionally, the CO_2 uptake capacity of SS-C-Li_4SiO_4-5, SS-C-Li_4SiO_4-10 and SS-C-Li_4SiO_4-20 sorbents evidently captured significantly less CO_2 compared to SS-C-Li_4SiO_4 sorbent. This indicates that the excess lithium inhibits the CO_2 uptake capacity of sorbents, which was previously discussed in section 5.2.2.

Similar regeneration performance can be observed in Figure 5.21, which shows the regeneration profiles of SS-B-Li_4SiO_4 sorbents at a) 600 ℃ and b) 700 ℃ with different amounts of excess lithium. It is evident that the overall amount of captured CO_2 by SS-B-Li_4SiO_4 sorbents at 700 °C (Figure 5.21b) decreased significantly compared to that at 600 °C (Figure 5.21a), comparable to SS-C-Li_4SiO_4 sorbents regeneration profiles observed in Figure 5.20. It is worthy to note that amount of excess lithium had the opposite effect on CO_2 uptake capacities in between both sorbents. This suggests that the dependency of the amount of excess lithium to improve overall CO_2 uptake capacities varies with the waste materials used to develop waste-derived Li_4SiO_4 CO_2 sorbents.

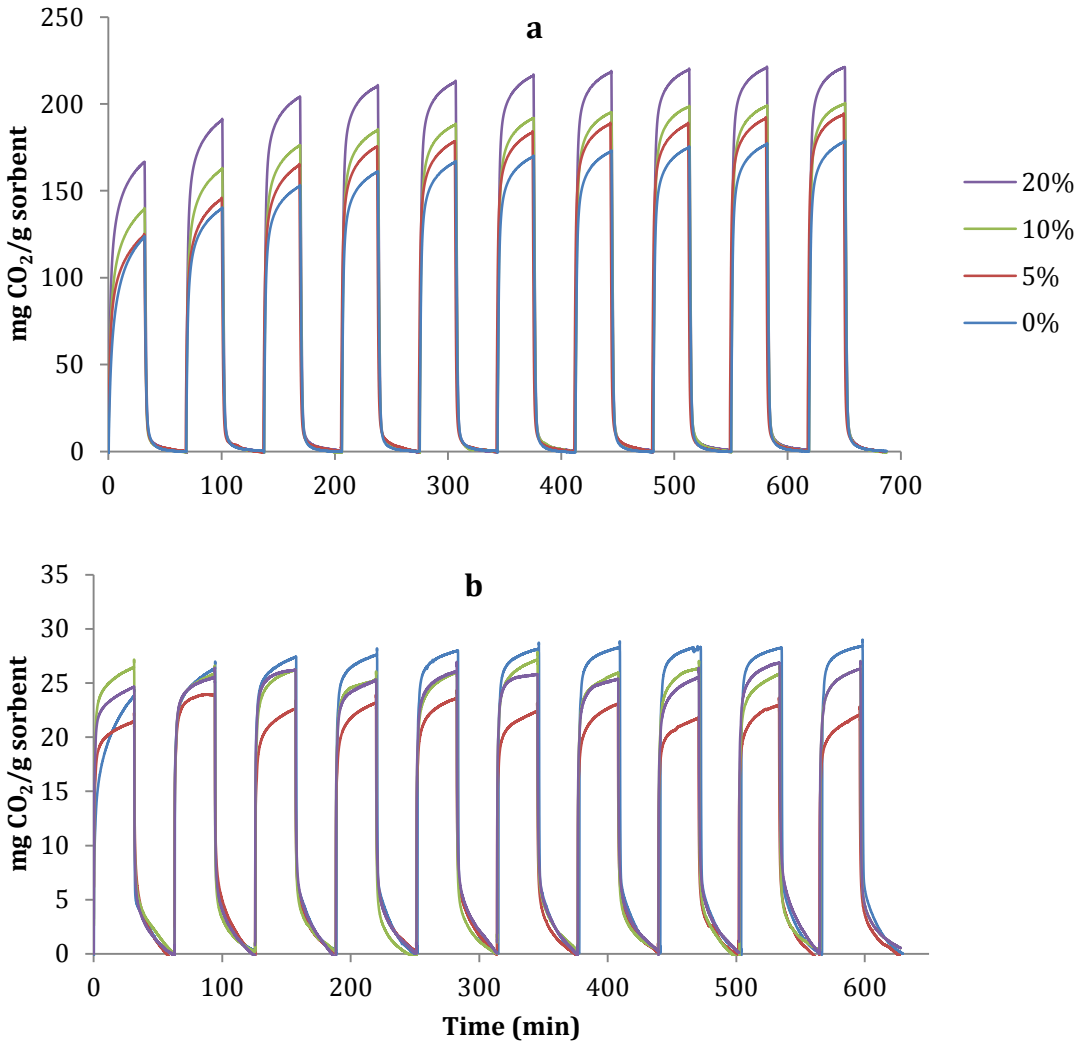

Figure 5.21 Regeneration profiles of SS-B-Li_4SiO_4 sorbents at a) 600 ℃ and b) 700 ℃ with different amounts of excess lithium in diluted CO_2 environment.

5.4. Effect of sorbent preparation method on CO_2 uptake capacity

Following the preparation of the pure and waste-derived Li_4SiO_4 sorbents, a study on the effect of sorbent's preparation method on the CO_2 uptake capacity of the sorbents was carried out. A wet impregnation method, namely, suspended

impregnation (SI) was implemented on the parent waste material POMBA. POMBA was selected as the waste material to be investigated in this study due to the highest CO_2 uptake capacity showed by SS-B-Li_4SiO_4 in comparison to other waste-derived Li_4SiO_4 sorbents, as reported in section 5.2.1.

It is worthy to note that only 20% excess lithium was added during preparation of the sorbent, as it was found that sorbents with this amount of excess lithium i.e. SS-B-Li_4SiO_4-20 captured the highest amount of CO_2 (257 mg CO_2/g sorbent). The preparation procedures of this method and the subsequent CO_2 capture analysis on the sorbent followed that of previously described in Section 3.2. The resulting sorbent deriving from this preparation method is labelled as SI-B-Li_4SiO_4-20. Furthermore, XRD analysis was carried out on SI-B-Li_4SiO_4-20 to verify the presence of Li_4SiO_4 in the sorbent prepared by this SI method.

Figure 5.22 shows XRD diffractograms of SI-B-Li_4SiO_4-20 resulting from SI preparation method and the previously prepared by solid state (SS) method, SS-B-Li_4SiO_4-20. It is observed that SI-B-Li_4SiO_4-20 exhibited sharp peaks representing Li_4SiO_4 comparable to SS-B-Li_4SiO_4-20 sorbent, denoting a successful attempt in producing a Li_4SiO_4-based sorbent using the procedures described in Section 3.2. Also, there seems to be no significant differences observed between both diffractograms, showing that a different preparation method did not seem to significantly change the mineral phase composition of the sorbent. Reaction products other than Li_4SiO_4 such as $LiAlSiO_4$ were expectedly detected, since there were significant amounts of aluminosilicates present in the parent waste material

(Table 4.2). The coexistence of Li_2SiO_3 in SI-B-Li_4SiO_4-20 is also expected, as this proved that the reaction between Li_2CO_3 and the SiO_2 in POMBA advanced according to equation 2.2 (Section 2.3.2).

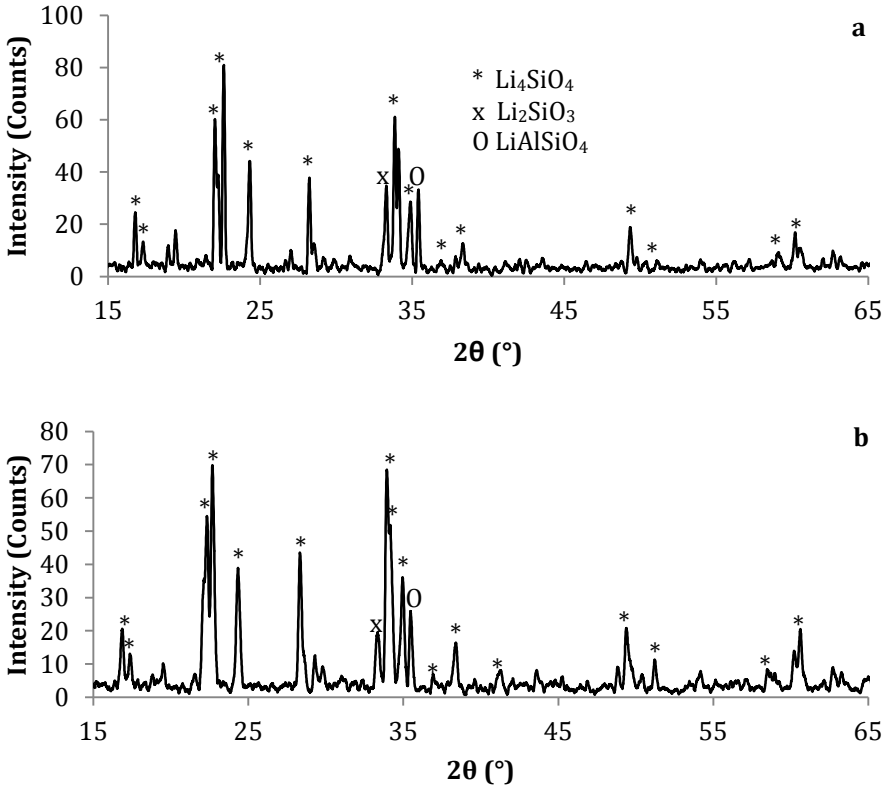

Figure 5.22 XRD diffractograms of a) SI-B-Li_4SiO_4-20and b) SS-B-Li_4SiO_4-20 sorbents.

Figure 5.23 shows the comparison of isothermal CO_2 profiles of SI-B-Li_4SiO_4-20 and SS-B-Li_4SiO_4-20 sorbents at sorption temperatures 500, 600 and 700 °C. Generally, CO_2 uptake capacity of SI-B-Li_4SiO_4-20 sorbent increased with sorption temperature (Figure 5.23a), although there was not much difference in uptake capacity between 600 and 700 °C towards the end of analysis duration. It was not observed that the CO_2 uptake capacity of the sorbent achieved sorption

equilibrium at lower sorption temperatures (500 and 600 °C). However, the CO_2 uptake capacity of the sorbent finally achieved sorption equilibrium at 700 °C. The highest CO_2 uptake capacity during the sorption duration was 197 mg CO_2/g sorbent at 700 °C, while the lowest uptake capacity was 144 mg CO_2/g sorbent at 500 °C.

Similar observations of increasing uptake capacity with sorption temperature were also detected for SS-B-Li_4SiO_4-20 (Figure 5.23b) as well as other waste-derived sorbents, as discussed in section 5.2.1. In addition, the sorption rate of both sorbents did not seem to change much, as indicated by the slope of the sorption isotherms. Kinetic parameters (Table 5.12) showed that there are no significant changes in the values of k_1 and k_2 of SI-B-Li_4SiO_4-20 compared to SS-B-Li_4SiO_4-20, with the exception of k_1 values at 500 °C (5.77×10^{-3} and 9.60×10^{-3} for SI-B-Li_4SiO_4-20 and SS-B-Li_4SiO_4-20, respectively). These observations indicate that the different in preparation method did not alter the overall trend of uptake capacity with respect to the sorption temperature.

Nevertheless, the overall CO_2 uptake capacity of SI-B-Li_4SiO_4-20 sorbent was lower (up to 197 mg CO_2/g sorbent) than that of SS-B-Li_4SiO_4-20 (up to 257 mg CO_2/g sorbent). This shows that although different preparation method did not drastically alter the overall kinetics performance, it seems to affect the maximum uptake capacity of the sorbents.

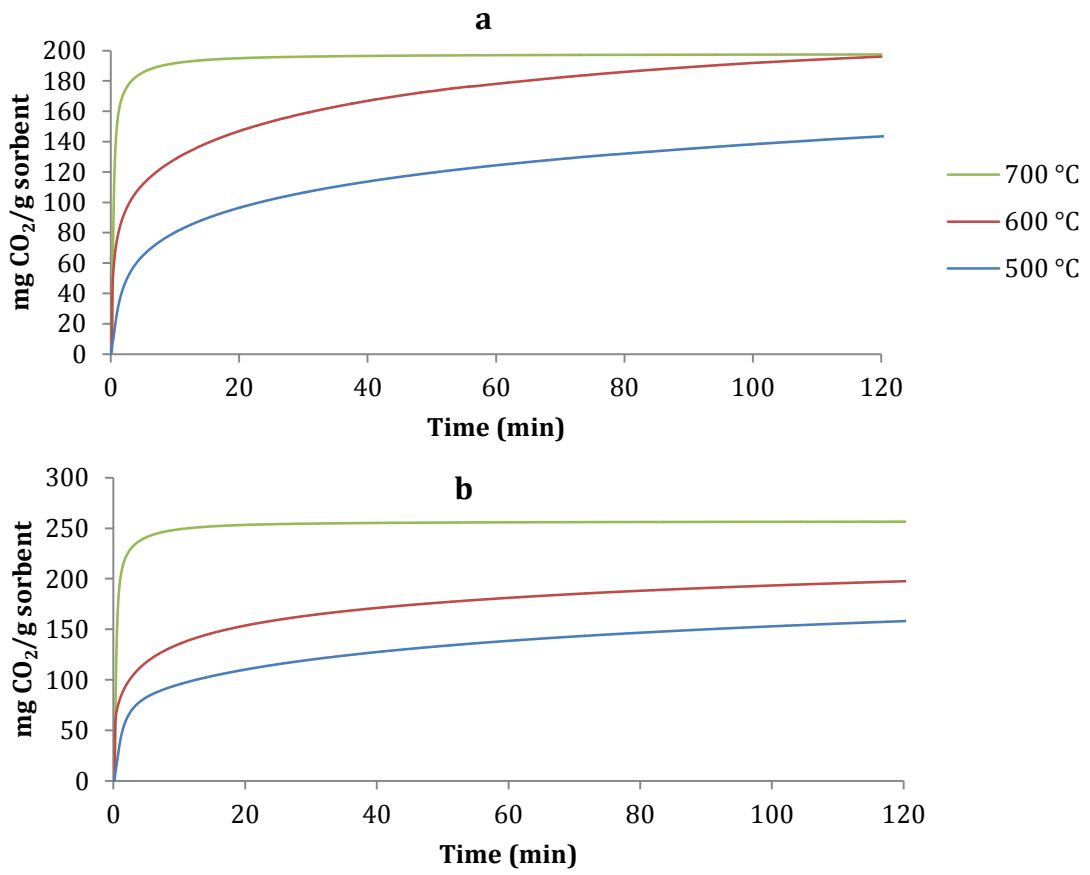

Figure 5.23 Isothermal CO_2 profiles of a) SI-B-Li_4SiO_4-20 and b) SS-B-Li_4SiO_4-20 sorbents at 500, 600 and 700 °C.

Table 5.12 Kinetic parameters and R^2 values comparison between SI-B-Li_4SiO_4-20 and SS-B-Li_4SiO_4-20.

Sorbents	Sorption temperature (°C)	k_1 (s^{-1})	k_2 (s^{-1})	R^2
SI-B-Li_4SiO_4-20	500	5.77×10^{-3}	3.25×10^{-4}	0.998
	600	1.20×10^{-2}	4.48×10^{-4}	0.995
	700	3.50×10^{-2}	2.46×10^{-3}	0.990
SS-B-Li_4SiO_4-20	500	9.60×10^{-3}	3.31×10^{-4}	0.999
	600	1.14×10^{-2}	4.73×10^{-4}	0.989
	700	3.17×10^{-2}	2.27×10^{-3}	0.986

5.5. Summary

Chapter 5 discussed the CO_2 capture by parent waste materials and their corresponding waste-derived Li_4SiO_4 sorbents. CO_2 capture analyses were conducted at isothermal sorption temperatures of 500, 600 and 700 °C in pure (100 vol%) and diluted (14 vol%) environments. Additionally, waste-derived Li_4SiO_4 sorbents were also analysed for their CO_2 sorption/desorption performances. Parent waste materials (CPFA, RPFA, FBA and POMBA) were not subjected to any pre-treatment method before the analysis to provide 'raw' CO_2 uptake capacity of waste materials prior to calcination process and also serves as the benchmark values for the progress of subsequent modification of the materials.

5.5.1. CO_2 uptake by parent waste materials

In general, it was found that the highest CO_2 uptake capacity of parent waste materials was about 4 mg CO_2/g sorbent by FBA. The CO_2 uptake values by waste materials are significantly lower than that of commercially available liquid solvent e.g. MEA (approximately 176 mg CO_2/g sorbent) (Samanta et al., 2012). This proves unsuitability of the waste materials as CO_2 sorbents if they were to be used without any pre-treatment. It was also observed that the CO_2 uptake profiles did not reach sorption equilibrium during the 120-minute analysis duration for CPFA, while others showed sorption equilibrium at 600 (RPFA and FBA) and 500 °C (POMBA). In addition, CO_2 uptake profiles were affected by sorption temperatures, depending on the residence time. Peaking behaviour was observed in all parent

waste materials, indicated by momentary maximum CO_2 uptake capacity before decreasing rapidly.

It was found that peaking behaviour of waste materials was due to the instability of the materials at high sorption temperatures. Additional experiments were carried out under N_2 flow in isothermal conditions 500, 600 and 700 °C confirmed this, as it was apparent that instability of the parent waste materials increased as a function of temperature.

Low CO_2 uptake by parent waste materials could be contributed by several factors, including low concentrations of metal oxides present on the surface of the waste materials. Significantly low concentrations (<10 wt%) of these metal oxides in waste materials was deemed to be key reason for the low CO_2 uptake. Pure metal oxides such as MgO and CaO are known to chemically absorb CO_2 at elevated temperatures of higher than 400 °C (Martavaltzi and Lemonidou, 2008; Hassanzadeh and Abbasian, 2010) producing $MgCO_3$ and $CaCO_3$, respectively.

5.5.2. CO_2 uptake by waste-derived Li_4SiO_4 sorbents in pure and diluted CO_2 environments

All pure (SS-P-Li_4SiO_4) and waste-derived (SS-C-Li_4SiO_4, SS-R-Li_4SiO_4, SS-F-Li_4SiO_4 and SS-B-Li_4SiO_4) sorbents presented direct correlations between the CO_2 uptake capacities in pure CO_2 environment and the sorption temperatures throughout the

duration of analyses. All sorbents captured the lowest amount of CO_2 at 500 °C and the highest at 700 °C, with intermediate amount of captured CO_2 at 600 °C.

This observation correlates well with the double shell CO_2 capture mechanism by Li_4SiO_4 proposed in previous studies (Essaki et al., 2005; Duran-Munoz et al., 2013). At low sorption temperature, two layers of shells covered the Li_4SiO_4 particle i.e. Li_2SiO_3 and Li_2CO_3 as CO_2 is chemically sorbed by Li_4SiO_4. Diffusion of Li^+ and O^{2-} ions from the bulk of Li_4SiO_4 particle is then activated at higher sorption temperature, allowing more CO_2 to be captured by the sorbent. In addition, the direct correlation between CO_2 uptake capacities of waste-derived Li_4SiO_4 sorbents and sorption temperatures is in good agreement with previous studies (Olivares-Marin et al., 2010; Wang et al., 2011).

In addition, all sorbents showed increase in sorption rate as the sorption temperature increased, as indicated by the slope of the CO_2 uptake capacity at the beginning of analysis. This observation is believed to be due to increased CO_2 diffusion activity within the Li_4SiO_4 particles, resulting in faster sorption rate compared to that at lower sorption temperature. Kinetic analysis was performed on SS-B-Li_4SiO_4 sorbents in an attempt to corroborate the data obtained in this study with the double exponential model, as this model was well-established to simulate the CO_2 sorption mechanism described earlier. As shown in Table 5.8, the kinetic parameters obtained following the kinetic analysis verified the diffusion step kinetically limits the overall CO_2 sorption on S-B-Li_4SiO_4 sorbents at sorption temperatures 500, 600 and 700 °C. This is indicated by the significantly larger k_1

values of the sorbents compared to k_2 values, which represent the chemisorption and diffusion rate of the process, respectively.

The addition of excess amounts of lithium seems to inhibit CO_2 uptake by SS-P-Li_4SiO_4 and fly ash-derived (SS-C-Li_4SiO_4 and SS-R-Li_4SiO_4) sorbents at lower sorption temperature (500 °C for SS-P-Li_4SiO_4 and 600 °C for SS-C-Li_4SiO_4 and SS-R-Li_4SiO_4 sorbents). As suggested by Duran-Munoz et al. (2013), it is assumed that there is insufficient thermal energy provided at this temperature to fully activate the diffusion of CO_2 through the bulk of Li_4SiO_4 particles, and therefore, the addition of excess lithium inhibits the overall sorption process (Duran-Munoz et al., 2013). As the sorption temperature increased to 600 and 700 °C, it is assumed that there is enough thermal energy to completely activate the diffusion process. The subsequent addition of excess amounts of lithium that previously acted as inhibitor now facilitates the sorption process instead, resulting in an increase in CO_2 uptake capacities by the sorbents.

Arrhenius plots of SS-B-Li_4SiO_4 sorbents seemed to support this theory, where the activated energy values associated with the diffusion step (E_{ad}) of the reaction increased with the addition of excess amount of lithium (Figures 5.11 to 5.14). This indicates that the diffusion step of the overall CO_2 sorption process is being kinetically limited by the addition of excess lithium. Moreover, the activated energy values associated with the chemisorption step (E_{ac}) decreased with increasing amount of excess lithium. This suggests that although the diffusion was kinetically limited, the chemisorption step was actually enhanced by the addition of excess lithium.

Comparing the CO_2 uptake capacity of pure and waste-derived Li_4SiO_4 sorbents, SS-P-Li_4SiO_4 sorbents captured significantly less amount of CO_2 (e.g. 24.47 mg CO_2/g sorbent by S-P-Li_4SiO_4-0 and 114.4 mg CO_2/g sorbent by SS-C-Li_4SiO_4-0 at 500 °C) despite pure SiO_2 was used in the preparation of the sorbents. The amorphous phase found in the waste-derived Li_4SiO_4 sorbents is believed to contribute to the enhanced CO_2 uptake performance of the sorbents due to the versatility of amorphous structure in capturing CO_2 molecules. In comparison to the more ordered structure of its crystalline counterpart which is predominantly found in SS-P-Li_4SiO_4 sorbents, the coexistence of amorphous Li_4SiO_4 is thought to have increased the CO_2 sorption capacity of the waste-derived sorbents. Faster diffusion of sorbate into amorphous structure than that in crystalline due to the atomic disorder (Sadoway, 2010) is also believed to increase the rate of CO_2 sorption of the sorbents.

In diluted CO_2 environment, the CO_2 uptake profiles of pure and waste-derived Li_4SiO_4 sorbents did not reach sorption equilibrium at the end of analyses. It is also observed that the amount of CO_2 uptake capacity by sorbents decreased accordingly in diluted (111.5 mg CO_2/g sorbent by SS-B-Li_4SiO_4-0 at 500 °C) CO_2 environment compared to that in pure (128.6 mg CO_2/g sorbent in pure CO_2 environment by SS-B-Li_4SiO_4-0 at 500 °C) one. This observation is in good agreement with a study by Essaki et al. (2005) which reported the CO_2 uptake capacity of pure Li_4SiO_4 pellets decreased significantly (from 27 wt% in 15 vol% CO_2 at 600 °C to 2 wt% in 5 vol% CO_2 at the same sorption temperature) as the partial pressure of CO_2 decreased (Essaki et al., 2005). Analysing the effect of

excess lithium on CO_2 uptake capacities of the sorbents in diluted CO_2 environment, almost no obvious correlations again were observed, although they followed the same trend as in the pure CO_2 environment. In addition, the rate of CO_2 sorption by all Li_4SiO_4 sorbents increased as a function of sorption temperature, also as observed in pure CO_2 environment.

Additionally, there is a distinctive trend of CO_2 uptake profiles in diluted CO_2 environment, where the amount of CO_2 uptake increased with sorption temperature up to 600 °C before decreasing significantly at 700 °C. The decrease in CO_2 uptake capacity is expected due to the substantially low CO_2 partial pressure making it harder for the sorbents to capture CO_2 efficiently. Seggiani et al. (2013) explained this occurrence to be attributed to the Gibbs free energy changes (ΔG) of the sorption reaction between CO_2 and Li_4SiO_4 (Seggiani et al., 2013). As the CO_2 sorption is an exothermic reversible gas-solid reaction with equilibrium constant equivalent to an inverse of CO_2 partial pressure, the lower the CO_2 concentration the lower the equilibrium emission temperature, which is the temperature where CO_2 sorption and regeneration both share the same temperature. Consequently, desorption process was initiated at lower (600 °C) temperature in diluted CO_2 sorption environment compared to the pure (700 °C) one (Seggiani et al., 2013).

5.5.3. Regeneration of waste-derived Li_4SiO_4 sorbents

While the addition of excess lithium improved the overall CO_2 uptake capacity in a single cycle at 600 °C (Table 5.3), it did not seem to affect the stability of the

sorbents in multiple cycles regeneration process at the same sorption temperature. In addition, the amount of CO_2 uptake capacity of sorbents did not reach sorption equilibrium. This is expected as the CO_2 uptake analysis of the same sorbents also did not attain sorption equilibrium during 120 minutes of analysis duration, as shown in Figure 5.5. It was also observed that the amount of CO_2 uptake capacity of sorbents progressively increasing despite the decreasing sorption rate with each regeneration cycle.

5.5.4. Effect of sorbent preparation method on CO_2 uptake capacity

The results showed that the preparation method via suspended impregnation (SI) decreased, albeit small changes, the overall CO_2 uptake capacity of SI-B-Li_4SiO_4-20 sorbent when compared to SS-B-Li_4SiO_4-20 sorbent, which was prepared using a dry impregnation method. The CO_2 uptake capacity decreased from 257 mg CO_2/g sorbent by SS-B-Li_4SiO_4-20 to 197 mg CO_2/g sorbent by SI-B-Li_4SiO_4-20. Although the CO_2 uptake capacity of SI-B-Li_4SiO_4-20 decreased with a wet impregnation method, other behaviour of the sorbent remained the same to that SS-B-Li_4SiO_4-20.

Chapter 6 Conclusions and recommendations for future work

This chapter summarises the results and conclusions derived from the experimental studies (Section 6.1). Suggestions for further work are presented in Section 6.2.

6.1. Conclusions

This study aimed to develop high temperature CO_2 sorbents using a selection of solid wastes from power generation plants. The principal results were derived from the preparation and characterisation of sorbents and CO_2 capture analyses. This section summarises the conclusions for these experimental studies.

The waste materials used as precursors to be developed into Li_4SiO_4-based sorbents include two samples of fly ashes (CPFA and RPFA) and two samples of bottom ashes (FBA and POMBA). Amongst these parent waste materials, three samples were coal-derived waste materials (CPFA, RPFA and FBA) while POMBA was a biomass-derived waste material. Different characterisation analyses were carried out on all parent waste materials, including particle size distribution, loss-on-ignition and major oxides composition and mineral phase composition analyses.

The CO_2 uptake capacities of parent waste materials were analysed to determine the benchmark capacity of the materials prior to be developed as high temperature

sorbents. The maximum of CO_2 sorption capacity of parent waste materials was found to be 4 mg CO_2/g sorbent, which was lower than that of a commercially available solvent (176 mg CO_2/g sorbent). This proved the unsuitability of the parent waste materials if they were to be used for CO_2 capture without any pre-treatment. The generally low sorption capacity of parent waste materials was believed to be contributed by the low contents of metal oxides that are capable of chemically absorbing CO_2, such as CaO and MgO.

The data obtained following the characterisation of parent waste materials and their corresponding waste-derived Li_4SiO_4 sorbents were used to predict the CO_2 uptake performance of the sorbents, as summarised in Section 4.3. Particle size of the parent waste materials was predicted to have an advantage over larger ones due to larger surface area that can be provided for the waste-derived Li_4SiO_4 sorbents for the CO_2 sorption to take place. This prediction was not exclusively accurate due to the inconsistent CO_2 uptake capacity of sorbents with the particle size of the parent waste materials used. For example, SS-B-Li_4SiO_4 which derived from parent waste material with the largest particle size distribution, i.e. POMBA, absorbed the highest amount of CO_2 at all sorption temperatures.

In addition to particle size, LOI values of the parent waste materials played an important role to anticipate the degree of decomposition caused by volatile matters in the waste materials. Although the LOI values of the parent waste materials did not directly correlate with the CO_2 uptake performance of the resulting Li_4SiO_4 sorbents, they certainly affected the CO_2 uptake capacities of

parent waste materials. Peaking behaviour was observed during CO_2 capture analysis on parent waste materials, as indicated by the maximum CO_2 sorption capacity observed before it decreased rapidly. This behaviour was caused by the instability of the materials at high sorption temperatures, which directly related to the LOI values of the materials.

Furthermore, at least 47 wt% of SiO_2 present in the parent waste materials was deemed sufficient to be developed into Li_4SiO_4-based sorbents. This conclusion was verified by the detection of crystalline and amorphous Li_4SiO_4 peaks in XRD diffractograms of waste-derived Li_4SiO_4 sorbents. Additionally, the presence of amorphous mineral phase of Li_4SiO_4 found in waste-derived Li_4SiO_4 sorbents was previously predicted to have an advantage over crystalline phase of Li_4SiO_4 which were predominantly found in pure SS-P-Li_4SiO_4 sorbents. This prediction seems to be accurate in the context of this study, as the CO_2 uptake capacity of waste-derived Li_4SiO_4 sorbents were higher than those of pure SS-P-Li_4SiO_4 sorbents. The versatility of amorphous structure in capturing CO_2 molecules compared to the more ordered structure of its crystalline counterpart, which is predominantly found in pure Li_4SiO_4 sorbents, is thought to be the cause of such observations (Sadoway, 2010).

Also, this study experimented for the first time the suitability of a palm oil mill boiler ash (POMBA) as a precursor for Li_4SiO_4-based high temperature CO_2 sorbent. It was found that not only it was suitable to be developed as a high temperature CO_2 sorbent, but the sorbents derived from POMBA obtained CO_2

sorption capacities higher (up to 257 mg CO_2/g sorbent) than some of the coal waste-derived Li_4SiO_4 sorbents developed in this study. In addition, the CO_2 sorption capacity of biomass-derived SS-B-Li_4SiO_4 sorbents were comparable not only to that of coal-derived SS-C-Li_4SiO_4 (up to 263 mg CO_2/g sorbent), SS-R-Li_4SiO_4 (216 mg CO_2/g sorbent) and SS-F-Li_4SiO_4 (199 mg CO_2/g sorbent) sorbents that were prepared in this study, but also to waste-derived Li_4SiO_4 sorbents from previously published work, namely, fly ash (up to 26 mg CO_2/g sorbent) (Olivares-Marin et al., 2010) and rice husk ash (up to 324 mg CO_2/g sorbent) (Wang et al., 2011). The results of CO_2 uptake capacity of waste-derived Li_4SiO_4 sorbents proved that the research objectives 1 and 2 (Section 1.3) have been successfully met.

Pure and waste-derived Li_4SiO_4 sorbents were mainly prepared using the solid-state (SS) impregnation method. This type of preparation method has been widely applied by previous studies (Essaki et al., 2005; Tang et al., 2009; Wang et al., 2011), but it was primarily adopted from Olivares-Marin et al. (2010). Compared to previous studies on lithium deprivation (Tang et al., 2009), this work investigated the effect of excess amounts of lithium (5, 10 and 20%) on CO_2 sorption performance. Depending on the waste materials used, it was found that excess amounts of lithium affected CO_2 sorption performance. The sorbents that were derived from fly ash samples (CPFA and RPFA) exhibited decreasing trend in CO_2 uptake capacity with increasing amount of excess lithium at lower sorption temperatures (500 and 600 °C), but increasing trend in uptake capacity at higher sorption temperature (700 °C). On the other hand, the bottom ash samples

showed increasing trend in uptake capacity with increasing amount of excess lithium.

It was also found that the CO_2 uptake capacities of pure SS-P-Li_4SiO_4 sorbents were constantly lower than that of waste-derived sorbents. It is believed that the impurities in the starting waste materials, e.g. K_2O, contributed to the improvement of CO_2 uptake capacities of waste-derived Li_4SiO_4 sorbents, in particular the SS-B-Li_4SiO_4 sorbents. This conclusion was derived from the observations of Wang et al. (2013), where the authors found a correlation between the content of impurities in the starting waste materials, such as K_2O and Na_2O, to be directly related to the enhancement of CO_2 uptake capacity of the resulting waste-derived sorbents.

The influence of different sorption temperatures (500, 600 and 700 °C) on CO_2 sorption capacity of the sorbents was also investigated in this study. It was found that the CO_2 uptake capacities of waste-derived sorbents significantly increased with each increment of sorption temperatures. This observation can be explained using the double shell CO_2 sorption mechanism where at low temperature, two layers of shells covered the Li_4SiO_4 particle i.e. Li_2SiO_3 and Li_2CO_3 as CO_2 is chemically sorbed by Li_4SiO_4 (Essaki et al., 2005). Diffusion of Li^+ and O^{2-} ions from the bulk of Li_4SiO_4 particle is then activated at higher sorption temperature, allowing more CO_2 to be captured by the sorbent (Duran-Munoz et al., 2013). With the establishment of the correlation between CO_2 uptake capacity of waste-derived

Li_4SiO_4 sorbents and sorption temperatures proved that the research objective 3 (Section 1.3) have been successfully met.

Kinetic analysis was performed on waste-derived Li_4SiO_4 sorbents with the highest CO_2 uptake capacity, i.e. SS-B-Li_4SiO_4, in an attempt to corroborate the double shell mechanism with the data obtained in this study. The results showed that the CO_2 sorption by SS-B-Li_4SiO_4 sorbents fit well with the double exponential model, and therefore, verified the double shell CO_2 sorption mechanism described earlier. The kinetic parameters obtained following the kinetic analysis verified the diffusion step kinetically limits the overall CO_2 sorption on SS-B-Li_4SiO_4 sorbents at sorption temperatures 500, 600 and 700 °C. This is indicated by the significantly larger k_1 values compared to that k_2, which represent the chemisorption and diffusion rate of the process, respectively. k_1 and k_2 values obtained in this study were also found to be in good agreement with published studies. Olivares-Marin et al. (2010) reported similar findings, where k_1 values were at least 1 magnitude higher than those of k_2 for fly ash-derived Li_4SiO_4 sorbents.

In addition to the dry preparation method, this study also investigated a wet, i.e. suspended impregnation (SI), method to explore the effect of wet and dry preparation methods on CO_2 sorption capacity and performance of the sorbents. The SI preparation method was adopted from Chang et al. (Chang et al., 2001). It was found that the wet SI preparation method decreased the CO_2 sorption capacity of the sorbent, while maintaining other sorption performances such as

temperature dependency of CO_2 uptake sorption and kinetic behaviour of the sorbents.

CO_2 sorption performance by waste-derived Li_4SiO_4 sorbents under diluted CO_2 environment was also studied. It was found that the sorption capacities of sorbents decreased drastically, particularly at sorption temperature 700 °C. This is because of the considerably reduced CO_2 partial pressure making it harder for the sorbents to capture CO_2 efficiently, as also reported in previous studies (Essaki et al., 2005). As the CO_2 sorption is an exothermic reversible gas-solid reaction with equilibrium constant equivalent to an inverse of CO_2 partial pressure, the lower the CO_2 concentration the lower the equilibrium emission temperature, which is the temperature where CO_2 sorption and regeneration both share the same temperature. Consequently, desorption process was initiated at lower (600 °C) temperature in diluted CO_2 sorption environment compared to the pure (700 °C) one (Seggiani et al., 2013). The results obtained following the study of CO_2 sorption by waste-derived Li_4SiO_4 sorbents under diluted CO_2 environment confirmed that the research objective 4 (Section 1.3) has been met.

Regeneration study of waste-derived Li_4SiO_4 sorbents uncovered the addition of excess lithium did not seem to affect the stability of the regeneration cycles of waste-derived sorbents. The inability of the sorbents to achieve sorption equilibrium during regeneration cycles was expected, as the CO_2 uptake analysis of the sorbents selected for regeneration study also did not achieve sorption equilibrium during 120 minutes of single cycle analysis. The results and

discussions presented following the regeneration performance study of waste-derived Li_4SiO_4 sorbents showed that research objective 5 has been met.

6.2. Recommendations for future work

There are several areas that are worthy of further studies. Firstly, further improvement of CO_2 uptake capacities of the sorbents could be done by adding K_2CO_3 to the waste-derived sorbents. A successful improvement of CO_2 uptake capacities by fly ash-derived Li_4SiO_4 sorbents was reported by a previously published study (Olivares-Marin et al., 2010).

The waste-derived sorbents could also be prepared with sodium as substitution of lithium, due to higher toxicity of the latter. A preliminary study of this preparation method was done by the author, as collaboration with another colleague within the research group. It was discovered that the sodium-based sorbents successfully captured CO_2, albeit in smaller amounts compared to that of lithium-based (Sanna et al., 2014). A future work of this would be to further improve the CO_2 uptake capacities of the sorbents, as well as to study their regeneration cycles.

Also, the CO_2 capture analysis of the waste-derived Li_4SiO_4 sorbents under CO_2 environment with varying sorption temperatures could also be analysed. This is to simulate fluctuating temperature, where it is a normal occurrence in industrial applications.

References

Borhan, M. N., Ismail, A., Rahmat, R. A., 2010. Evaluation of Palm Oil Fuel Ash (POFA) on Asphalt Mixtures. Australian Journal of Basic and Applied Sciences, 4(10): 5456-5463.

Change, G.C., 2004. United Nations Framework Convention on Climate Change. United Nations Publications: Geneva, Switzerland.

Choi, S., Koyama, S., Watanabe, T., Park, D.-W., n.d. Preparation of Amorphous Li_4SiO_4 Nanoparticles from Crystalline Raw Material by RF Thermal Plasma.

Choudhary, A., 2012. Synthesis and characterization of lithium silicate ceramic for the test blanket module (TBM) in fusion reactors. NATIONAL INSTITUTE OF TECHNOLOGY, ROURKELA.

Consoli, N. C., Heineck, K. S., Coop, M. R., et al., 2007. Coal bottom ash as a geomaterial: Influence of particle morphology on the behaviour of granular materials. Journal of Soil and Foundations, Vol. 47, No. 2, 361-373.

Dash, S., Sood, D. D., Prasad, R., 1996. Phase diagram and thermodynamic calculations of alkali and alkaline earth metal zirconates, Journal of Nuclear Materials 228, 83-116

Durán-Muñoz, F., Romero-Ibarra, I.C., Pfeiffer, H., 2013. Analysis of the CO_2 chemisorption reaction mechanism in lithium oxosilicate (Li_8SiO_6): A new option for high-temperature CO_2 capture. Journal of Materials Chemistry A 1, 3919. doi:10.1039/c3ta00421j

Essaki, K., Kato, M., Uemoto, H., 2005. Influence of temperature and CO_2 concentration on the CO_2 absorption properties of lithium silicate pellets. Journal of materials science 40, 5017–5019.

Etheridge, D.M., Steele, L.P., Langenfelds, R.L, Francey, R.J., Barnola, J.-M. and Morgan, V.I. 1998. Historical CO2records from the Law Dome DE08, DE08-2, and DSS ice cores. In *Trends: A Compendium of Data on Global Change*. Carbon Dioxide Information Analysis Center, Oak Ridge National Laboratory, Oak Ridge, Tenn., U.S.A.

Figueroa, J. D., T. Fout, et al. (2008). "Advances in CO_2 capture technology - The U.S. Department of Energy's Carbon Sequestration Program." International Journal of Greenhouse Gas Control 2(1): 9-20.

Gauer, C., Heschel, W., 2006. Doped lithium orthosilicate for absorption of carbon dioxide. Journal of Materials Science 41, 2405–2409. doi:10.1007/s10853-006-7070-1

GCEP, G. C. a. E. P. (2005). An Assessment of Carbon Capture Technology and Research Opportunities. GCEP Energy Assessment Analysis. Stanford University: 20.

Gray, M. L., K. J. Champagne, et al. (2008). "Performance of immobilized tertiary amine solid sorbents for the capture of carbon dioxide." International Journal of Greenhouse Gas Control 2(1): 3-8.

Hassanzadeh, A., Abbasian, J., 2010. Regenerable MgO-based sorbents for high-temperature CO_2 removal from syngas: 1. Sorbent development, evaluation, and reaction modeling. Fuel 89, 1287-1297.

Ida, J., Lin, Y.S., 2003. Mechanism of High-Temperature CO_2 Sorption on Lithium Zirconate. Environmental Science & Technology 37, 1999–2004. doi:10.1021/es0259032

IEA, International Energy Agency (2004). Prospects for CO_2 capture and storage. Simon and Schuster.

IPCC, Intergovernmental Panel on Climate Change, Working Group III (2005). “IPCC special report on carbon dioxide capture and storage.” Cambridge University Press for the Intergovernmental Panel on Climate Change, Cambridge.

IPCC, Intergovernmental Panel on Climate Change (2007). Climate Change 2007: Synthesis Report. Contribution of Working Groups I, II and III to the Fourth Assessment Report of the Intergovernmental Panel on Climate Change: 60.

IUPAC, International Union of Pure and Applied Chemistry (1985). “Reporting physisorption data for gas/solid systems.” Pure & Appl. Chem., Vol. 57, No. 4, pp. 603-619.

Kato, M., K. Essaki, et al. (2003). “Novel CO_2 Absorbents Using Lithium-Containing Oxides.” Greenhouse Gas Control Technologies - 6th International Conference. J. Gale and Y. Kaya. Oxford, Pergamon: 1579-1582.

Klara, S. M., R. D. Srivastava, et al. (2003). "Integrated collaborative technology development program for CO_2 sequestration in geologic formations--United States Department of Energy R&D." Energy Conversion and Management 44(17): 2699-2712.

Kumar, P., Mal, N., Oumi, Y., et al., 2001. Mesoporous materials prepared using coal fly ash as the silicon and aluminium source. J. Mater. Chem., 11, 3285-3290

Levandowski J., Kalkreuth W., 2009. Chemical and petrographical characterization of feed coal, fly ash and bottom ash from the Figuera Power Plant, Parana, Brazil. International Journal of Coal Geology 77, 269-281.

López Ortiz, A., Escobedo Bretado, M.A., Guzmán Velderrain, V., Meléndez Zaragoza, M., Salinas Gutiérrez, J., Lardizábal Gutiérrez, D., Collins-Martínez, V., 2014. Experimental and modeling kinetic study of the CO_2 absorption by Li_4SiO_4. International Journal of Hydrogen Energy 39, 16656–16666. doi:10.1016/j.ijhydene.2014.05.015

Lu, C. H., Lee, W. C., 2000. Reaction mechanism and kinetics analysis of lithium nickel oxide during solid-state reaction. J. Mater. Chem., 10, 1403-1407

MacDowell, N., Florin, N., Buchard, A., Hallett, J., Galindo, A., Jackson, G., Adjiman, C.S., Williams, C.K., Shah, N., Fennell, P., 2010. An overview of CO2 capture technologies. Energy & Environmental Science 3, 1645. doi:10.1039/c004106h

Martavaltzi, C. S., Lemonidou A. A., 2008. Development of new CaO based sorbent materials for CO_2 removal at high temperature. Journal of Microporous and Mesoporous Materials 110, 119-127.

Medina, A., Gamero, P., Querol, X., et al., 2010. Fly ash from a Mexican mineral coal I: Mineralogical and chemical characterization. Journal of Hazardous Materials 181, 82-90.

Mejía-Trejo, V.L., Fregoso-Israel, E., Pfeiffer, H., 2008. Textural, Structural, and CO_2 Chemisorption Effects Produced on the Lithium Orthosilicate by Its Doping with

Sodium ($Li_{4-x}Na_xSiO_4$). Chemistry of Materials 20, 7171–7176. doi:10.1021/cm802132t

Olivares-Marín, M., T. C. Drage, et al. (2010). "Novel lithium-based sorbents from fly ashes for CO_2 capture at high temperatures." International Journal of Greenhouse Gas Control 4(4): 623-629.

Ooi, Z., X., Ismail, H., Bakar, A. A., 2013. Characterization of oil palm ash (OPA) and thermal properties of OPA-filled natural rubber compounds. Journal of Elastomers and Plastics, 1-15.

Ortiz-Landeros, J., Martinez-dlCruz, L., Yanez, C. G., Pfeiffer, H., 2011, Towards understanding the thermoanalysis of water sorption on lithium orthosilicate (Li_4SiO_4). Thermochemica Acta 5151, 73-78.

Pfeiffer, H., Knowles, K. M., 2004. Reaction mechanisms and kinetics of the synthesis and decomposition of lithium metazirconate through solid-state reaction. Journal of European Ceramic Society 24, 2433-2443.

Qiu, H., Lv, L., Pan, B., Zhang, Q., Zhang, W., Zhang, Q., 2009. Critical review in adsorption kinetic models. Journal of Zhejiang University SCIENCE A 10, 716–724. doi:10.1631/jzus.A0820524

Rao, A. B. and E. S. Rubin (2002). "A Technical, Economic, and Environmental Assessment of Amine-Based CO_2 Capture Technology for Power Plant Greenhouse Gas Control." Environmental Science & Technology 36(20): 4467-4475.

Rodríguez-Mosqueda, R., Pfeiffer, H., 2010. Thermokinetic Analysis of the CO_2 Chemisorption on Li_4SiO_4 by Using Different Gas Flow Rates and Particle Sizes. The Journal of Physical Chemistry A 114, 4535–4541. doi:10.1021/jp911491t

Samanta A., Zhao An, Shimizu G. K. H., Sarkar P., and Gupta R., (2012). "Post-Combustion CO_2 Capture Using Solid Sorbents: A Review." Industry and Engineering Chemistry Research 51: 1438–1463.

Sanna A., Ramli I., Maroto-Valer M. M., 2014. Novel Na-silicates CO_2 Sorbents from Fly Ash. Energy Procedia 63, 739-744.

Scripps Institute of Oceanography (2014) *The Keeling Curve*, [Online], Available: https://scripps.ucsd.edu/programs/keelingcurve/ [12 Aug 2014].

Seggiani, M., Puccini, M., Vitolo, S., 2011. High-temperature and low concentration CO_2 sorption on Li_4SiO_4 based sorbents: Study of the used silica and doping method effects. International Journal of Greenhouse Gas Control 5, 741–748. doi:10.1016/j.ijggc.2011.03.003

Seggiani, M., Puccini, M., Vitolo, S., 2013. Alkali promoted lithium orthosilicate for CO_2 capture at high temperature and low concentration. International Journal of Greenhouse Gas Control 17, 25–31. doi:10.1016/j.ijggc.2013.04.009

Shan, S. Y., Jia, Q., M., Jiang L., H., 2012. Preparation and kinetic analysis of Li_4SiO_4 sorbents with different silicon sources for high temperature CO_2 capture. Journal of Chinese Science Bulletin 57, 2475-2479.

UNFCCC, United Nations Framework convention on climate Change (2012) *The Doha Climate Gateway,* [Online], Available: http://unfccc.int/key_steps/doha_climate_gateway/items/7389.php [4 Jul 2013].

UNFCCC, United Nations Framework convention on climate Change (2007) *The Bali Roadmap,* [Online], Available: http://unfccc.int/key_steps/bali_road_map/items/6072.php [4 Jul 2013].

UNFCCC, United Nations Framework convention on climate Change (2010) *The Cancun Agreement,* [Online], Available: http://unfccc.int/key_steps/cancun_agreements/items/6132.php [4 Jul 2013].

UNFCCC, United Nations Framework convention on climate Change (2011) *Durban Outcomes,* [Online], Available: http://unfccc.int/key_steps/durban_outcomes/items/6825.php [4 Jul 2013].

UNFCCC, United Nations Framework convention on climate Change (2013) *Warsaw Outcomes,* [Online], Available: http://unfccc.int/key_steps/warsaw_outcomes/items/8006.php [1 Mar 2014].

US E.I.A., 2013. International Energy Outlook 2013 With Projections to 2040. Government Printing Office.

Tang, T., Zhang, Z., Meng, J. B., Luo, D. L., 2009. Synthesis and characterization of lithium silicate powders. Journal of Fusion Engineering and Design 84, 2124-2130.

Thy, P., Jenkins, B. M., Grundvig, S., et al., 2006. High temperature elemental losses and mineralogical changes in common biomass ashes. Fuel 85, 783-795.

Vassilev, S. V., Vassileva, C. G., Karayigit A. I., et al., 2005. Phase-mineral and chemical composition of composite samples from feed coals, bottom ashes and fly ashes at the Soma power station, Turkey. International Journal of Coal Geology 61, 35-63.

Veliz-Enriquez, M. Y., Gonzalez G., Pfeiffer, H., 2007. Synthesis and CO_2 capture evaluation of $Li_{2-x}K_xZrO_3$ solid solutions and crystal structure of a new lithium-potassium zirconate phase. Journal of Solid State Chemistry 180, 2485-2492.

Venegas, M.J., Fregoso-Israel, E., Escamilla, R., Pfeiffer, H., 2007. Kinetic and Reaction Mechanism of CO_2 Sorption on Li_4SiO_4 : Study of the Particle Size Effect. Industrial & Engineering Chemistry Research 46, 2407–2412. doi:10.1021/ie061259e

Wang, K., Guo, P., Wang, F., Zheng, C., 2011. High temperature capture of CO_2 on lithium-based sorbents from rice husk ash. Journal of Hazardous Materials 189, 301-307.

Wang, K., Zhao, P., Guo, X., Li, Y., Han, D., Chao, Y., 2014. Enhancement of reactivity in Li_4SiO_4-based sorbents from the nano-sized rice husk ash for high-temperature CO_2 capture. Energy Conversion and Management 81, 447–454. doi:10.1016/j.enconman.2014.02.054

WEC, World Energy Council (2003). “Drivers of the Energy Scene: A Report of the World Energy Council.” World Energy Council, London.

Wondraczek, L., Deubener, J., Misture, S.T., Knitter, R., 2006. Crystallization Kinetics of Lithium Orthosilicate Glasses. Journal of the American Ceramic Society 89, 1342–1346. doi:10.1111/j.1551-2916.2005.00861.x

Yamaguchi, T., T. Niitsuma, et al. (2007). "Lithium silicate based membranes for high temperature CO_2 separation." Journal of Membrane Science 294(1-2): 16-21.

Yinjie, W., Jiping, L., 2011. The Influencing Factor for CO_2 Absorption of Li_4SiO_4 at High Temperature. IEEE, pp. 839–841. doi:10.1109/ICMTMA.2011.782

Zainudin N. F., Lee, K. T., Kamaruddin A. H., et al., 2005. Study of adsorbent prepared from oil palm ash for flue gas desulfurization. Separation and Purification Technology 45, 50-60.

Appendix

Figures A.1 to A.3 show the isothermal CO_2 uptake profiles of SS-R-Li_4SiO_4, SS-F-Li_4SiO_4 and SS-B-Li_4SiO_4 sorbents in diluted CO_2 environment. As previously stated in section 5.2.2, these isotherms exhibit similar trend to that of SS-C-Li_4SiO_4 sorbents and therefore, are presented here in the Appendix section.

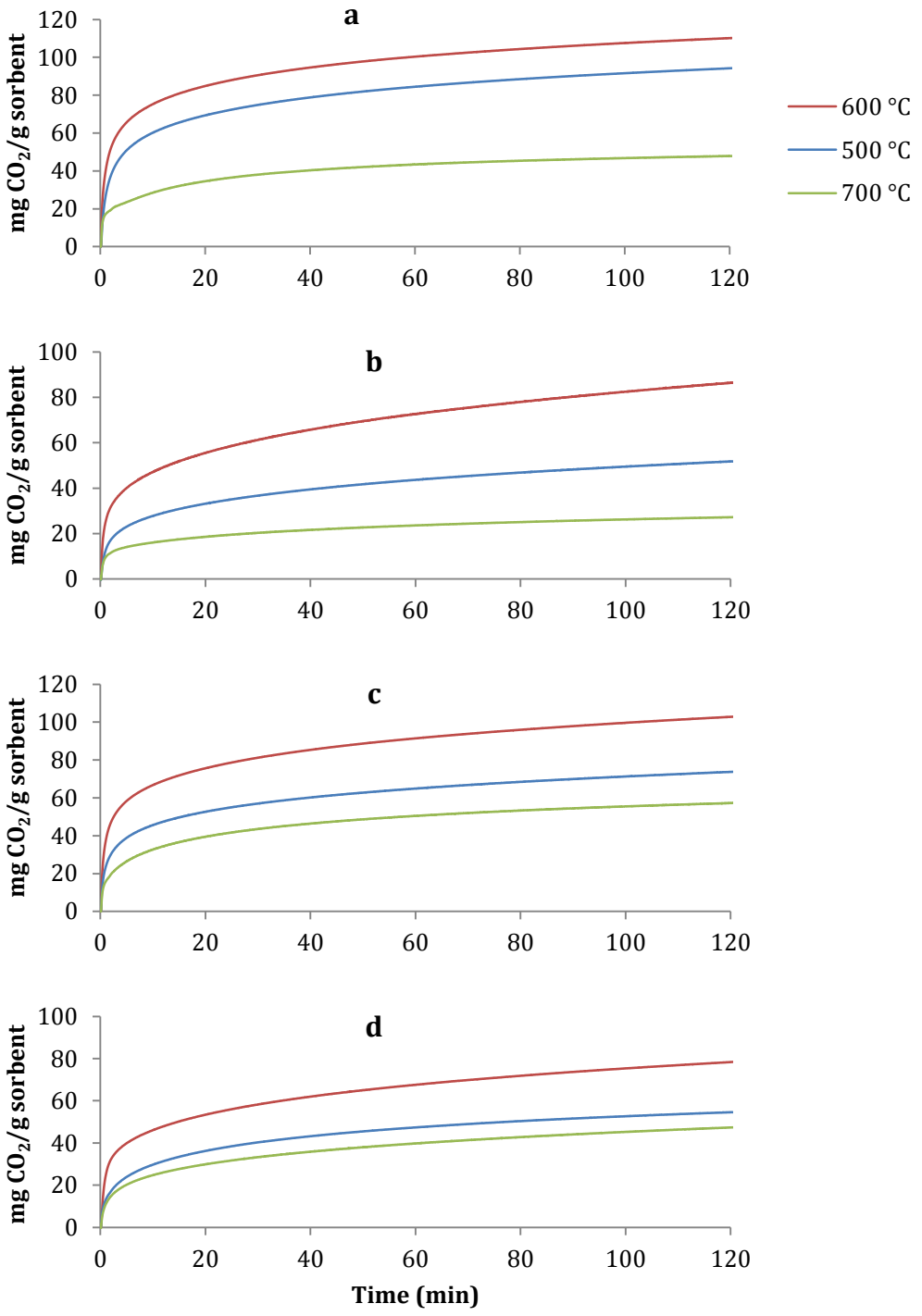

Figure A.1 Isothermal CO_2 uptake profiles of a) SS-R-Li_4SiO_4-0; b) SS-R-Li_4SiO_4-5; c) SS-R-Li_4SiO_4-10 and d) SS-R-Li_4SiO_4-20 in diluted CO_2 (14 vol%) environment.

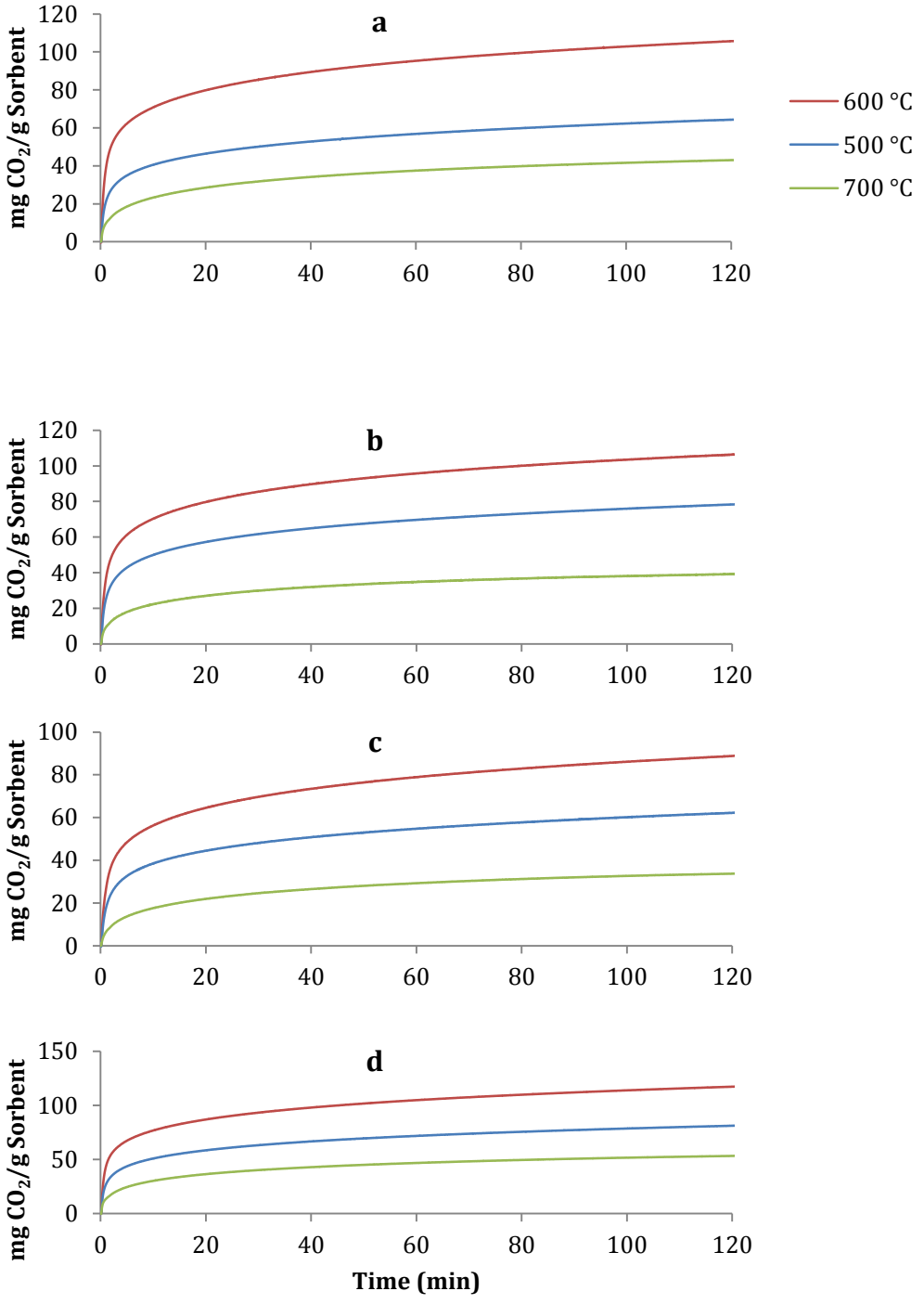

Figure A.2 Isothermal CO_2 uptake profiles of a) SS-F-Li_4SiO_4-0; b) SS-F-Li_4SiO_4-5; c) SS-F-Li_4SiO_4-10 and d) SS-F-Li_4SiO_4-20 in diluted CO_2 (14 vol%) environment.

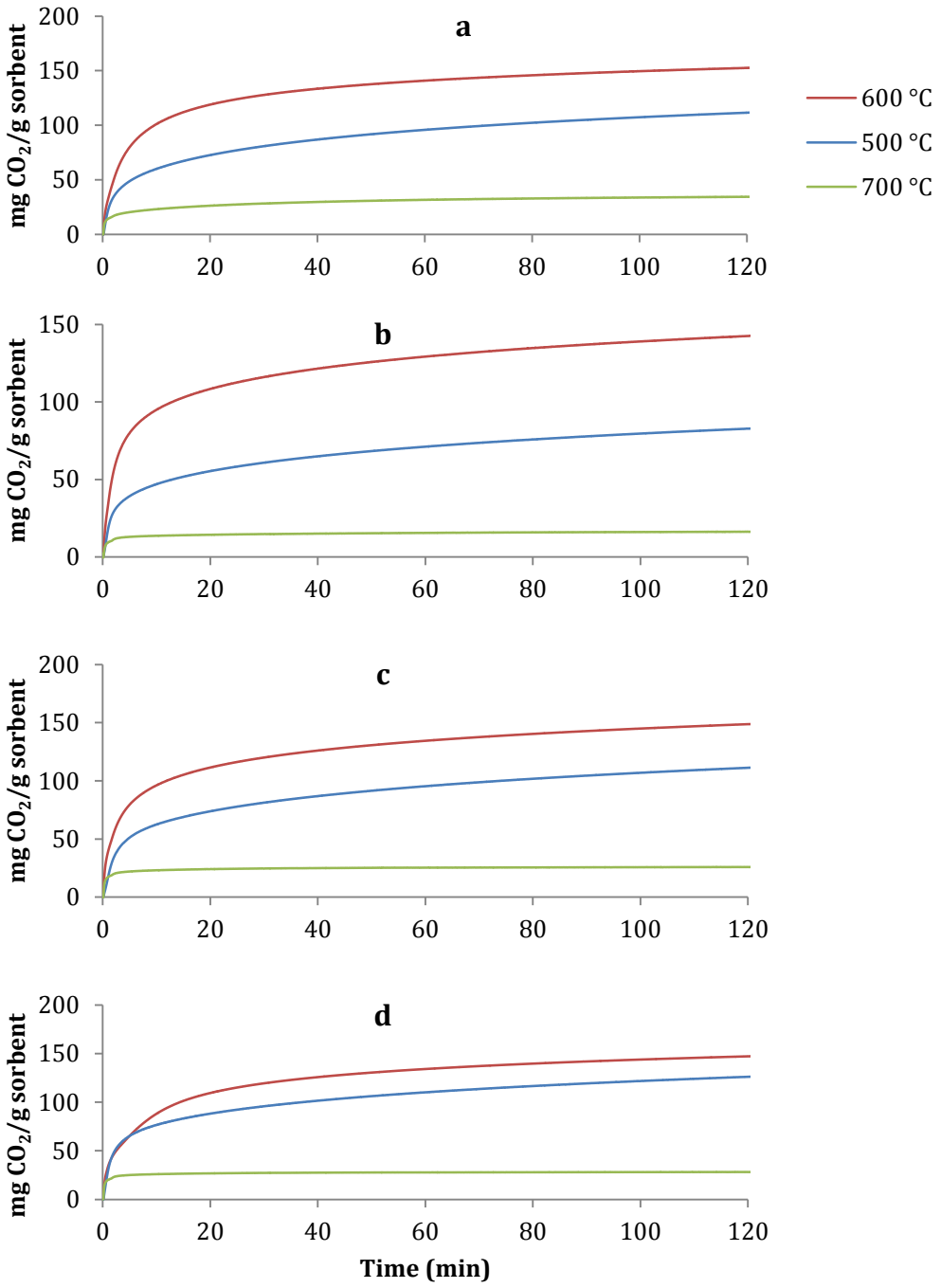

Figure A.3 Isothermal CO_2 uptake profiles of a) SS-B-Li_4SiO_4-0; b) SS-B-Li_4SiO_4-5; c) SS-B-Li_4SiO_4-10 and d) SS-B-Li_4SiO_4-20 in diluted CO_2 (14 vol%) environment.